PERFORMANCE INVESTIGATION OF ELECTRIC VEHICLE CHARGING IN A BIPOLAR DC MICROGRID

Thesis

Submitted in partial fulfillment of the requirements for the degree of

DOCTOR OF PHILOSOPHY

by

NISHA K S

DEPARTMENT OF ELECTRICAL AND ELECTRONICS ENGINEERING,
NATIONAL INSTITUTE OF TECHNOLOGY KARNATAKA,
SURATHKAL, MANGALORE -575025

May, 2024

DECLARATION

by the Ph.D. Research Scholar

I hereby *declare* that the Research Thesis entitled **" Performance Investigation of Electric Vehicle Charging in a Bipolar DC Microgrid"** which is being submitted to the **National Institute of Technology Karnataka, Surathkal** in partial fulfillment of the requirement for the award of the Degree of **Doctor of Philosophy** in **Electrical and Electronics Engineering** is a *bonafide report of the research work carried out by me.* The material contained in this Research Thesis has not been submitted to any University or Institution for the award of any degree.

Nisha.K.S

.....

Nisha K S, 187EE012

Department of Electrical and Electronics Engineering

Place: NITK-Surathkal

Date: 17-05-2024

CERTIFICATE

This is to *certify* that the Research Thesis entitled " **Performance Investigation of Electric Vehicle Charging in a Bipolar DC Microgrid**" submitted by **Nisha K.S** (Register Number:187120EE012) as the record of the research work carried out by her, is *accepted as the Research Thesis submission* in partial fulfillment of the requirements for the award of degree of **Doctor of Philosophy**.

20/05/2024

Dr. Dattatraya N. Gaonkar
(Research Guide)

Dr. Debasmita Mishra
(Chairman-DRPC, EEE dept.)

PROFESSOR AND HEAD
DEPARTMENT OF ELECTRICAL AND ELECTRONICS ENGINEERING
NATIONAL INSTITUTE OF TECHNOLOGY KARNATAKA
SRINIVASNAGAR, SURATHKAL, MANGALORE - 575 025, INDIA

Acknowledgements

It gives me immense pleasure and a great sense of satisfaction to express my heartfelt gratitude to those who made this dissertation possible.

Firstly, I would like to express my sincere gratitude to my Ph.D supervisor *Dr. Dattatraya Narayan Gaonkar*, Professor, Department of Electrical and Electronics Engineering, for his patient guidance, and incessant support throughout my research journey. I am forever thankful for giving me freedom to explore research areas which align to my interests and being the best research guide I could have asked for. He has been a constant source of encouragement in this entire journey.

I thank *National Institute of Technology Karnataka, Surathkal (NITK)* for giving me an opportunity to pursue research and *Ministry of Human Resource Department*, Government of India for awarding research scholarship.

I wish to thank my research progress assessment committee (RPAC) members, *Dr. A Karthikeyan* and *Dr Pathipati Srihari*, for their constructive feedback and guidance.

I also would like to thank HOD, *Prof.Dattatraya Narayan Gaonkar*, and former HODs, *Prof. B Venkatesa Perumal*, *Prof. Gururaj S Punekar*, *Prof. Shubhanga K N*, for extending the facilities and resources in the department at different stages of the research work.

I also wish to express my thanks to all my colleagues and friends in NITK, especially *Vishnu Sidharthan P*, *Asif Abdullah*, *Sreeram V Kulkarni*, *Vikas Singh*, *Teena Johnson*, *Anvit Khare*, and *Subradip Mondal* for the mental support and assistance throughout the course of my research.

I also want to express my regards to all faculties of EEE department in NITK, especially *Dr.Krishnan C.M.C*, *Prajof. P*, and *Dr. Dastagiri Reddy* for the motivation by setting a exemplary path of career to follow.

I would like to express my deepest gratitude towards my parents Mr. Sathian K K and Smt. Vasanthy K, and brother Akshay Sathian for their unconditional love and support. Their support and belief in me selecting my own paths is the foundation of whatever I have achieved in my life.

I would like to mark my words specially for my husband, who started this journey of research together with me. Thank you for your inputs and unending support in completion of my research work.

I would like to dedicate this dissertation as a mark of gratitude and affection to all mentors and institutes who instilled a research spirit in me, especially in Centre for Materials for Electronics Technology (C-MET),National Institute of Technology Calicut, National Institute of Technology Warangal and finally National Institute of Technology Karnataka Surathkal.

Finally, I thank *almighty God* for all the blessings and strength to keep going and pursue my goals at the times of difficulty.

Nisha. K. S

Abstract

Transportation electrification and charging infrastructure in India has to gain momentum in accordance to development of electric vehicle technology. Charging of electric vehicles is going to be a major electrical load in the near future, as more and more population shift to electric automotives from internal combusted engine-powered vehicles. Integration of electric vehicle charging stations might even burden the existing grid to a point of collapse or grid failure. Thus, an alternate grid structure is a necessity in the near-futures, for the powering the EV loads. Emergence of distributed energy sources and compatible technologies makes dc microgrids more popular compared to ac grids. Besides electric vehicle loads is primarily a battery which is dc in nature. Setting up charging stations integrated to microgrids can avoid the overburdening of the primary utility grid, by benefiting the distributed energy resources. The bipolar DC microgrid is a far better microgrid structure than the unipolar microgrid structure in many aspects like reliability, flexibility, and controllability. It can provide multiple voltage level interfaces according to the load demands, which is very apt for different charging levels of electric vehicles. Thus bipolar dc microgrid is the best answer we can put forward for the new age power grid.

Establishing charging infrastructure interfaced with bipolar DC microgrids along the roads and highways is the most realistic and feasible solution to avoid the overburdening of the existing power system. Operation of multiple sources and loads connected to bipolar DC microgrid will affect voltage regulation, and overall stable operation of the grid. Along with this, intermittent nature of renewable energy resources and unpredictable charging and discharging behaviour of EVs aggravate the power imbalance between two poles of dc microgrid. This leads to voltage unbalance issues in bipolar dc microgrid.

This thesis proposes bipolar converter configurations and fast acting nonlinear control strategies which can address voltage balancing and power sharing issues efficiently as well as integrate electric vehicle charging stations to bipolar dc grid. A bipolar dc grid in this research work consists

of photovoltaic power generation, DC loads and a battery system as auxiliary energy storage. Three level boost converter derived from neutral point clamped converter configuration is used for connecting PV systems to bipolar dc grid. Bipolar converter based on three level buck boost converter is used to connect battery energy storage system to microgrid. This bidirectional converter is operated such that auxiliary battery storage bridges the power gap between load demand power and generated power. Discrete state space modelling of the three level converters is done and model predictive control is developed, which is fast acting and more robust than PI control. With model predictive control, voltage regulation, pole capacitance voltage balancing, MPPT tracking and overall stable operation of the bipolar dc microgrid is ensured.

Simulation of the proposed model predictive control with three level converters is done in Typhoon Schematic Editor and Simulink. Hardware in loop testing of the model predictive control of the bipolar dc microgrid is done with Typhoon HIL 402 and validated in virtual and real time hardware in loop environment. EV load profile is developed for a cluster of vehicles considering different driving profiles and different vehicle dynamics. V2G and G2V regulation and control is implemented in integrating this EV load profile to bipolar dc grid. Multi-port three level converter is proposed for connecting electric vehicle charging stations. An overall decentralized model predictive control of multi-node bipolar dc grid with EV load profile, PV generation, BESS and dc loads is implemented effectively and analysed under dynamic grid conditions.

Contents

List of Figures

List of Tables

List of Abbreviations

DER	Distributed energy resources
NYCC	New york city cycle
WLTP	Worldwide harmonized light vehicles test procedure
BESS	Battery energy storage system
PV	Photovoltaic
HWFET	High way fuel economy test
IDC	Indian driving cycle
$FTP-75$	Federal test procedure
PHEV	Plugin hybrid electric vehicle
MPC	Model predictive control
PID	Proportional integral derivative
SOC_{EV}	EV state of charge
SOC_{BESS}	Battery state of charge
EVCS	Electric vehicle charging station
EV	Electric vehicle
MPPT	Maximum power point tracking
TLC	Three level converter
NPC	Neutral point clamped converter
TLBC	Three level boost converter
TLBDC	Three level bidirectional converter
G2V	Grid to vehicle charging
V2G	Vehicle to grid charging

List of Symbols

M	Gross weight of vehicle
Cd	drag coefficient
f_r	Rolling resistance coefficient
λ	Weighing factor
P_{gen}	Total generated power from solar PV
P_{gen1}	Generated power from PV system-1
P_{gen2}	Generated power from PV system-2
P_{load}	Total load power demand
P_{load1}	Load power connected in +ve dc bus
P_{load2}	Load power connected in -ve dc bus
P_{bat}	Battery power
I_{charg}	Total charging current demanded by EV load profile
I_{reg}	Total discharging/regulation current demanded by EV load profile
V_{bat}	Nominal voltage of battery pack
V_{pv}	Output voltage of PV
i_{pv}	Output current of PV
i_{C1}	Current through DC-link capacitor C1
i_{C2}	Current through DC-link capacitor C2
i_{01}	Load current through +ve pole
i_{02}	Load current through -ve pole
V_{C1}	voltage across the DC link/pole capacitor C1
V_{C2}	voltage across the DC-link/pole capacitor C2
V_{dc}	DC source voltage at battery side of three-level converter
V_{grid}	Bipolar dc microgrid voltage
V_O	Output voltage of multi-interleaved buck converter
V_S	Source voltage of multi-interleaved buck converter
i_{dc}	Current at battery side of three-level converter
R_{pv}	Series resistance of L_{pv}
R_{dc}	Series equivalent resistance of L_{dc}
L_{pv}	Inductance of three-level boost converter connected to PV
L_{dc}	Inductance of three-level bidirectional converter connected to BESS

L_{int}	Inductance of interleaved buck converter connecting EV load
Δi_{int}	Ripple current through interleaved inductor
R_{01}	DC load connected across +ve dc pole and neutral
R_{02}	DC load resistance across -ve dc pole and neutral
C_1	DC-link capacitor connected across +ve dc pole and neutral
C_2	DC-link capacitor connected across -ve dc pole and neutral
C_{int}	Output capacitor of interleaved buck converter
d_{eff}	Effective switching duty ratio of TLBDC
d_{s2}	Switching duty ratio of IGBT switch S2
d_{s3}	Switching duty ratio of IGBT switch S3
D	Interleaved buck converter duty cycle
f_s	Switching frequency of three-level converters
f_{int}	Switching frequency of multi-interleaved buck converter
S_1, S_2, S_3, S_4	Three level bidirectional converter switches
D_1, D_2, D_3, D_4	Diodes across TLC switches S1,S2,S3, and S4

Chapter 1

Introduction

The aftereffects of environmental pollution, such as global warming and extreme climate change, have become too grave to ignore in the past few years. The world is dealing with it on a daily basis in the form of frequent occurrence of massive floods, heat waves, dry spells, forest fires etc. The transportation industry contributed a significant chunk of the toxic pollutant and greenhouse gas emissions in the last decades. It adds up to more than 26% of total CO_2 across the globe. Depletion of oil resources, hike in fuel costs, and environmental pollution from poisonous gases are the major issues in the transportation industry. The population depending on its own mode of transportation is substantial, which creates a fast increment in such issues to the environment and humanity.

All the buzz and excitement around Electric Vehicle (EV) technology is that it has the potential for efficient de-carbonization of the automotive industry in the following decades (UNFCCC, 2015), thus pitching in to achieve the targets stated in the Paris Agreement by 2030. Nowadays, world is witnessing a drastic transformation from internal combustion engine vehicle technology to electric vehicle technology. EV technology is most advantageous in terms of cost-effectiveness, zero toxic gas emission, environment friendly, silent working, comfort, and very fewer maintenance (Bull, 2001). EV technology is at a fast pace in the domains of advanced motor drives, effective control methods, incorporation of hybrid sources, and state-of-the-art charging stations (Rafi and Bauman, 2021). State-of-the-art EV technology is in a stable state in the areas of motor drives and efficient controllers, but still extensive research needs to be done in the faster charging system development.

With the sudden increase in the number of EVs, there arises necessity for charging infrastructure development. Electric vehicle charging stations (EVCS) and electric vehicle supply equipment (EVSE) needed to be installed just like the petrol pumps on the highways and roads. It will burden the existing power system with ev loads. This situation is further worsened by the unconstrained and intermittent charging behavior of EVs (Lucas et al., 2015) as well as fast charging stations demanding more power from the utility grid within short intervals of time (Yong et al., 2015). So the existing power grid will be incompliant even in developed countries when a paradigm shift to EV happens. An alternative power grid structure is needed. India's aggressive electric vehicle target should also contribute to integration of EV charging stations to microgrid as to ensure adequate electric supply to meet surging demand. Charging stations for these plug-in hybrid electric vehicle (PHEVs) and gridable electric vehicles (GEVs) is calling for major infrastructure upgradation in the power grid structure.

1.1 Microgrid Classification

Microgrid is a group of interconnected distributed energy resources and loads within clearly defined electrical boundaries that acts as a single controllable entity with respect to the grid. Indian climatic conditions and renewable abundance point to a thriving microgrid markets for off grid and on-grid systems. In India, microgrids can step up to bridge the gap created by unreliable and insufficient primary utility grid, to involve off-grid customers, reduce power cost and pollution. For generations, diesel generators were used for power back up in Indian house holds. But now it is replaced by solar PV inverter and battery. Distributed energy resources (DERs) have attained more significance (Bevrani et al., 2017) on the account of the dip in costs of semiconductors in the past two decades. Among DERs, solar photovoltaic energy has the most promising and matured technology among the distributed energy resources considering the year around sunlight availability in Indian subcontinent (Debnath and Chatterjee, 2015). Hence, solar PV systems can be considered as a primary generation source for microgrid.

Based on the type voltage and current assumed, microgrid can be classified as ac microgrid, dc-microgrid and ac and dc hybrid microgrid (Kim et al., 2014). The classification of microgrid is illustrated in fig.1.1. AC microgrid make use of an ac bus system for connecting distributed and renewable energy sources and loads. It

is advantageous when needed to be connected with primary utility grid, ac loads or ac power generation units directly. But ac microgrid prone to lower conversion efficiency, power relaibility issues, and complex control owing to frequency and power factor related problems. Ac microgrids can be classified based on frequency, voltage and phase. Out of this, major classification is based on frequency. Line frequency ac microgrid operates at lower frequency, usually at the frequency of the utility grid, i.e. 50Hz or 60Hz. High frequency ac microgrid operates at higher frequencies. These microgrids usually makes use of high frequency transformers. High frequency operation is advantageous for higher voltage operation and significant size reduction of electrolytic capacitor used. But it is prone to more voltage drop and power losses at higher frequency. Dc microgrid on the other hand , makes use of direct current bus system for connecting distributed and renewable energy sources, energy storage devices and loads. It is much simpler owing to the absence of frequency and power factor problems, improved converter efficiency and lesser loss. Dc microgrid is considered to have many advantages compared to ac microgrid. Hybrid microgrid is an interconnection of AC and DC microgrids with power converters, hence possess both the advantage of dc and ac counterparts. But, it is too costly, requires more converters and complex operation.

1.2 Bipolar DC Microgrid

Dc microgrid is more beneficial than ac microgrids due to various factors. Most of the distributed energy resources (DERs) inherently produce dc power, hence dc–ac conversion stages can be eliminated if dc microgrid are established. Due to this, it also guarantee lesser conversion energy losses and better efficiency. Power quality issues due to power factor, reactive power, and frequency deviations are absent in dc microgrids, which reduces the complexity of control. Dc microgrid is less susceptible to failure due to main grid disturbances. Power quality problems associated with the high penetration of renewable resources that show varying power output are easily controlled with robust control of the dc bus voltage. Advances in power electronics and the semiconductor industry also favor the emergence of dc microgrids. Energy store devices like battery, supercapacitors, fuel cells etc are in dc form. Expected proliferation of electric vehicles in future needs fast dc battery chargers. All these factors advocates for the dc microgrid than the ac microgrid in the future.

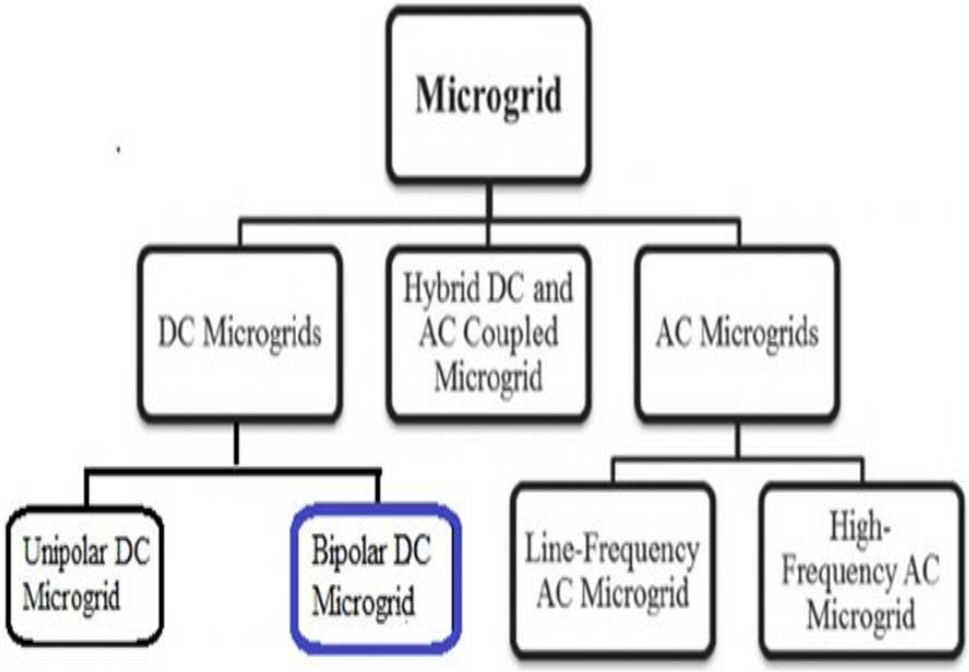

Figure 1.1: Microgrid Classification

DC microgrids have two structures; unipolar and bipolar dc grid configuration which is illustrated in fig.1.2. Mono polar dc grids have limitation in power handling capability. To enhance the power handling capability and reliability, bipolar dc micro grid topologies are developed. A bipolar structure dc microgrid has two poles, one positive pole and one negative pole and neutral in between. Loads can be connected between neutral and any of the two poles or between two poles. Bipolar structure of grid gives better control and flexibility in terms of load sharing, stability in times of disturbances, voltage regulation, balanced operation etc (Kakigano et al., 2010). The advantages of a bipolar dc grid are the availability of multiple voltage levels, continuity of power, load sharing, voltage regulation, balanced operation and flexibility. In short, bipolar grid structure gives better stability and control under dynamic conditions. Hence bipolar dc microgrid is a better dc microgrid configuration than the conventional unipolar dc microgrid configuration (Zubieta, 2016).

Driven by the need for higher reliability and power quality, advancements in power electronics, distributed energy resource technologies like PV panels, fuel cells etc, idea of dc microgrids is gaining attention worldwide. Some factors which advocates for

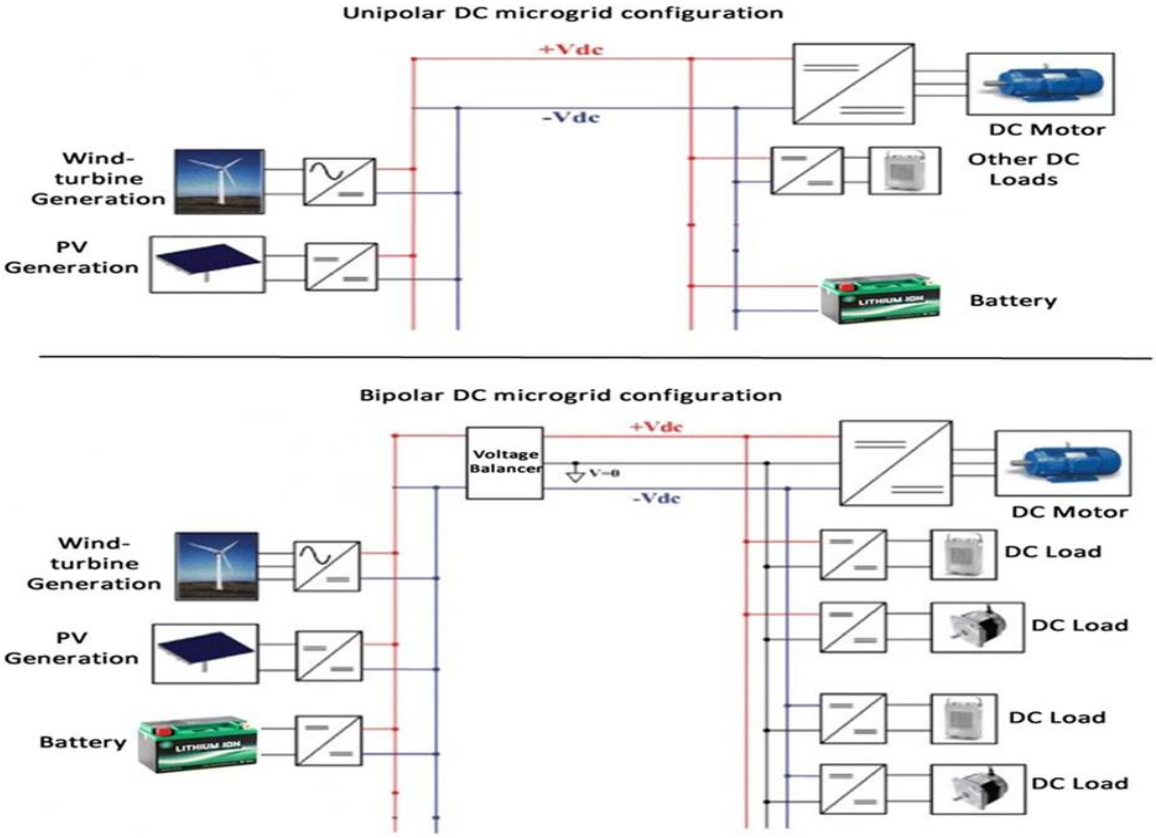

Figure 1.2: Configuration of Unipolar and Bipolar DC Grid

bipolar dc microgrid in future are:

- DC Home: concept of dc home is becoming more relevant as more and more household loads shifts to dc form like mobile phones, laptops, ovens, lights, battery storage etc.

- Data Centers : prefer dc distribution systems owing to factors like better efficiency, battery energy storage and cable size.

- Energy Park: generally, RESs harvested in dc form can be connected to common dc link bus and form collector grids.

- Telecommunication : need power at highly reliable, efficient and lesser cost.

- Traction: dc based public traction systems like metros,trams, buses are becoming more widespread around the urban population.

- Energy storage systems: major energy storage devices like battery, fuel cells, supercapacitors etc require dc power for better efficiency, prolonged life, power density, etc.

1.3 Electric Vehicle Charging Infrastructure

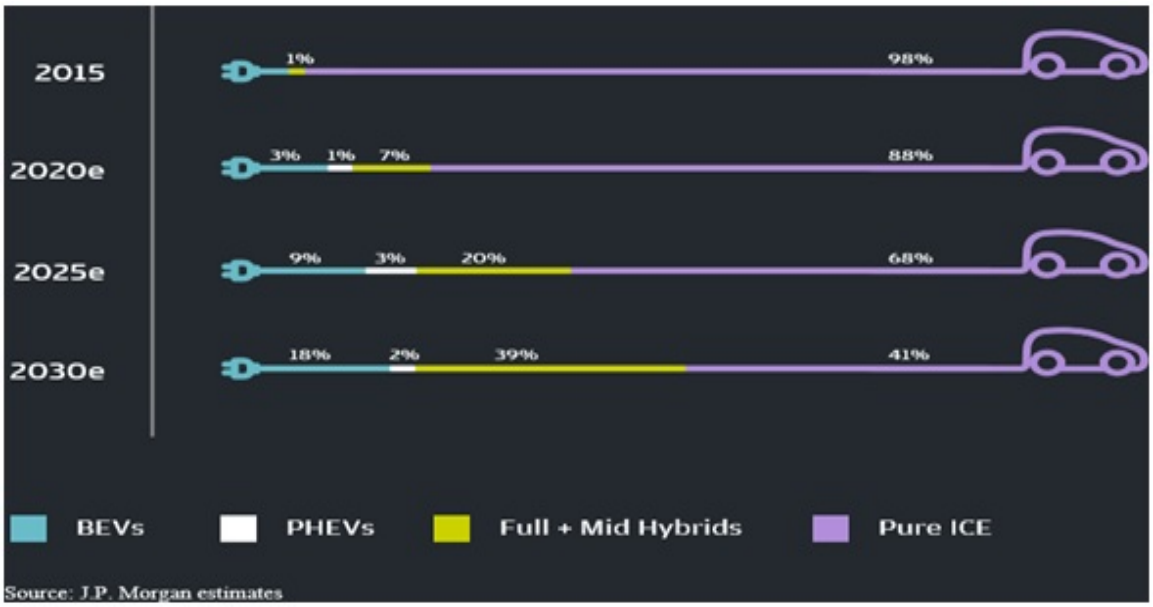

Figure 1.3: Forecast of electric vehicle usage in coming decade (JPMorgan, 2018)

Petroleum based fuels crisis which is going to worsen in the coming decades will set a trend on replacement of gasoline engine vehicles with different types of electric vehicles like hybrid EV, plugin HEV, gridable EV etc. EVs are playing major role by setting itself as an excellent mode of transportation which can solve the problems created like petroluem based fuel exhaustion and environmental pollution due to its combustion. A leap of growth in the electric vehicle is predicted by studies conducted by J.P.Morgan estimates and it is illustrated in fig.1.3. According to this research, 60% of pure ICE vehicles is going to be replaced by hybrid/ or full EVs by 2030 (JPMorgan, 2018). This leads to development of improved technologies in EV which emphasis them in transportation industry across the globe. Transportation electrification and charging infrastructure has to gain momentum in order to go hand-in-hand with advances of electric vehicle technology. As a result, electric vehicle

charging stations and electric vehicle supply equipment needed to be installed just like the petrol pumps in the highways and roads.

1.3.1 Electric Vehicle Supply Equipment

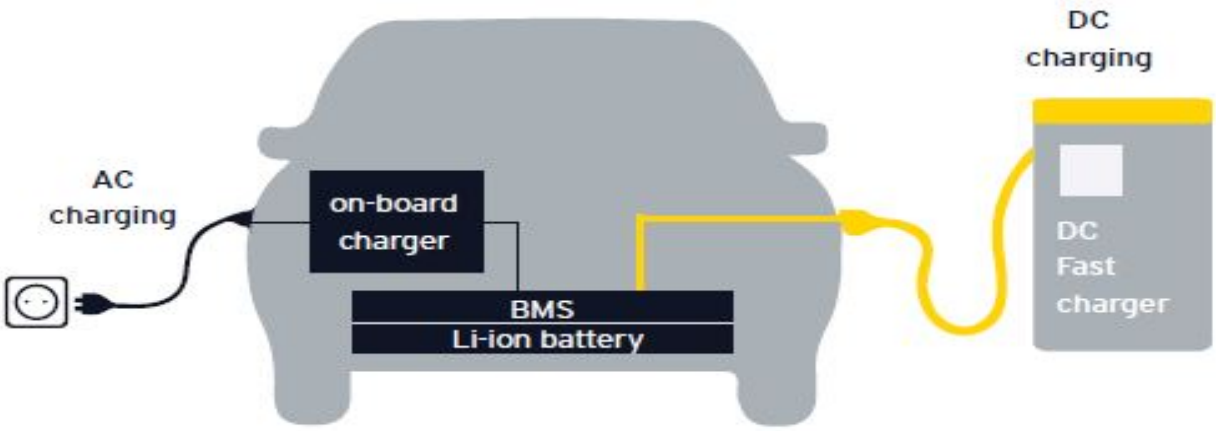

Figure 1.4: AC and DC Charger

Electric Vehicle Supply Equipment (EVSE) constitutes of devices dedicated for supplying electrical power to an electric vehicle. It can be connected to grid or be a standalone installation. Fig.1.4 gives a general idea about the difference between onboard charging and off board charging. Onboard chargers are usually AC chargers which consists of a power factor correcting AC-DC converter (inverter/rectifier) installed inside the vehicle and usually powered is taken from utility grid. Off board chargers are generally DC-DC chargers placed outside the vehicle, in a charging station. These dc chargers are directly connected to battery of vehicle, hence less conversion losses. EVSEs are classified into different types based on nature of charging power, charging speed, charging levels, connector type and based on communication protocols. The table and detailed classifications is given below:

- **By EVSE output - AC or DC** : Onboard charger are generally used in AC type EVSE. Onboard charger usually consists of a PFC AC-DC inverter-rectifier. Power ratings of an AC EVSE spans from 3.3 kW to 43 kW. While a DC type EVSE are usually dc-dc converter and are offboard chargers. DC EVSE can provide higher power spanning from 10 kW to 240+ kW.

- **By EVSE power rating – Levels I,II,III** : AC & DC EVSE have different power rating. They are seggregated as Level-I, Level-II, and Level-III. Different power level for AC and DC chargers as shown in Tbl. 1.1 and Tbl. 1.2.

Table 1.1: Power ratings for AC Chargers

	AC Chargers
Level I	120 V,1 phase AC (upto 1.9 kW, 16 A)
Level II	240 V single phase AC (upto 19.2kW, 80A)
Level III	Greater than 20 kW

Table 1.2: Power ratings for DC Chargers

	DC Chargers
Level I	200-450 V DC (upto 36 kW, 80 A)
Level II	200-450 V DC (upto 90kW, 200A)
Level III	200-600 V DC (upto 240kW, 40 A)

- **By charging speed – slow, fast or ultra-fast** : Time taken to charge an EV battery is based on the chargers used and battery capacity. For a 100kWh battery, 10kW charger is slow charging. For a 10kWh battery, it can act as a fast charger. Slow charging is when charging time spans around 4-8 hours. Fast charging is usually within one hour and charging done within 30 minutes is known as ultra fast charging. The fastness of charger also depends on battery size, type and thermal management.

- **By charging communication and connector type – CCS, GB/T,CHAdeMO** : Tbl. 1.3 below briefs about the various charging protocols. Certain standards are required for communication between EV battery, charger for effective charging. Otherwise, it will lead to overcharging, short circuits etc. This is referred as EVSE-EV communication protocols. Internationally accepted standards for charging are SAE J1722, GB/T-20234 and IEC 62196-4. They follow charging and communication protocols of CCS, GB/T and Chademo chargers respectively. Type of connectors, communication standard, charging power type, voltage levels of each of this standards is given in 1.3 .

Table 1.3: Prominent charging protocols

Country following	**Worldwide adopted**	**China**	**Worldwide adopted**
Charging standard	SAE J1722	GB/T-20234	IEC 62196-4
EVSE-EV communication	PLCC	CAN	CAN
Communication Protocol	CCS	GB/T	CHAdeMO
Type of charging	AC and DC	AC and DC	DC
Charging limit	1000V,350A, 350kW	750V,200A, 150kW	500V,125A, 400kW

1.3.2 India EVSE Related Standards

Business models and approaches chosen by numerous countries across the world for the better adoption of EV technology and EVSE system are different. India is in the forefront of this EV revolution with number of start up company already seizing the market and planning for products for future. is gearing up to unleash an EV revolution. In 2016, on the behalf of India Smart Grid Forum (ISGF), Bureau of Indian Standards (BIS) setup ETD 51 Committee for the formation of Indian Standards to be followed for EVSE. Since the EVs now in market mostly uses an onboard charger, they are required to be connected to primary utility grid for charging EV. Hence there should be a compliance with power system grid code just like other electrical devices used. Indian power grid system follows IEC standards and our grid power specifications aligns with that of the European standards, i.e. 230V, 50Hz. Whereas the US standard is different (110V and 60Hz).

Ministry of Heavy Industries also supported and agreed to the recommendation of national standards by BIS for better adoption of EVSE and EV charging infrastructure. BIS came up with two national standards for electric vehicle charging stations as Bharat EV Charger AC-001 and Bharat EV Charger DC-001. The standards IS:17017-1 published by BIS in August 2018 recommends both CCS-2 and CHAdeMO. In 2017, Department of Heavy Industries (DHI) commitee issued specifications based on GB/T charging protocols (which is put forward and used by China) for Bharat AC and DC chargers. According to this, Bharat EV Charger AC001 is

the standard for AC chargers and Bharat EV Charger DC001 is the standard for DC chargers. Both these EV chargers gives a dc output of maximum 120 V only and are slow chargers. Currently, BMS of EVs in Indian market does not support dc fast charging. BIS has adopted and will retain these standards in India, until new battery management system and evolved batteries are present in EV market. These standards needs to be withered and revisioned as more innovated EVs rolled out into roads with supercapacitors and batteries capable of fast charging with 400-500 V DC output. In India, right now all the EV standards adopted by major countries like China, US,Europe coexist. CCS and Chademo are standards adopted world wide, and GB/T is the standard adopted by China. In India, EV market can adopt with any of these standards.

Tesla is yet to enter the EV market in India and Ola Electric is already planning tie up with them. Ola Electric also have announced their new EV Four wheeler and super chargers. They also plan to set up 500+ super charging points exclusively for their customers, just like Tesla did in United States. Delhi has established charging ports in 50 of its sub-stations in the city. Bangalore, has also established electric bikes points near metro stations (Yulu) and also equipped parking spaces in malls and offices with charging points for electric cars. The Indian market for EVs is at an exciting stage, with the biggest market and competition in two wheeler sector , and slowly shifting focus to modified three wheelers. Mahindra Reva is the pioneer and main established electric car manufacturer in India with a legacy of 20 years and Tata Nexon in the electric car of India at the moment. More and more players are coming forward to grab a chunk of this evolving EV market in India. It is stated in a study that India's fossil fuel import from foreign nations decreased from 70% to 82% in 2012.

In India, IS 15886 was drafted for standardization of electric and hybrid vehicles and their components by Bureau of Indian Standards (BIS). Some standards were drafted by Automotive Research Association of India (ARAI). ARAI is a leading automotive R& D institute based in pune , formed by Indian Government for the sole purpose of better adoption of evolving EV technology and better development of charging infrastructure. These standards include:

- **AIS-138 (Electric Vehicle Conductive AC Charging System) :** for DC charging system for electric vehicles with assistance from existing international standards including IEC 61851-1(General Requirements), IEC 61851- 23

(electric vehicle charging station) and IEC 61851-24 (Digital communication)

- **Automotive Indian Standards AIS-102 & AIS-123 :** ARAI has published document including AIS-102 (Part 1 and 2) on CMVR Type Approval for Hybrid Electric Vehicles, AIS-123 on CMVR Type Approval of Hybrid Electric System Intended for Retro-fitment and AIS 131 on type Approval Procedure for Electric and Hybrid Electric Vehicles introduced in market for pilot/ demonstration projects intended for government schemes.

- **Bharat AC Charger and DC Charger:** In late 2017, the Ministry of Heavy Industries instituted "Committee on Standardization of Protocol for Electric Vehicles" which framed draft standards for charging stations – Bharat EV charger AC – 001 and Bharat EV charger DC – 001.

1.4 Literature Review

1.4.1 Bipolar DC Microgrid Operation and Control

Considering the growing ratio of dc loads and DERs, dc microgrid is more beneficial than ac microgrids because of efficiency and easier control. (Zubieta, 2016) proposed as the dc microgrids provide great benefits to the local distribution system than ac counterparts. (Kakigano et al., 2010) proposed low voltage bipolar dc microgrid as the next big thing in high quality distribution systems with three-wire dc line. A bipolar system has low-rated operation voltage of converters thereby securing cost effectiveness of converters and high reliability,stability since neutral terminal is grounded. However, bipolar system brings about unbalance problem between two poles if each load has different power rating. Control strategies are used for managing bipolar dc microgrid need to take care of various aspects like energy management of the renewable energy sources, battery, load etc connected to the grid, handling the power quality problems arising (mainly voltage profile variations since dc grid), maintaining the voltage balance between bipolar grid structure. Taha. A (Ahmadi et al., 2018a) presented a standardised hierarchial control of ac and dc microgrids, which consists of primary control based on droop control method, secondary control allows restoration of deviations and tertiary control manages the power flow between grid and external electrical distribution system. A method is proposed in (Ahmadi

et al., 2018b) to adaptively adjust the virtual resistance to reduce the circulating current between converters, so as to improve the load voltage and the performance of the power grid in the low voltage DC microgrid. However, this method needs to collect all node currents for multi-node converters, which means that the communication pressure of the whole system will be great, and the cost will be raised. In (Ahmadi, 2021), a new converter topology and unified control strategy is proposed to achieve unified control of power-sharing and voltage balance in a bipolar DC microgrid. In this work, voltage deviation can be maintained in the set range by collecting the droop coefficient of VSI in the bipolar DC microgrid.Voltage balancing converters tend to balance the voltage of BPDCMG buses with active sources or transferring the power from one bus to another one and batteries. This power sharing strategy does not guarantee an optimum performance of the entire system. So a hierarchical control strategy (Ahmadi, 2020) including a tertiary control with optimization method for achieving efficient operation and system damping improvement in a bipolar DC microgrid, a secondary control to regulate the output voltage decreased by primary droop control and to adjust the system damping when VRs change is implemented to three-port multidirectional DC–DC converter in this work. Adaptive droop control of unbalanced voltage in the multi-node bipolar DC microgrid based on fuzzy control is explored by , in which new voltage unbalance coefficient and voltage deviation index are defined to obtain more accurate parameters to describe the degree of voltage imbalance (Guo et al., 2022). X. Zhang .et.al (Zhang et al., 2015) three level voltage balancer derived from conventional TLC in a bipolar dc grid of 800V. Small signal modelling and new control strategy of conducting time extension of partial switch devices with PI controllers. In (Tavakoli, 2013), effective voltage balance control for bipolar dc microgrid is proposed with three level dc-dc fast charger which is combination of NPC converter connected with three level boost converter and uses PI control.

1.4.2 EV Integration to Microgrid

EV batteries themselves can play a significant role in microgrid systems, storing solar energy for when it's needed. The Indian government is planning on offering a 'EV as a Service' financial model to all citizens, putting the government in a position to possibly utilize EV batteries as a grid resource to meet national renewable targets (Pillai

et al., 2018). Analysis and design of a photovoltaic-based DC microgrid system is done by(Xiong and Yang, 2020). Operations of a 2.1 kW solar-fed EV charging station connected with the grid at Santa Monica is discussed in (Ingersoll and Perkins, 1996). The feasibility of charging EVs at workstations in the Netherlands using solar energy and data from the Dutch Meteorological Institute is explored in (R. Chandra Mouli et al., 2016). In the review paper (Du et al., 2010), non-isolated bi-direction dc dc converters for plug-in hybrid electric vehicle charge station application at municipal parking deck charging station has been proposed with the functionalities of normal and rapid charging, grid support such as reactive and real power (V2G mode) injection, current harmonic filtering and load balance. The proposed charging station has a DC power distribution bus, which can be considered as a microgrid, to interface with DC-DC chargers, distributed renewable power generations and energy storage system. An online power management based on the fuzzy logic (Gharibeh et al., 2021) is implemented for fuel cell based PHEV with PV uses the demanded power of the vehicle, battery and supercapacitor SoCs, as well as the vehicle speed as inputs to optimize the grid-vehicle operation. A combination of supercapacitors and batteries is used to improve the EV's performance and mileage. A coordinated control of battery energy storage (BESS) and plugin electric vehicles (PEVs) is presented for frequency regulation in a smart grid (Jamroen and Dechanupapritta, 2019) to eliminate frequency fluctuation caused by the dynamic behavior of load and intermittent nature of renewable sources. In the study, the BESS power utilization is decreased by 18.41% by the coordination of PEVs charging control and frequency regulation. In review paper (Yilmaz and Krein, 2013) , various aspects regarding implementation of V2G interfaces, challenges, cost, communication protocols, battery chargers, charging power levels, and infrastructure for plug-in and hybrid vehicles are detailed. Future aspects like roadbed charging is also discussed. (Singh et al., 2020), presents a newly integrated converter for plug-in electric vehicles with various modes of vehicle operation like plug-in charging or power factor correction (PFC), propulsion and regenerative braking etc is presented. Moreover, a non-linear carrier control method is used for PFC operation which saves the voltage sensor requirement for continuous conduction mode of operation. Reduction of feedback circuitry enhances the compactness of the converter, making it more suitable for on-board charger. Several non-isolated bidirectional DC-DC converters suited for charge station applications have been reviewed and compared. In (Du et al., 2010), a 10kW EV charging setup using a three-level

bidirectional converter in the vehicle parking area is realized, giving fixed switching pulses, i.e. only implemented open loop control. (Goli and Shireen, 2014) designed a smart charging station for Plug-in Hybrid Electric Vehicle (PHEV), in which PHEV is powered by solar or the utility grid or both, depending upon the dc link voltage. In a work done by (Huang et al., 2021), an off-grid DC EV Charging Station fed by PV is presented, which provides a total of 890 kW for 20 EVs with a novel hybrid control that has merits of both master-slave and droops control. A transformer less bipolar dc- dc converter based on series-connected submodules (D Broeck et al., 2019)for managing power flow for medium/high-voltage dc grids. This proposed converter is based on full bridge converters connected in modular arrangement, hence very bulky and requires large number of switches. Yu Du, Xiaohu Zhou et al.(Zhao et al., 2020) reviewed non-isolated bi-direction dc-dc converters for plug-in hybrid electric vehicle charge station application at municipal parking deck charging station with the functionalities of normal and rapid charging, grid support such as reactive and real power (V2G mode) injection, current harmonic filtering and load balance. The proposed charging station has a DC power distribution bus, which can be considered as a microgrid, to interface with DC-DC chargers, distributed renewable power generations and energy storage system. (Kang et al., 2013) presents a simple and cost-effective stand-alone rapid battery charging system of 30kW for electric vehicles. The proposed system mainly consists of active front-end rectifier of neutral point clamped 3-level type and non-isolated bi-directional dc-dc converter of multiphase interleaved half-bridge topology. The optimal discharging algorithm for V2G operation has been adopted to maintain the discharging current of 1C and proposed charging system is able to reach the full-charge state within less than 16min for the battery capacity of 8kWh by supplying the rated charging current of 78A.

1.4.3 Bipolar Converters and its Control

Bipolar dc grid have major issues of voltage balancing between grid terminals during dynamic conditions of changes in dc loads and power generation etc. Usual unipolar bidirectional converters (isolated and non-isolated) cannot be used for integrating energy storage systems like battery, super capacitor pack, fuel cells. Bipolar bidirectional converters with voltage balancing capability need to be integrated between bipolar grid and ESS to achieve stable and balanced operation of grid during load

disturbance and power generation fluctuations. (Kim et al., 2014) has stated through his work that this voltage unbalance problem can be addressed by bipolar converters or voltage balancers. Voltage balancers are derived from neutral point clamped multilevel inverters/converters(Kim et al., 2018), specifically NPC inverters. A voltage balancer ensure smoothing capacitors over each pole equally charged ,hence pole voltages balanced. Later three level voltage balancers were introduced to reduce the voltage stress on the device. (Zhang et al., 2015) depicted a three level voltage balancer with new control strategy of conducting time extension of partial switch devices with PI controllers in a bipolar dc grid of 800V. Mitigation of voltage unbalance by using static load transfer switch in bipolar LV DC distribution system is (Fan et al., 2015) presented, but there is complexity of load positioning and re-configuring based on data measured involved with this SLTS method. A transformerless bipolar dc- dc converter based on series-connected submodules for managing power flow for medium/high-voltage dc grids. This proposed converter is based on full bridge converters connected in modular arrangement,hence very bulky and requires large number of switches. Promising configurations of coupled inductor and switched capacitor based bipolar converters (Wang et al., 2017) and voltage balancers are proposed in (Xiong and Yang, 2020), which can be modified to get bipolar bidirectional converters with leser voltage stress on switches and voltage balancing similar to the three level converters.

Pulse delayed control of TLC is proposed in (**?**) Control approach based on flatness control of three level boost converter is discussed in (Garcia et al., 2006). In (Ingersoll and Perkins, 1996), a 10kW experiment prototype of three-level bi-directional DC-DC converter in municipal parking deck charge station application is done, but it is done with some test switching pulses with constant duty cycle, i.e. no controller. This has V2G and G2V options.

L.Tan, Bin Wu, V.Yaramasu, et al in (Tan et al., 2016) proposed effective voltage balance control for bipolar dc microgrid with three level dc-dc fast charger for EV charging station. Proposed VBC is a combination of NPC converter connected with three level boost converter which uses neutral point current to do the balancing work. A new modulation technique using PID controller is used for voltage balancing. . In (Tavakoli et al., 2017) , effective voltage balance control for bipolar dc microgrid is proposed with three level dc-dc fast charger which is combination of NPC converter connected with three level boost converter and uses PI control. A modified three level

boost converter is implemented for power factor correction with interleaved current sensorless control. Control approach based on flatness control of three level boost converter is discussed in literature. Work by Sebastian Rivera, Bin Wu,Samir Kuo, V.Yaramasu (Yaramasu and Wu, 2014) proposes a different dc-bus charging station concept, using a bipolar dc bus, enabled by a grid-tied 3 phase NPC with an additional fourth leg to act as the grid interface. A four-leg three-phase NPC converter offers superior harmonic performance and higher power handling capabilities. An additional leg is incorporated to act as a balancing circuit. A balancing inductor Lb is connected at mid point of capacitor and neutral point. In the paper by Xinbo Ruan (Xiong and Yang, 2020), origin of TL converters and their basic topological variations are described and a feedforward controlled Half Forward Bridge TL topology is first presented. Review of different bipolar converters /voltage balancers derived from normal converters like Buck-Boost,Cuk type, Super-Sepic/Zeta-type, interleaved type and three level converter (TLC) are stated in (Du et al., 2010). Promising configurations of coupled inductor and switched capacitor based bipolar converters and voltage balancers are proposed in (Wang et al., 2017), which can be modified to get bipolar bidirectional converters with lesser voltage stress on switches and voltage balancing similar to the three level converters. A very few papers depicts operation of TLC boost mode for voltage regulation and dc link capacitor voltage balancing issues. A modified three level boost converter is implemented for power factor correction with interleaved current sensorless control. Literature is available for three level buck converter and three level voltage balancers enabling controlled power flow in one direction. TLC converter is used for applications like battery electric vehicle charging, ultra-capacitor charging, power factor correction electric drives, interlinking between ac grid side and NPC inverter (Tavakoli, 2013). But all these works are either on TL buck converter or on TL boost converter and depicts controlled power flow only in one direction. We focus on developing three level converter with both buck and boost operation (i.e, with controlled bidirectional power flow) and voltage balancing capability.

(Akter et al., 2015) in their works has applied model predictive control for the operation of bidirectional ac-dc converter for energy storage applications and G2V -V2G applications in electric vehicle battery charger. Unlike the conventional linear control approach, model predictive control (MPC) technique is so desirable because it doesn't need the tuning of PID parameters for changes in the reference voltages and

currents (Tavakoli et al., 2017). It avoids the complexities of PWM modulation and other coordinate transformations. Moreover, model predictive method gives better performance in µgrid with renewable energy sources like PV, wind under fluctuating conditions of solar irradiation, wind speed etc (Golchoubian and Azad, 2017). It gives lesser oscillations and peaks during transients and gives faster control (Rodriguez and Cortes, 2012). Predictive control of TL boost with NPC inverter for wind energy conversion system in (Tan et al., 2016) is an interesting work, but doesn't have bidirectional power flow capability. A continuous set MPC is applied for unbalanced loads in bipolar dc grid in certain work (Sadiq et al., 2022). Suitable fast acting predictive control techniques has to be developed for elimination of voltage balancing and load sharing issues occurring in bipolar dc grid due to load disturbances and variations in power supplied by distributed energy sources like solar PV, wind farms etc.

1.5 Motivation

Microgrid based distributed energy resources need to be set up for powering upcoming electric loads in future. Many renewable energy sources like solar photovoltaic and fuel cell generate dc power. Most of these sources supply power to an ac utility grid through costly and inefficient power converters, even where the power may ultimately be delivered to a dc device, like EV battery. With the development of cost-effective and efficient power electronic converters, a dc micro-grid can become a promising solution than ac grid. Dc microgrid have two structures; unipolar and bipolar dc grid configuration. Mono polar dc grids have limitation in power handling capability. To enhance the power handling capability and reliability, bipolar DC micro grid topology are developed. Bipolar structure of grid gives better control and flexibility in terms of load sharing and stability in times of disturbances.

But bipolar dc grid have major issues of voltage imbalance between grid terminals during dynamic conditions. Pole voltages shifts with variations in input power generated and load changes. Using regular converter configurations with unipolar structure cannot provide power sharing between two poles, hence cannot mitigate voltage unbalance issues. Moreover, number of converters in the system increases when unipolar converters used for connection to bipolar dc grid. This automatically increase the semiconductor switches and complexity of control. Unpredictable charg-

ing and discharging tendencies of electric vehicle will also cause power quality issues on the bipolar dc grid. Dc link capacitance voltages need to be maintained constant and balanced irrespective of grid conditions. Bipolar dc microgrid need novel three level converter configurations suitable for the bipolar structure of the grid to connect with PV generation system, battery energy storage, electric vehicle charging stations etc and to achieve stable, balanced operation of grid during dynamic conditions.

1.6 Research Gaps

With the literature study explained in previous section, some vital problems are identified which need to be addressed to improve the performance of the proposed system of bipolar dc microgrid integrated electric vehicle charging stations in this work.

1. Unpredictable charging and discharging tendencies of electric vehicle will cause power quality issues on the primary ac grid. It will also burden the existing power system with ev loads with fluctuating behavior. Alternate grid system or new provisions should be added to existing system to tackle this problem.

2. Bipolar dc voltage unbalance is the major issue that faced in the bipolar dc microgrid. Pole voltages shifts with variations in input power generated and load changes. DC capacitance voltages need to be maintained constant and balanced irrespective of PV irradiation conditions and load.

3. Bipolar dc microgrid need novel three level converter configurations suitable for the bipolar structure of the grid to connect with PV generation system, battery energy storage, electric vehicle charging stations etc. Using regular converter configurations with unipolar structure cannot provide power sharing between two poles, hence will cause unbalanced power. Also number of converters in the system also increases, hence increase the semiconductor switches.

1.7 Author Contributions

This research work put forward three level converters and its predictive control for bipolar dc grid and electric vehicle charging stations. Significance of bipolar dc mi-

crogrid in future transportation electrification is emphasized through this research. The major contributions of this research work are:

1. Modelling and design of three level converters for a bipolar dc grid with PV generation and battery energy storage for addressing voltage balance and regulation problems under normal/abnormal grid conditions.

    - Design and modelling of three level buck/boost converters for integration of battery energy stoarge with bipolar dc microgrid.
    - Voltage unbalance mitigation and enabling power sharing between poles of the grid.
    - Regulation of grid voltage, and minimization of fluctuations during varying load and solar irradiation conditions.
    - Investigation of operation with PI controller under dynamic grid conditions.

2. Developing model predictive controller to regulate and mitigate stability issues of bipolar dc microgrid during dynamic conditions.

    - Developed model predictive control of TLC to meet control objectives; voltage regulation, voltage balancing, mppt tracking and bidirectional power flow.
    - Simulation and hardware in loop validation of the proposed MPC controller
    - Energy management strategy formulated for bidirectional power flow without any complexity for a wide range of Pgen/ Pload .
    - Efficient and faster voltage balancing, grid voltage regulation and power sharing achieved within 0.2sec in bipolar dc microgrid.

3. Performance investigation of multi-node bipolar dc grid under different EV charging profiles and develop V2G/G2V energy management system.

    - Development of EV charging profiles which reflects vehicle dynamics and EV battery conditions
    - Developed V2G/G2V energy management system for EV load profile- grid interfacing.

- Improved bipolar bidirectional converter configuration suitable for integrating Electric Vehicle Charging Stations to bipolar dc microgrid.
- Effective decentralized control of all the components of multi-node bipolar dc microgrid (BESS, PV, EVCS and DC loads).

1.8 Outline of the Dissertation

The whole thesis is organized into five chapters as follows as shown in fig 1.5:
Chapter 1: A brief introduction to the bipolar dc microgrid and basics of electric vehicle charging is covered in this chapter. An extensive literature survey of the power electronic interface and control techniques to overcome voltage unbalance issues in bipolar dc grid, and microgrid integration of EV are reviewed. Identified research gaps leading to the major contributions of this research works.

Chapter 2: Modelling and design of the bipolar dc microgrid is discussed in this chapter. It details mathematical modelling of PV cells, Li-ion battery, circuit description and state space modelling of bipolar converters and PI controller implementation.

Chapter 3: Implementation of the model predictive controller and an energy management strategy which mitigates voltage unbalance issues and ensures stable operation of proposed bipolar dc microgrid are discussed in this chapter. Further, hardware in loop testing is done to validate the effectiveness of the predictive controller.

Chapter 4: Modelling of EV load profiles which reflects the variations in driving cycles, vehicle dynamics and battery conditions EV load profile is discussed in this chapter. V2G/G2V energy management system suitable for bipolar dc microgrid and its effective operation in the proposed bipolar dc microgrid is also explained. Moreover, an improved bipolar bidirectional converter suitable for integrating electric vehicle charging stations to bipolar dc microgrid is also put forward.

Chapter 5: This chapter concludes the contributions of the proposed research work and also discusses the scope for possible future works which enhances the significance of bipolar dc microgrid in the transportation electrification.

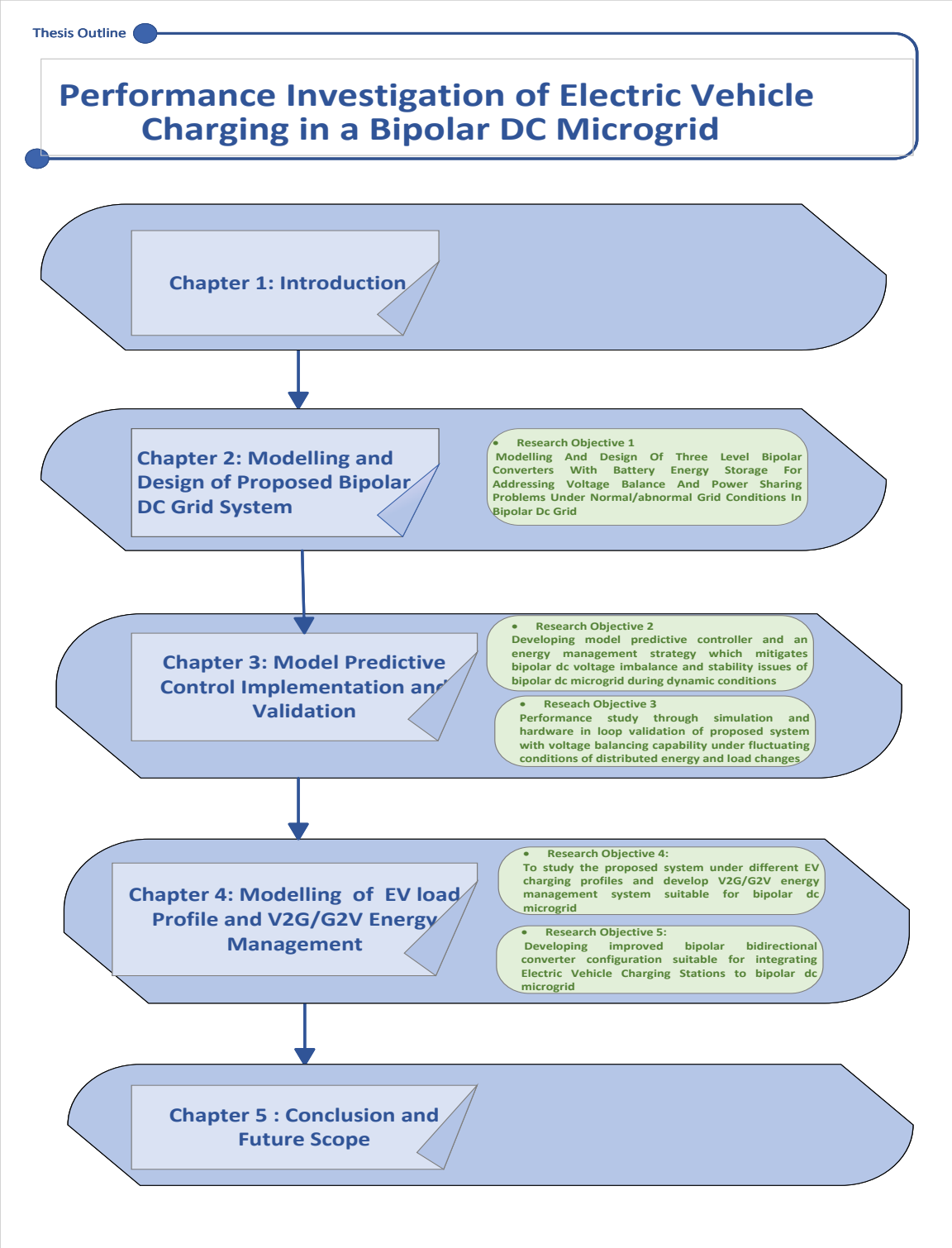

Figure 1.5: Thesis organisation.

Chapter 2

Modelling and Design of Three Level Converters for Bipolar DC Microgrid

2.1 Introduction

This chapter introduces the structure of a bipolar dc microgrid system, which can be used for powering electric vehicle charging stations. Modelling and design of three level or bipolar converters suitable for bipolar dc grid is detailed in this chapter, followed by the operation of the bipolar dc microgrid with PI controller. The ideas explained are from the available literature as well as those observed in the process of further analysis, and simulation studies.

2.2 Configurations of Bipolar DC Microgrid

Typical Bipolar dc grid gives a provision of connecting heavy loads between two poles or light loads can be connected to one pole and common. The bipolar dc microgrid can be considered as an effective solution to the applications where a high level of reliability and efficiency is required. Schematics of the bipolar dc micro grid is with two power generation units of solar pv system, battery and dc loads are considered for study in this work. In fig 2.1, 2-L boost converters extract maximum power from PV panels for corresponding irradiations and feed to grid. There is no voltage regulation or voltage balancing between bipolar grid during load disturbance

or fluctuating power generation. For regulating the power flow in the grid, battery energy storage (BES) is introduced to the bipolar grid. It can deliver or absorb power from the bipolar microgrid by 2-L bidirectional converters connected compensating for excess deficiency of power due to transient conditions. But two battery systems with two bidirectional converters are required to regulate the grid voltage and control the power flow,but the voltage balancing issue still persists. Moreover, it needs two BES which is bulky. Configuration in fig 2.3 with 3-level bidirectional buck boost converter with single BES eliminates the disadvantages of configuration in fig 2.1 and fig.2.2. PV panels are interfaced through a three level boost converter to extract the maximum power and three level buck-boost converter with appropriate control strategy can balance the dc bus voltage and also maintain regulation. In the bipolar dc microgrid configurations shown in fig.2.3, EV fast charging stations can also be set up using three level bidirectional buck/boost converter.

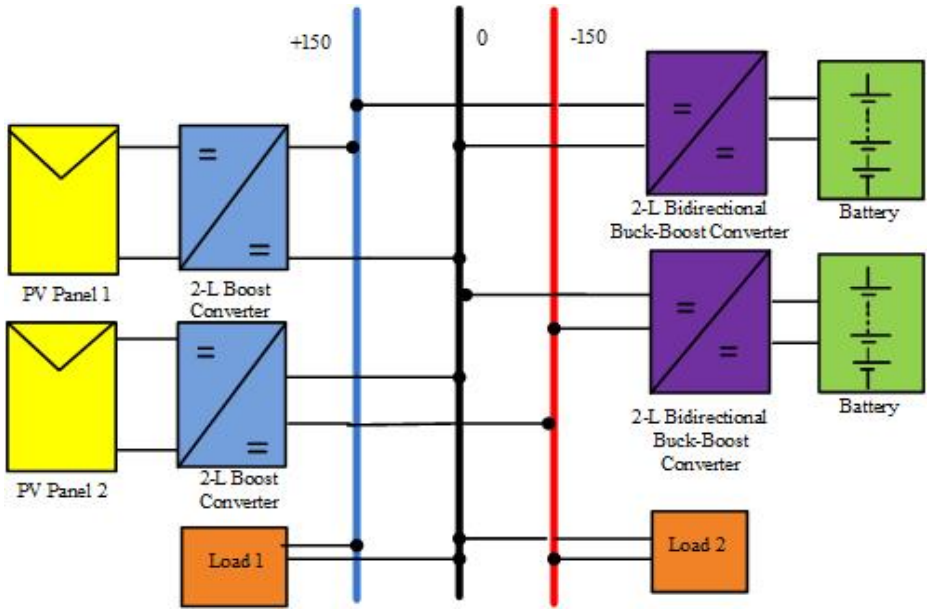

Figure 2.1: Bipolar DC grid: configuration-1

2.3 System Description

The basic architecture of bipolar dc microgrid used for study and research is illustrated in fig 2.4. System composed of distributed energy resources, energy storage system, local dc loads, electric vehicle charging ports, different converters for con-

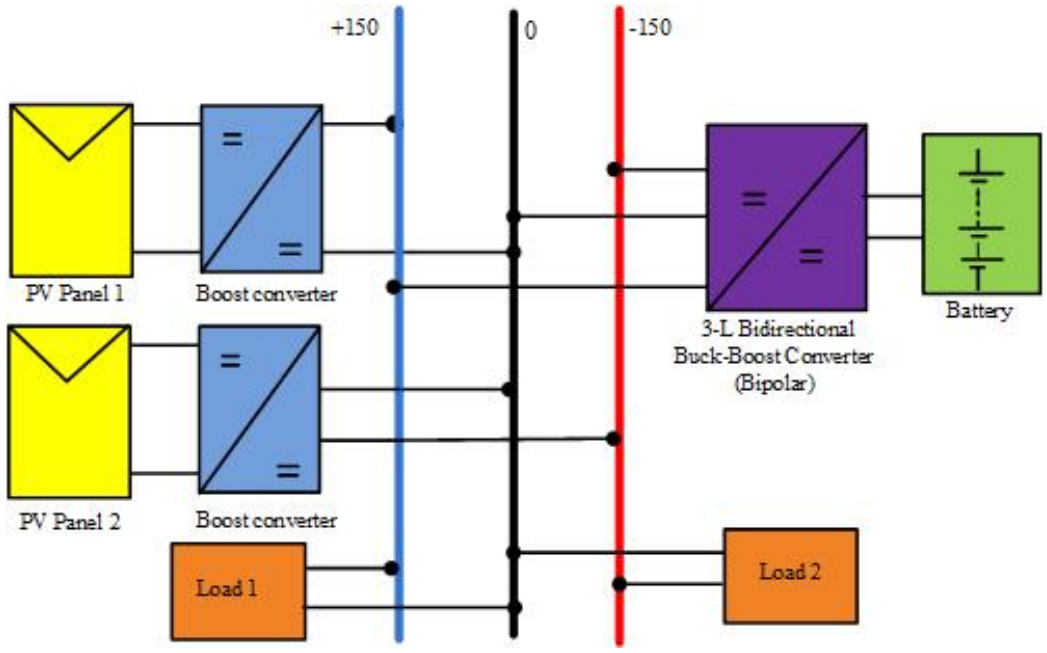

Figure 2.2: Bipolar DC grid: configuration-2

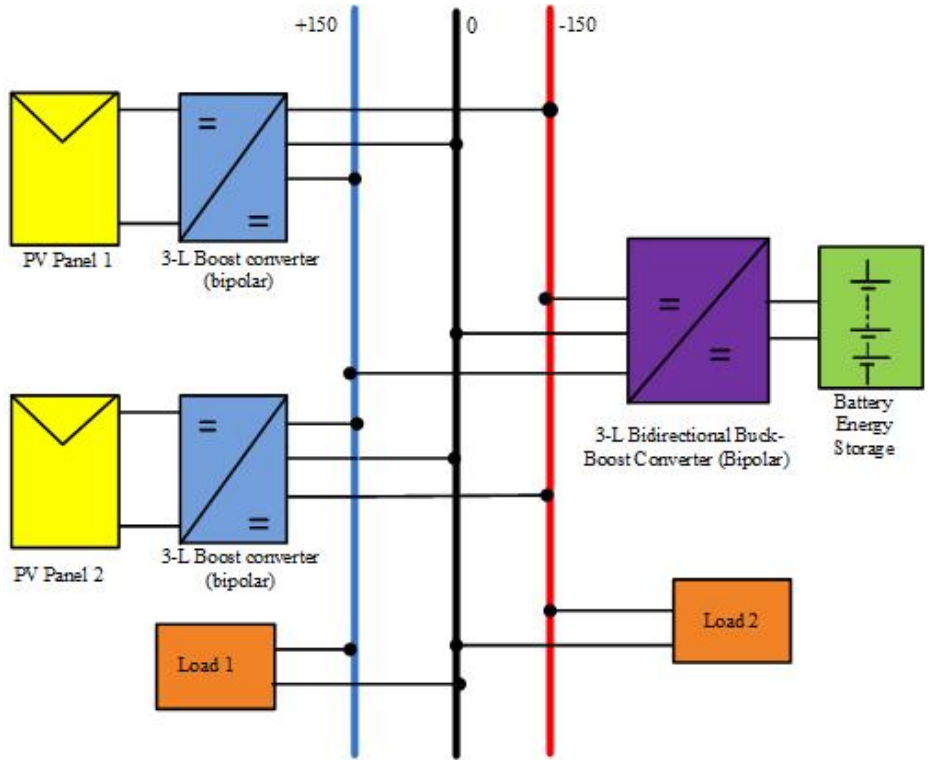

Figure 2.3: Bipolar DC grid: configuration-3

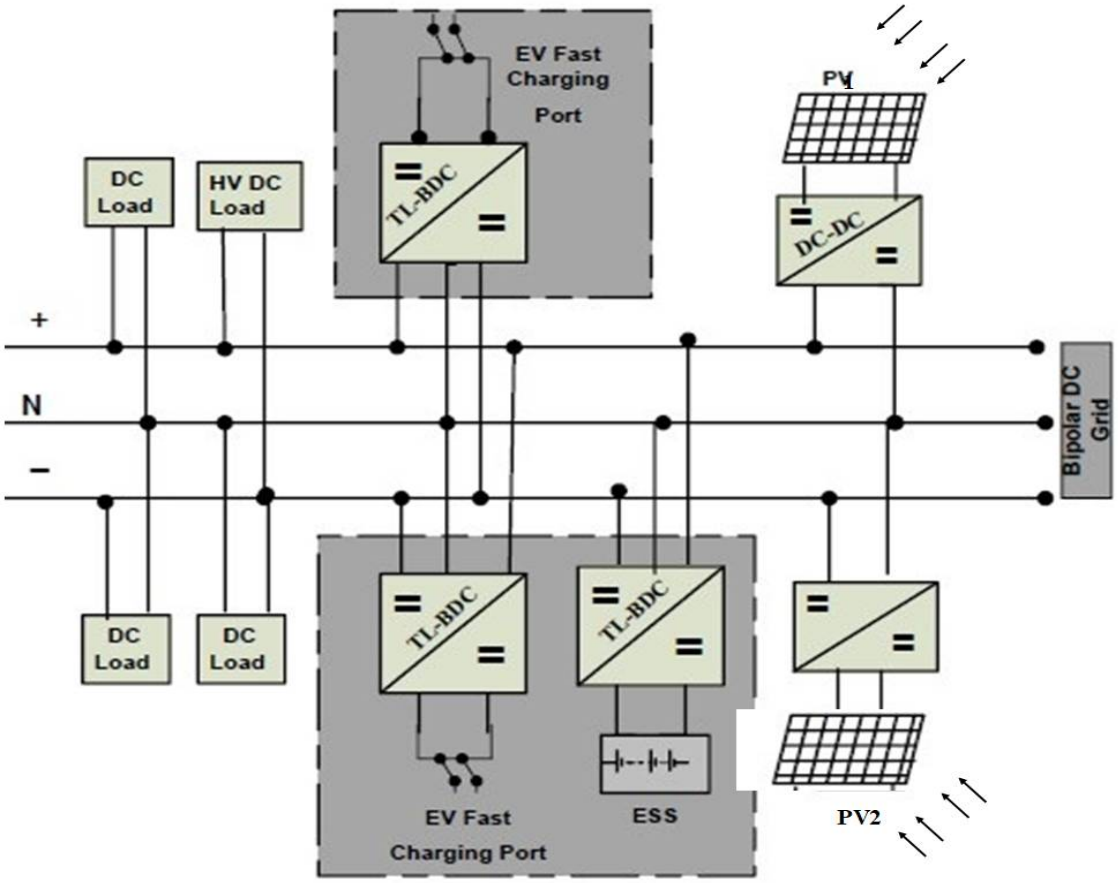

Figure 2.4: Schematics of Bipolar DC Microgrid System

trol and conversion. The topology of various voltage balancing converters which can be reconfigured as bipolar bidirectional converters which can be applied for ESS or EVCS integration with bipolar microgrid. In above configuration, three level configurations has simpler switching sequence and operation. The topology of bipolar converter of our interest is three level buck-boost converter. Thus, three level (bipolar) bidirectional buck/boost converter is the most suitable converter configuration to be used as interlinking converter between bipolar dc microgrid and battery energy storage (BES) or for integrating electric vehicle fast charging stations to bipolar dc microgrid. There are several control issues related to the bipolar dc microgrid, including voltage balancing between the two poles of the dc microgrid, load sharing, voltage control among parallel converters, maximum power point tracking and energy storage. Suitable bipolar converters are needed for integration of ESS, EVSE, DERs etc to the bipolar dc microgrid. Also, bidirectional power flow is essential when ESS

, EV s etc are connected to grid. The intention of this proposed work is on development of bipolar converters suitable for integration of dc fast charging stations and battery energy storage systems with bipolar dc microgrid. It also focusses on suitable control strategies for elimination of voltage balancing and load sharing issues occuring in bipolar dc grid due to load disturbances and variations in power supplied by distributed energy sources like solar PV, wind farms etc. of the dc grid due to load disturbances and distributed generation output fluctuations.

2.4 Bipolar / Three Level Converters

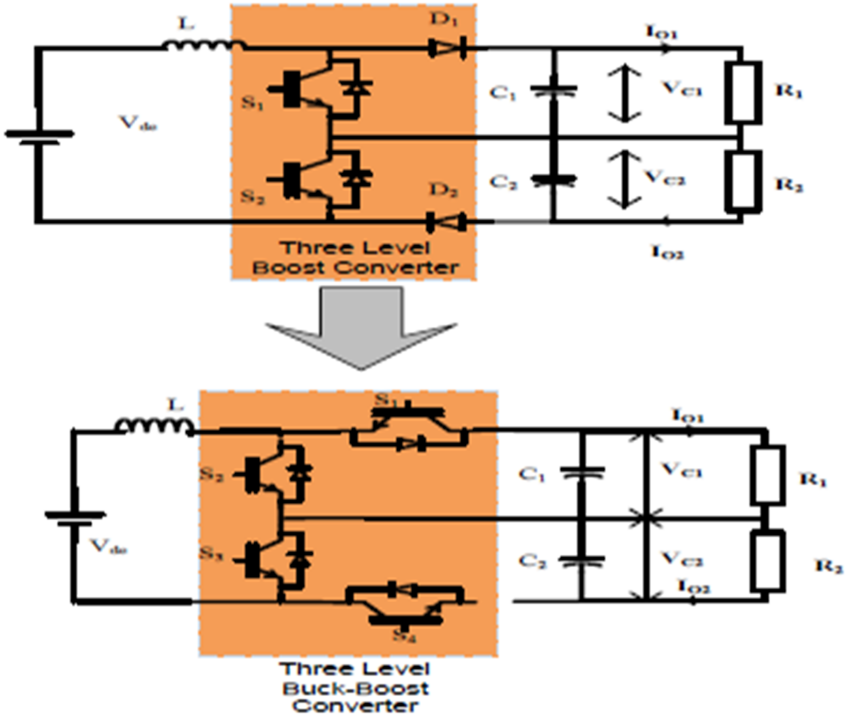

Figure 2.5: Schematics of TLC Derived Converters

Three level dc-dc converter (TLC), as in fig.2.5 is derived from neutral point clamped architecture of multi-level converters. This three-level configuration gives it a bipolar structure (+ve, -ve and neutral). This structure has numerous advantages ; two switches are connected in series in a single leg which reduce the voltage stress across the switch, inherent capacitance voltage balancing, different voltage levels at the output. Conventional Three level converter (TLC) have only 2 switches and two

diodes. Hence, bidirectional power flow is not possible. The circuit topology for three level bidirectional buck/boost dc-dc converter (TL-BDC) is derived from TLC by replacing diodes D1, D2 by IGBT switches S1, S2 respectively.

2.5 Three Level PV Converter

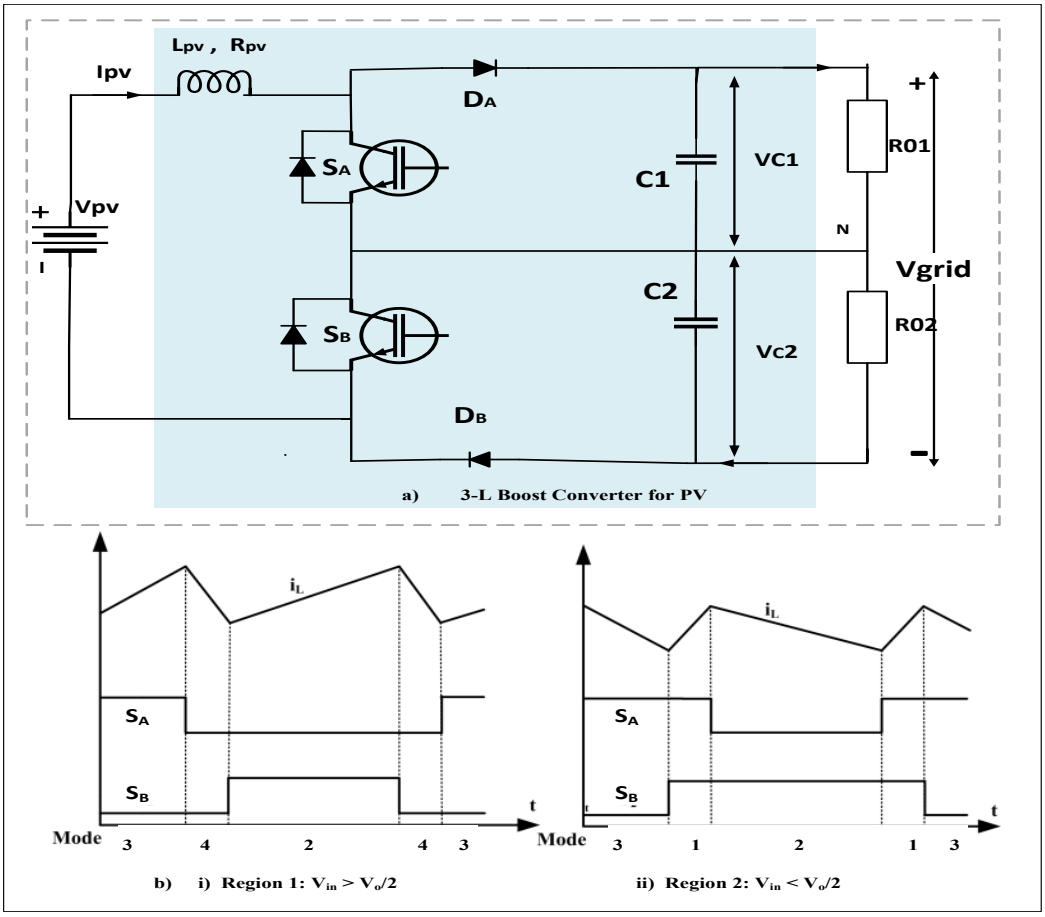

Figure 2.6: Three-level boost converter for PV.

PV converters are needed to extract the maximum power from the PV units. Instead of a normal boost converter, a three-level boost converter is used to connect it to the bipolar DC grid. This converter has two switches in series which reduce the voltage stress across the switch by half. Another advantage of using a three-level or bipolar converter is power sharing between two poles; i.e. power from each generation unit can be fed equally to both poles of the bipolar DC grid.

The circuit diagram of TL-Boost converter is given in fig. 2.6. The circuit consists of two IGBT switches S_A, S_B, diodes D_A, D_B, capacitors C_1, C_2, inductor L_{pv} and equivalent series resistance of inductor R_{pv}. TL boost can be operated in four modes corresponding to the states of switches S_A, and S_B and it is shown in Fig. 2.6.b. L_{pv} discharge and charge in 4 and 1 modes respectively. In mode 2 and 3, rising inductor current direction depend on voltages V_{C1} and V_{C2}. The modes of operation of TL boost converter is depicted in fig. 2.7, with red colour lines indicate the conduction path and switching states 1==ON and 0==OFF, for the switches S_A, and S_B.

Mode	S_A	S_B	Configuration
Mode 1	1	1	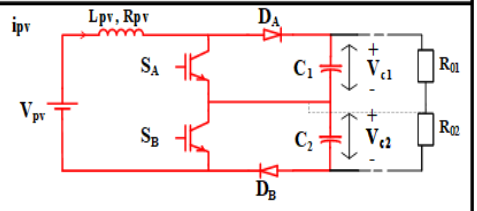
Mode 2	0	1	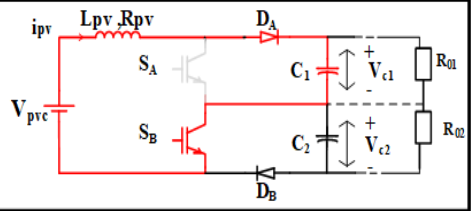
Mode 3	1	0	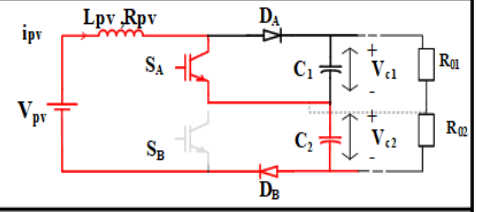
Mode 4	0	0	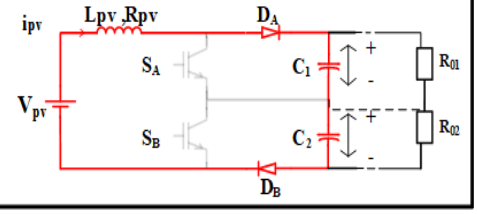

Figure 2.7: Modes of operation of three-level boost converter for PV.

2.5.1 Modelling of Three Level PV Converter

For obtaining the continuous time model of the TL boost converter, the different modes of operation are analyzed. Kirchoff's Current and Voltage laws are applied for

four modes of operation to get the following Eqns. 2.1- 2.14.

Mode I: During mode 1 operation, switches S_A, S_B are ON. PV current i_{pv} flows through L_{pv} and R_{pv}. Applying Kirchoff's voltage law (KVL) to the circuit in mode 1 in the figure **??**, we get Eqns. 2.1.

$$V_{pv} - R_{pv}.i_{pv} - L_{pv}.\frac{di_{pv}}{dt} = 0; \tag{2.1}$$

Current flow during boost operation is such that $i_c = i_{pv} - i_0$, where i_c is the pole capacitance current, i_0 is the load current, and i_{pv} is the pv source current. In mode 1, i_{pv} is flowing entirely through S_A and S_B. Capacitors C_1, and C_2 is discharging to loads R_{01} and R_{02} respectively. Hence applying Kirchoff's Current law (KCL), we get Eqns. 2.2-2.3;

$$i_{c1} = i_{pv} - i_{01} = 0 - i_{01} \tag{2.2}$$

$$i_{c2} = i_{pv} - i_{02} = 0 - i_{02} \tag{2.3}$$

Rewriting i_{c1} and i_{01} in terms of V_{C1} and rewriting i_{c2} and i_{02} in terms of V_{C2}, we get the following Eqns. 2.4- 2.5.;

$$C_1.\frac{dV_{C1}}{dt} = 0 - \frac{-V_{C1}}{R_{01}}; \tag{2.4}$$

$$C_2.\frac{dV_{C2}}{dt} = 0 - \frac{V_{C2}}{R_{02}}; \tag{2.5}$$

Mode II : During mode II operation switches S_B and D_A are conducting. Capacitor C_1 is charged through S_B and D_A by i_{pv} and C_2 is discharged to load R_{02}. Applying KVL and KCL in a similar way as in mode I operation, we get Eqns. 2.6, 2.7, and 2.8.

$$V_{pv} - V_{C1} - R_{pv}.i_{pv} - L_{pv}.\frac{di_{pv}}{dt} = 0; \tag{2.6}$$

$$i_{c1} = i_{pv} - i_{01}; i.e, C_1.\frac{dV_{C1}}{dt} = i_{pv} - \frac{V_{C1}}{R_{01}}; \tag{2.7}$$

$$i_{c2} = 0 - i_{02}; i.e, C_2.\frac{dV_{C2}}{dt} = 0 - \frac{V_{C2}}{R_{02}}; \tag{2.8}$$

Mode III : During mode III operation, switches S_A and D_B is conducting. Capacitor C_2 is charged by i_{pv} and C_1 is discharged to load R_{01}. Applying KVL and KCL,

we get Eqns. 2.9,2.10, 2.11.

$$V_{pv} - V_{C2} - R_{pv}.i_{pv} - L_{pv}.\frac{di_{pv}}{dt} = 0 \tag{2.9}$$

$$i_{c1} = 0 - i_{01}; i.e, C_1.\frac{dV_{C1}}{dt} = -\frac{V_{C1}}{R_{01}}; \tag{2.10}$$

$$i_{c2} = i_{pv} - i_{02}; i.e, C_2.\frac{dV_{C2}}{dt} = i_{pv} - \frac{V_{C2}}{R_{02}}; \tag{2.11}$$

Mode IV :During mode IV operation, switches S_A, S_B are in turned off condition and diodes D_A, D_B conducting. Capacitors C_1, and C_2 is getting charged by i_{pv}. Applying KVL and KCL, we get Eqns. 2.12,2.13 and 2.14.

$$V_{pv} - V_{C1} - V_{C2} - R_{pv}.i_{pv} - L_{pv}.\frac{di_{pv}}{dt} = 0; \tag{2.12}$$

$$i_{c1} = i_{pv} - i_{01}; i.e, C_1.\frac{dV_{C1}}{dt} = i_{pv} - \frac{V_{C1}}{R_{01}}; \tag{2.13}$$

$$i_{c2} = i_{pv} - i_{02}; i.e, C_2.\frac{dV_{C2}}{dt} = i_{pv} - \frac{V_{C2}}{R_{02}}; \tag{2.14}$$

where V_{C1}, V_{C2} are the voltage across pole capacitance C_1, C_2 ; i_{pv} is the inductor current, i_{01}, i_{02} are pole currents flowing through +ve and -ve poles of the DC grid ; R_{01}, R_{02} are loads connected to bipolar grid, R_{pv}, L_{pv} are the equivalent series resistance and inductance of the bipolar/three level PV converter. Taking i_{01}, i_{02} as pole currents of the grid, current flow during boost operation is such that $i_{pv} = i_0 + i_c$. From above equations, state space model of the presented converter can be written in matrix form as shown in Eqn 2.15;

$$\begin{bmatrix} \frac{di_{pv}}{dt} \\ \\ \frac{dV_{c1}}{dt} \\ \\ \frac{dV_{c2}}{dt} \end{bmatrix} = \begin{bmatrix} \frac{-R_{pv}}{L_{pv}} & \frac{-\bar{S_A}}{L_{pv}} & \frac{-\bar{S_B}}{L_{pv}} \\ \\ \frac{\bar{S_A}}{C_1} & \frac{-1}{R_{01}.C_1} & 0 \\ \\ \frac{\bar{S_B}}{C_2} & 0 & \frac{-1}{R_{02}.C_2} \end{bmatrix} \begin{bmatrix} i_{pv} \\ V_{C1} \\ V_{C2} \end{bmatrix} + \begin{bmatrix} \frac{1}{L_{pv}} & 0 & 0 \end{bmatrix} \begin{bmatrix} V_{pv} \\ 0 \\ 0 \end{bmatrix} \tag{2.15}$$

where $\bar{S_A} = 1 - S_A$ and $\bar{S_B} = 1 - S_B$.

2.6 Three Level Bidirectional Buck/Boost Converter

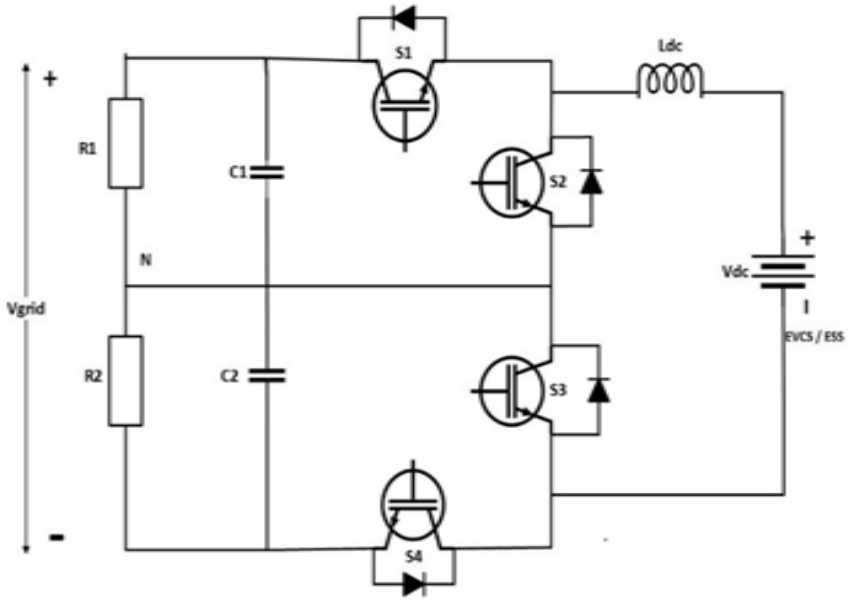

Figure 2.8: Three Level Bidirectional Buck/Boost Converter

Three level bidirectional buck/boost converter, (fig.2.8) is composed of four switches S1-S4, their respective anti-parallel diodes D1-D4, the main inductor Ldc, the capacitors C1-C2, dc voltage Vdc and the output loads. R1,R2 connected to bipolar dc grid. The capacitance of C1 and C2 have the same value. Operation of switches S1, S2 and S3, S4 are complimentary. High voltage is at the grid side, V_{grid} and low voltage is the battery /EVCS side, V_{dc}. The converter is made to operate in four distinctive modes each in buck operation and boost operation. Distinctive switching states of S_1, S_4 controls buck mode and S_2, S_3 controls boost mode operation respectively. The converter operation is confined to eight modes of operation, four modes defined for boost operation and four modes defined for buck operation.

2.6.1 Modes of Boost Operation:

- ON-state: both S_3 and S_2 are ON and the shoot-through current passes through the inductor L_{dc}. During this state, load currents are supplied by C_1 and C_2 .

- Balancing-state: balancing function of the converter is activated in this state. If $R_1 \leq R_2$, (R_1 absorbs more current), S_2 is OFF and S_3 is kept ON.

- Balancing state: if $R_1 \geq R_2$, S2 is ON and S_3 is OFF.
- OFF-state: both S_2 and S_3 are OFF

2.6.2 Modes of Buck Operation:

- ON-state: both S1 and S4 are ON and current passes through the inductor L to the capacitor C1, C2 and load R1 and R2.
- Balancing-state: balancing function of the converter is activated in this state. If $R_1 \leq R_2$ (R1 absorbs more current),S_1 is OFF and S_4 is kept ON.
- Balancing state: Alternatively, if $R_1 \geq R_2$, S_1 is kept ON and S_4 is OFF.
- OFF-state: both S_1 and S_4 are OFF

2.6.3 Switching Equation

Analyzing the four modes of boost and buck operation, the switching equations are derived. In boost mode, power flows from battery (lv side) to dc microgrid (hv side). Grid capacitor C_1 is charged by D_1-D_4 conducting or S_3-D_1 conducting. Hence necessary condition for charging of V_{C1} is conduction of antiparallel diode, D_1. i.e. nonconducting state of S_2. Similarly charging paths of V_{C2} are through S_1-D_4 or D_1-D_4. Hence, a necessary condition for charging V_{C2} is that S_3 is in a nonconducting state. Switching of S3 controls the voltage across V_{C2}. Switching of S_2 control charging of V_{C1}. Hence, switching equation is eqn.2.16 :

$$Vdc = V_{C1} * (1 - S_2) + V_{C2} * (1 - S_3) \tag{2.16}$$

In buck operation (power flow from grid to battery), V_{C1} gets discharged to battery when S_1-S_4 is conducting or S_1-D_3 conducting. Necessary condition for discharging of V_{C1} is the conducting state of S_1. Similarly, V_{C2} gets discharged to battery when S_1-S_4 is conducting or D_2-S_4 is conducting. Necessary condition for discharging of V_{C2} is S_4 conducting. Hence switching equation is 2.17:

$$V_{dc} = V_{C1} * S_1 + V_{C2} * S_4 \tag{2.17}$$

2.6.4 Design of the Circuit Elements

The design equations for the three level bidirectional converter is given 2.18 - 2.27.

$$\Delta I_{dc} = \frac{V_o * d_{eff} * (1 - d_{eff})}{L * fs} \tag{2.18}$$

where for boost,

$$d_{\text{eff}} = d_{\text{S2}} - 0.5 + d_{\text{S3}} - 0.5 = 2d - 1 \tag{2.19}$$

for buck

$$d_{\text{eff}} = d_{\text{S2}} + d_{\text{S3}} = 2d \tag{2.20}$$

$$\Delta V_C = \frac{i_{dc} * d_{eff} * (1 - d_{eff})}{C * fs} \tag{2.21}$$

Applying d_{eff} in (3), we get for d $\leq$ 0.5,

$$\Delta I_{bat}(d) = \frac{Vo * 2 * 1 - 2d}{L * fs} \tag{2.22}$$

For d $\geq$ 0.5 ,

$$\Delta I_{bat}(d) = \frac{Vo * (1 - d) * (2d - 1)}{L * fs} \tag{2.23}$$

Voltage gain ratio,

$$\frac{V_o}{V_{bat}} = \frac{2}{1 - d_{eff}}, \tag{2.24}$$

where for d $\geq$ 0.5

$$d_{eff=}d_{S2} - 0.5 + d_{S3} - 0.5 = 2d - 1 \tag{2.25}$$

Voltage gain ratio,

$$\frac{Vo}{V_{bat}} = \frac{2}{2 - d_{eff}} \tag{2.26}$$

where d $\leq$ 0.5

$$d_{eff=}d_{S2} + d_{S3} = 2d \tag{2.27}$$

2.7 Modelling of Three Level Bidirectional Converter

Applying KCL and KVL for analysing modes of operation in fig.2.9, by considering V_{C1}, V_{C2}, I_{dc} as the state variables and V_{dc} as the input, state space model of the converter in continuous time can be found.

Mode	S2	S3	Configuration
Mode 1	1	1	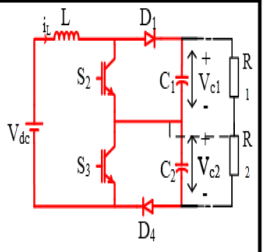
Mode 2	0	1	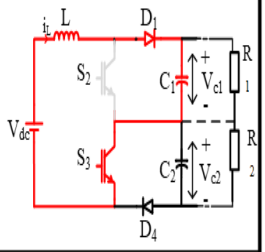
Mode 3	1	0	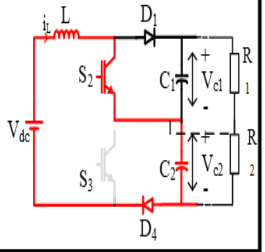
Mode 4	0	0	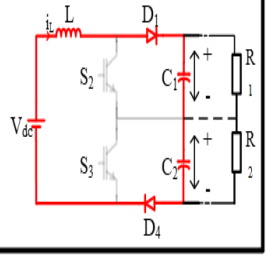

Mode	S1	S4	Configuration
Mode 1	1	1	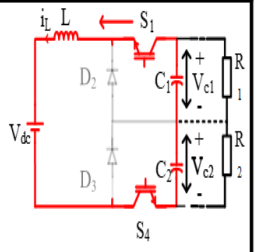
Mode 2	0	1	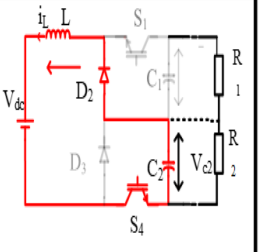
Mode 3	1	0	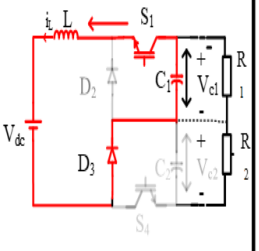
Mode 4	0	0	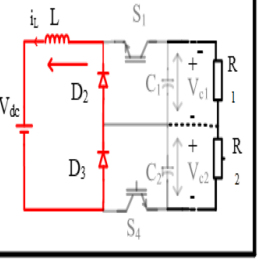

Figure 2.9: Modes of operation of TL Bidirectional Converter

2.7.1 State Space Analysis of Boost Operation

For obtaining the continuous time model of TL Bidirectional converter for boost operation, the different modes of operation are analyzed. Kirchoff's Current and Voltage laws are applied for four modes of operation to get the following Eqns. 2.28-2.42.

Mode I: During mode 1 operation, switches S_2, S_3 are ON. Inductor current i_{dc} flows through L_{dc} and R_{dc}. Applying Kirchoff's voltage law (KVL) to the circuit in mode 1 in the figure 2.9, we get Eqns. 2.28.

$$V_{dc} - R_{dc}.i_{dc} - L_{dc}.\frac{di_{dc}}{dt} = 0; \tag{2.28}$$

Current flow during boost operation is such that $i_c = i_{dc} - i_0$, where i_c is the pole capacitance current, i_0 is the load current, and i_{dc} is the inductor current. In mode 1, i_{dc} is flowing entirely through S_2 and S_3. Capacitors C_1, and C_2 is discharging to loads R_{01} and R_{02} respectively. Hence applying Kirchoff's Current law (KCL), we get Eqns. 2.29-2.30;

$$i_{c1} = i_{dc} - i_{01} = 0 - i_{01} \tag{2.29}$$

$$i_{c2} = i_{dc} - i_{02} = 0 - i_{02} \tag{2.30}$$

Rewriting i_{c1} and i_{01} in terms of V_{C1} and rewriting i_{c2} and i_{02} in terms of V_{C2}, we get the following Eqns. 2.31- 2.32.;

$$C_1.\frac{dV_{C1}}{dt} = 0 - \frac{-V_{C1}}{R_{01}}; \tag{2.31}$$

$$C_2.\frac{dV_{C2}}{dt} = 0 - \frac{V_{C2}}{R_{02}}; \tag{2.32}$$

Mode II : During mode II operation switches S_3 and D_1 are conducting. Capacitor C_1 is charged through S_3 and D_1 by i_{dc} and C_2 is discharged to load R_{02}. Applying KVL and KCL in a similar way as in mode I operation, we get Eqns. 2.33, 2.34, and 2.35.

$$V_{dc} - V_{C1} - R_{dc}.i_{dc} - L_{dc}.\frac{di_{dc}}{dt} = 0; \tag{2.33}$$

$$i_{c1} = i_{dc} - i_{01}; i.e, C_1.\frac{dV_{C1}}{dt} = i_{dc} - \frac{V_{C1}}{R_{01}}; \tag{2.34}$$

$$i_{c2} = 0 - i_{02}; i.e, C_2.\frac{dV_{C2}}{dt} = 0 - \frac{V_{C2}}{R_{02}}; \tag{2.35}$$

Mode III : During mode III operation, switches S_2 and D_4 is conducting. Capacitor C_2 is charged by i_{dc} and C_1 is discharged to load R_{01}. Applying KVL and KCL, we get Eqns. 2.36,2.37, 2.38.

$$V_{dc} - V_{C2} - R_{dc}.i_{dc} - L_{dc}.\frac{di_{dc}}{dt} = 0 \tag{2.36}$$

$$i_{c1} = 0 - i_{01}; i.e, C_1.\frac{dV_{C1}}{dt} = -\frac{V_{C1}}{R_{01}}; \tag{2.37}$$

$$i_{c2} = i_{dc} - i_{02}; i.e, C_2.\frac{dV_{C2}}{dt} = i_{dc} - \frac{V_{C2}}{R_{02}}; \tag{2.38}$$

Mode IV :During mode IV operation, switches S_2, S_3 are in turned off condition and diodes D_1, D_4 conducting. Capacitors C_1, and C_2 is getting charged by i_{dc}. Applying KVL and KCL, we get Eqns. 2.39,2.40 and 2.41.

$$V_{dc} - V_{C1} - V_{C2} - R_{dc}.i_{dc} - L_{dc}.\frac{di_{dc}}{dt} = 0; \tag{2.39}$$

$$i_{c1} = i_{dc} - i_{01}; i.e, C_1.\frac{dV_{C1}}{dt} = i_{dc} - \frac{V_{C1}}{R_{01}}; \tag{2.40}$$

$$i_{c2} = i_{dc} - i_{02}; i.e, C_2.\frac{dV_{C2}}{dt} = i_{dc} - \frac{V_{C2}}{R_{02}}; \tag{2.41}$$

where V_{C1}, V_{C2} are the voltage across pole capacitance C_1, C_2 ; i_{dc} is the inductor current, i_{01}, i_{02} are pole currents flowing through +ve and -ve poles of the bipolar DC grid ; R_{01}, R_{02} are loads connected to bipolar grid, R_{dc}, L_{dc} are the equivalent series resistance and inductance of the battery side of three level buck/boost converter. Taking i_{01}, i_{02} as pole currents of the grid, current flow during boost operation is such that $i_{dc} = i_0 + i_c$. From above equations, state space model of the presented converter can be written in matrix form as shown in Eqn 2.42;

$$\begin{bmatrix} \frac{di_{dc}}{dt} \\ \\ \frac{dV_{c1}}{dt} \\ \\ \frac{dV_{c2}}{dt} \end{bmatrix} = \begin{bmatrix} \frac{-R_{dc}}{L_{dc}} & \frac{-\bar{S_2}}{L_{dc}} & \frac{-\bar{S_3}}{L_{dc}} \\ \\ \frac{\bar{S_2}}{C_1} & \frac{-1}{R_{01}.C_1} & 0 \\ \\ \frac{\bar{S_3}}{C_2} & 0 & \frac{-1}{R_{02}.C_2} \end{bmatrix} \begin{bmatrix} i_{dc} \\ V_{C1} \\ V_{C2} \end{bmatrix} + \begin{bmatrix} \frac{1}{L_{dc}} & 0 & 0 \end{bmatrix} \begin{bmatrix} V_{dc} \\ 0 \\ 0 \end{bmatrix} \tag{2.42}$$

where $\bar{S_2} = 1 - S_2$ and $\bar{S_3} = 1 - S_3$.

2.7.2 State Space Analysis of Buck Operation

For obtaining the continuous time model of the TL bidirectional converter for the buck operation, the different modes of operation are analyzed. Kirchoff's Current and Voltage laws are applied for four modes of operation to get the following Eqns. 2.43- 2.56.

Mode I: During mode 1 operation, switches S_4 and S_1 are conducting. Capacitor C_1, C_2 charging the battery through S_1, and S_4 (refer 2.9), we get eqns. 2.43.

$$V_{C1} + V_{C2} - V_{dc} - R_{dc}.i_{dc} - L_{dc}.\frac{di_{dc}}{dt} = 0; \tag{2.43}$$

$$i_{c1} = i_{01} - i_{dc}; \quad i.e, \quad C_1.\frac{dV_{C1}}{dt} = \frac{V_{C1}}{R_{01}} - i_{dc}; \tag{2.44}$$

$$i_{c2} = i_{02} - i_{dc}; \ i.e, \quad C_2.\frac{dV_{C2}}{dt} = \frac{V_{C2}}{R_{02}} - i_{dc}; \tag{2.45}$$

Mode II : During mode II operation switches S_4 and D_2 are conducting. Capacitor C_2 is discharging to battery V_{dc} and R_{02}. C_1 is discharged to load R_{01}. Applying KVL and KCL in a similar way as in mode I operation, we get Eqns. 2.46, 2.47, and 2.48.

$$V_{C2} - R_{dc}.i_{dc} - L_{dc}.\frac{di_{dc}}{dt} - V_{dc} = 0; \tag{2.46}$$

$$i_{c1} = i_{01} - 0; i.e, \quad C_1.\frac{dV_{C1}}{dt} = \frac{V_{C1}}{R_{01}} - 0; \tag{2.47}$$

$$i_{c2} = i_{02} - i_{dc}; \quad i.e, \quad C_2.\frac{dV_{C2}}{dt} = \frac{V_{C2}}{R_{02}} - i_{dc}; \tag{2.48}$$

Mode III : During mode III operation, switches S_1 and D_3 is conducting. Capacitor C_1 is discharging to V_{dc} and load R_{01}. C_2 is discharged to load R_{02}. Applying KVL and KCL, we get Eqns. 2.49, 2.50, 2.51.

$$V_{C1} - R_{dc}.i_{dc} - L_{dc}.\frac{di_{dc}}{dt} - V_{dc} = 0; \tag{2.49}$$

$$i_{c1} = i_{01} - i_{dc}; i.e, C_1.\frac{dV_{C1}}{dt} = \frac{V_{C1}}{R_{01}} - i_{dc}; \tag{2.50}$$

$$i_{c2} = i_{02} - 0; i.e, \quad C_2.\frac{dV_{C2}}{dt} = \frac{V_{C2}}{R_{02}} - 0; \tag{2.51}$$

Mode IV :During mode IV operation, switches S_1, S_4 are in turned off condition and diodes D_2, D_3 conducting. Capacitors C_1, and C_2 is getting discharged to R_{01} and R_{02}. i_{dc} discharges to the battery V_{dc}. Applying KVL and KCL, we get Eqns. 2.52, 2.53 and 2.54.

$$0 - R_{dc}.i_{dc} - L_{dc}.\frac{di_{dc}}{dt} - V_{dc}; \tag{2.52}$$

$$i_{c1} = i_{01} - i_{dc} = i_{01} - 0 \tag{2.53}$$

$$i_{c2} = i_{02} - i_{dc} = i_{02} - 0 \tag{2.54}$$

Rewriting i_{c1} and i_{01} in terms of V_{C1} and rewriting i_{c2} and i_{02} in terms of V_{C2}, we get the following Eqns. 2.55- 2.56.;

$$C_1.\frac{dV_{C1}}{dt} = \frac{-V_{C1}}{R_{01}} - 0; \tag{2.55}$$

$$C_2.\frac{dV_{C2}}{dt} = \frac{V_{C2}}{R_{02}} - 0; \tag{2.56}$$

where V_{C1}, V_{C2} are the voltage across pole capacitance C_1, C_2 ; i_{dc} is the inductor current, i_{01}, i_{02} are pole currents flowing through +ve and -ve poles of the DC grid ; R_{01}, R_{02} are loads connected to bipolar grid, R_{dc}, L_{dc} are the equivalent series resistance and inductance of the three level bidirectional converter. Taking i_{01}, i_{02} as pole currents of the grid, current flow during buck operation is such that $i_o = i_c + i_{dc}$. From above equations, state space model of the presented converter can be written in matrix form as shown in Eqn 2.57;

$$\begin{bmatrix} \frac{di_{dc}}{dt} \\ \\ \frac{dV_{c1}}{dt} \\ \\ \frac{dV_{c2}}{dt} \end{bmatrix} = \begin{bmatrix} \frac{-R_{dc}}{L_{dc}} & \frac{S_1}{L_{dc}} & \frac{S_4}{L_{dc}} \\ \\ \frac{-S_1}{C_1} & \frac{1}{R_{01}.C_1} & 0 \\ \\ \frac{-S_4}{C_2} & 0 & \frac{1}{R_{02}.C_2} \end{bmatrix} \begin{bmatrix} i_{dc} \\ V_{C1} \\ V_{C2} \end{bmatrix} + \begin{bmatrix} \frac{1}{L_{dc}} & 0 & 0 \end{bmatrix} \begin{bmatrix} V_{dc} \\ 0 \\ 0 \end{bmatrix} \tag{2.57}$$

2.8 Control of Interfacing Converters

The modelling and design of three level bidirectional converter was dealt in previous section. Modes of operation were defined and switching equations discussed too.This section details the closed loop PI control developed and MPPT control applied for three level bidirectional converter and PV boost converter respectively for effective operation of bipolar dc grid during dynamic conditions.

2.8.1 MPPT for Two Level PV Boost Converter

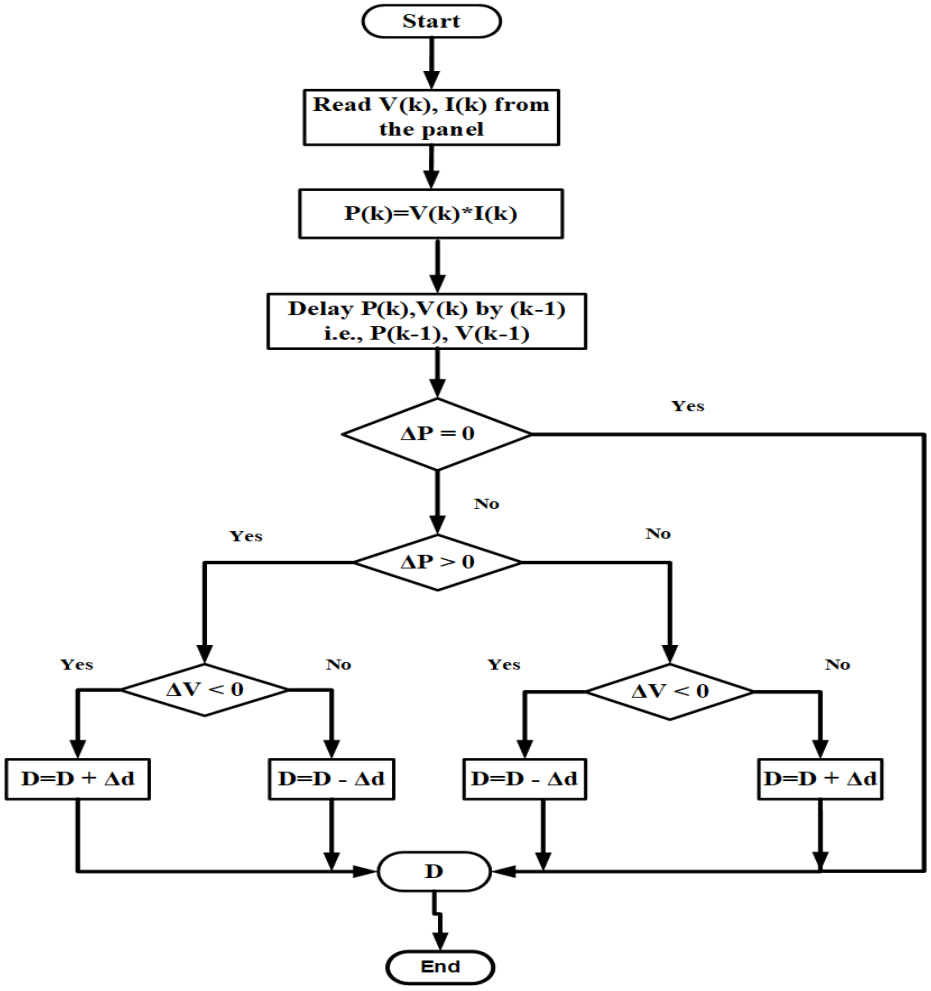

Figure 2.10: Perturb and Observe MPPT Algorithm

MPPT control technique (Perturb & Observe) can be used for switching of Solar PV boost converter. Either simple two level boost or three level boost converter can be

used for interlinking PV panels to grid. Here, two-level boost converters are operated to extract maximum power corresponding to each irradiation level with conventional perturb and observe MPPT technique, of which control algorithm flow is given in fig.2.10. MPPT method gives tracks the point of maximum power by adjusting the duty cycles of the boost converter,such that maximum power is generated from PV panel for respective irradiation.

2.8.2 PI Control of Three Level Buck-Boost Converter

Conventional PI controllers is implemented for controlling TLC converter interlinking BESS and bipolar dc grid. Double loop with inner current control loop and outer voltage loop with PI controllers is developed for the bidirectional operation of three level buck -boost converter. Block diagram of the PI controller for voltage balancing and regulation is shown in 2.11. Buck/boost modes of operation is initiated by monitoring the following conditions;

Buck Mode: $SOC_{max} \geq SOC$ & $P_G \geq P_L$
Boost Mode: $SOC \geq SOC_{min}$ & $P_G < P_L$
Float Mode: $SOC > SOC_{max}$ or $SOC < SOC_{min}$.

Main control objective are grid voltage restoration and balancing of the two capacitive voltages V_{C1}, V_{C2} of the bipolar buses for dynamic conditions of load and power generations. Grid voltage regulation controller compares the grid voltage V_{grid}, with reference voltage 300V and the error is given to the inner current controller loop which compares it with neutral point current, I_n. Gate signal thus obtained is given to S_2 and S_4 , to attain voltage regulation. Likewise, capacitance voltage balancing controller compares the voltages V_{C1} and V_{C2} and the error is given to the inner current controller loop which compares it with inductor current, I_l. Switching pulses obtained are given to S_3 and S_1, to eliminate capacitive voltage unbalance issues. These PI controllers, depending upon the power gap , $\Delta P = P_G - P_L$, operates the converter in buck or boost such that grid voltage is regulated at 300V and V_{C1}, V_{C2} balanced at 150V under dynamic conditions. Gating signals to S_1, S_2, S_3, S_4 is initiated, only if the SOC condition of the battery is within the safe limits $SOC_{max} \geq SOC \geq SOC_{min}$. SOC_{max} is taken as 0.9 and SOC_{min} is taken as 0.35. If SOC conditions not satisfied, converter goes to floating mode. Logic gate AND is used to check these battery conditions. PI controller is designed and control parameters obtained by frequency

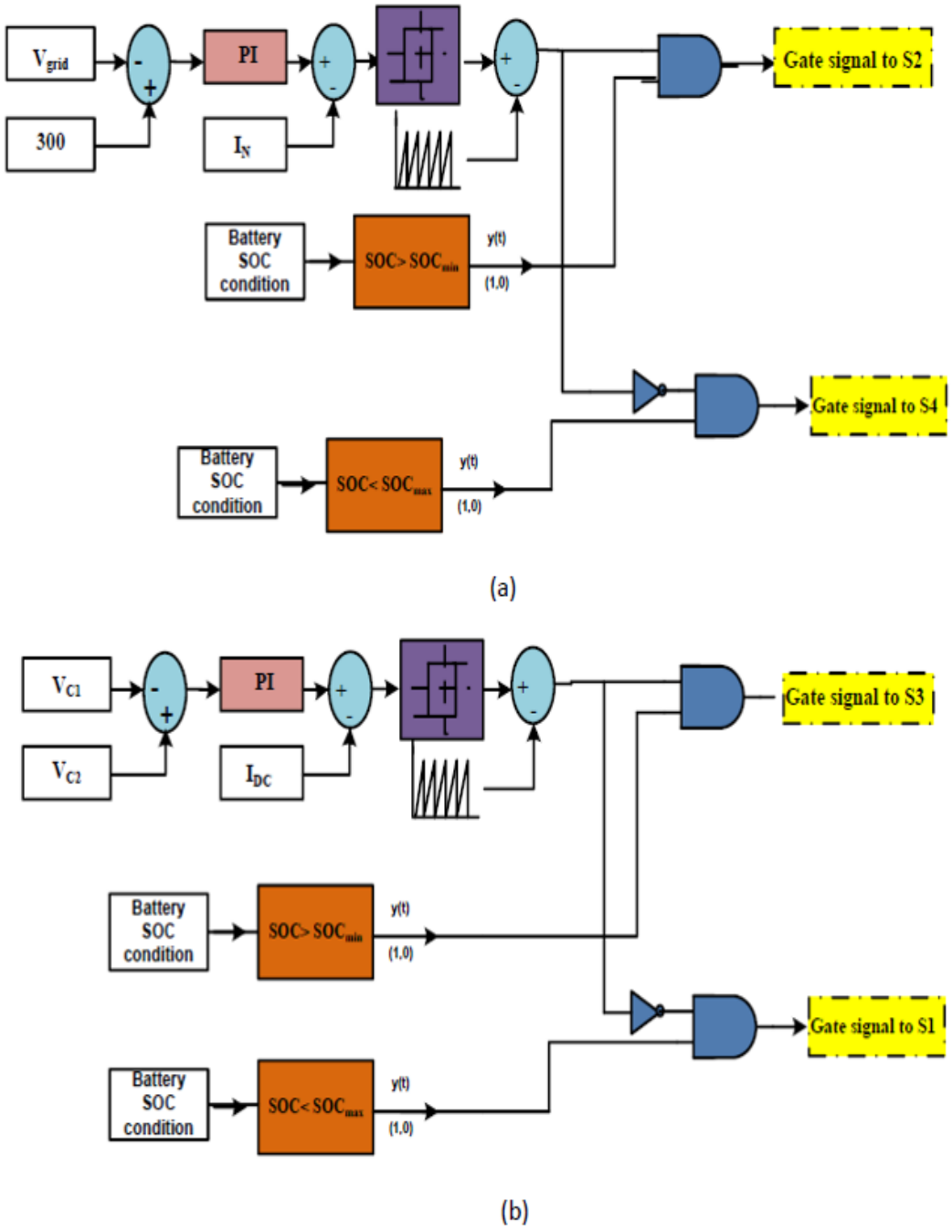

Figure 2.11: PI Control. a) Voltage regulation b) Capacitance voltage balancing

domain plots for desired phase margin and bandwidth using MATLAB/PID tuning tool for stability. Parameters of PI controller loops is given in Tbl.2.1.

Table 2.1: Controller loops parameters

Sl no.	Parameters	Values
1	Bandwidth of inner current battery loop	rad/sec
2	Phase margin of inner current battery loop	60 °
3	Control parameters current loop	Kp = 0.045 ,Ki = 5
4	Bandwidth of outer voltage loop	rad/sec
5	Phase margin of outer voltage loop	55 °
6	Control parameters outer voltage loop	Kp = 0.4 ,Ki =10

2.9 Battery Modelling

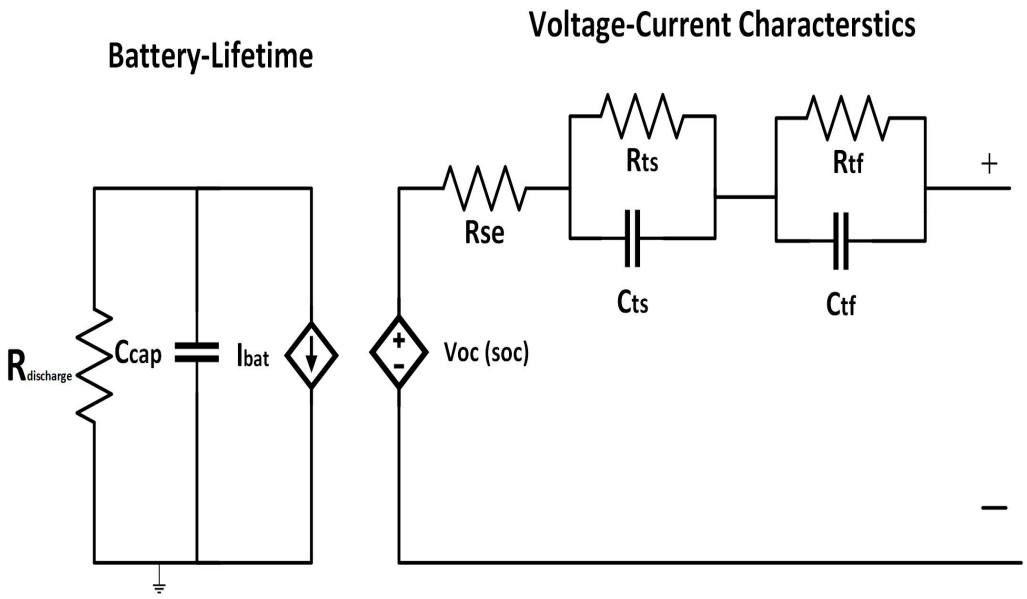

Figure 2.12: Accurate battery equivalent circuit

Li-ion battery is mathematically modelled based on accurate electrical battery model (Chen and Rincon-Mora, 2006). This model takes into consideration the effects of operating temperature and battery life. It also represents slow and fast transient response in the equivalent electrical circuit. Equations depicting the battery equivalent model for Li-ion battery and its extracted parameters for various SOC

conditions and room temperature is taken from (Tremblay et al., 2007). Parameter used for modelling a Li-ion battery pack (100V, 15Ahr) is given in Table. 2.2. Simulation diagram of Li-ion battery done in MATLAB Simulink is given in fig 2.13. Battery capacity is at least half of that of the power fed to the dc grid.

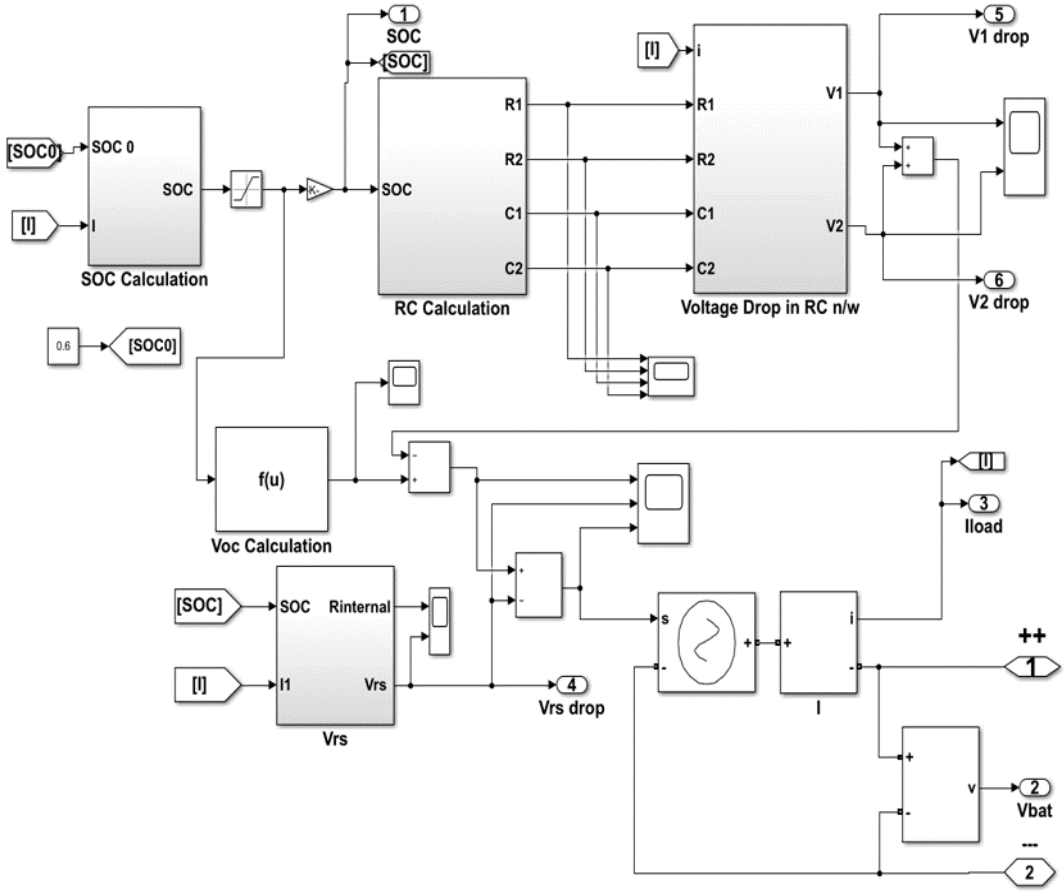

Figure 2.13: Mathematical modelling of Li-ion Battery

$$SOC = SOC_0 - \int \frac{I_{bat}.dt}{Q} * 3600 \tag{2.58}$$

$$V_{BAT} = V_{OC} - V_1 - V_2 - V_{rs} \tag{2.59}$$

$$V_1 = \frac{1}{s} * [\frac{I}{C} - \frac{V_1}{R.C}] = V_2 \tag{2.60}$$

Equations depicting the battery accurate equivalent model is given as above from 2.58 -2.60, where V_{BAT} is the terminal battery voltage , V_1 ,V_2 are voltage drop due to RC parallel components(transient response) and Vrs is the ohmic voltage drop due to

series resistance. Extracted parameters for Li-ion battery for various SOC conditions and room temperature is given by equations 2.61-2.66 , where V_{OC} is the open circuit voltage, SOC is the state of charge , R_{se} is the equivalent series resistance, $R_{(ts)}$ is the slow transient resistance, R_{tf}, is the fast transient resistance C_{ts} is the slow transient capacitance, C_{tf} is the fast transient capacitance.

$$V_{oc}(soc) = 1.031.e^{-35.SOC} + 0.2156.SOC - 0.1178.SOC^2 + 0.3201.SOC^3 \quad (2.61)$$

$$R_{se}(soc) = 0.1562.e^{(-24.37.SOC)} + 0.07446 \quad (2.62)$$

$$R_{(ts)}(soc) = 0.3208.e^{(-29.14.SOC)} + 0.04669 \quad (2.63)$$

$$R_{tf} = 6.603.e^{(-15.52.SOC)} + 0.04984 \quad (2.64)$$

$$C_{ts} = -752.9.e^{(-13.57.SOC)} + 703.6 \quad (2.65)$$

$$C_{tf} = 6006.e^{(-15.52.SOC)} + 4475 \quad (2.66)$$

Table 2.2: Li-ion Battery Parameters

Symbol	Parameter	Value
Ah	Rated Capacity	15Ahr
Vbat	Terminal Voltage	100V
Nsb	No of cells in series	28
Nsp	No of cells in parallel	15
SOC_0	Initial SOC	60%

2.10 Result Analysis using PI controller

Case I: Changes in irradiation level

Simulated waveforms for fluctuation in irradiation level in buck and boost operation are evaluated in fig 2.14. DC load of 900W each is connected to bipolar grid. Irradiation level is kept at $400W/m^2$ each initially for the PV system. Here PG $\leq$

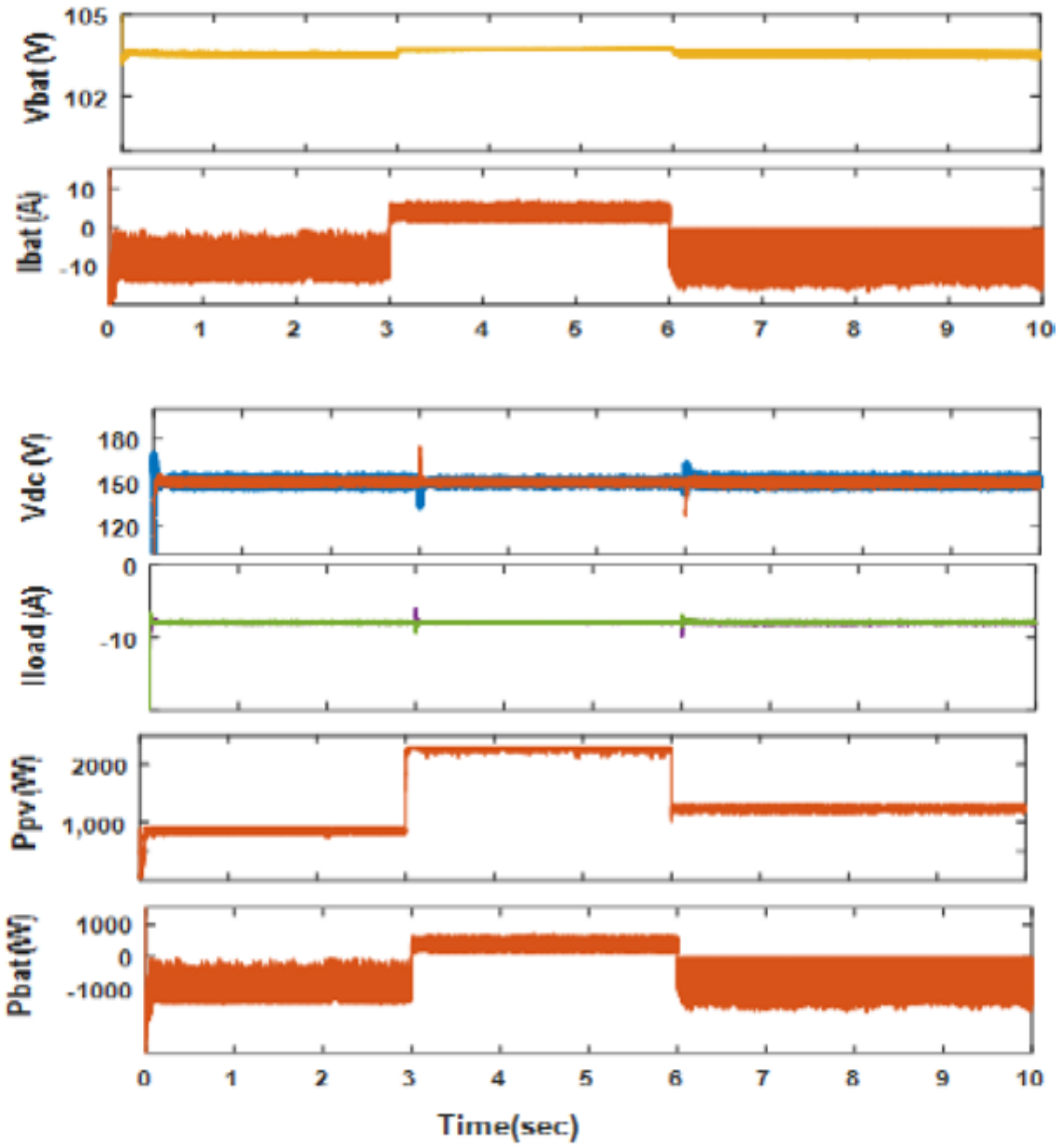

Figure 2.14: Simulation results for irradiation change with PI

PL (960 $\leq$ 1800W). Deficient power is provided by battery. At t=3sec,irradiation is increased to 1000 W/m^2 and 900W/m^2 respectively for PV1 and PV2. Here PG $\geq$PL (2280W $\geq$ 1800W). Hence the converter goes from boost to buck operation and the excess power is taken by the battery. Battery gets charged with I_{bat} = 4.8A. At t= 6s, irradiation is changed to 500W/m^2 and 600W/m^2. Converter goes from buck

stage to boost operation and battery is discharges, delivering the deficient power.

Case II: .Changes in DC load connected

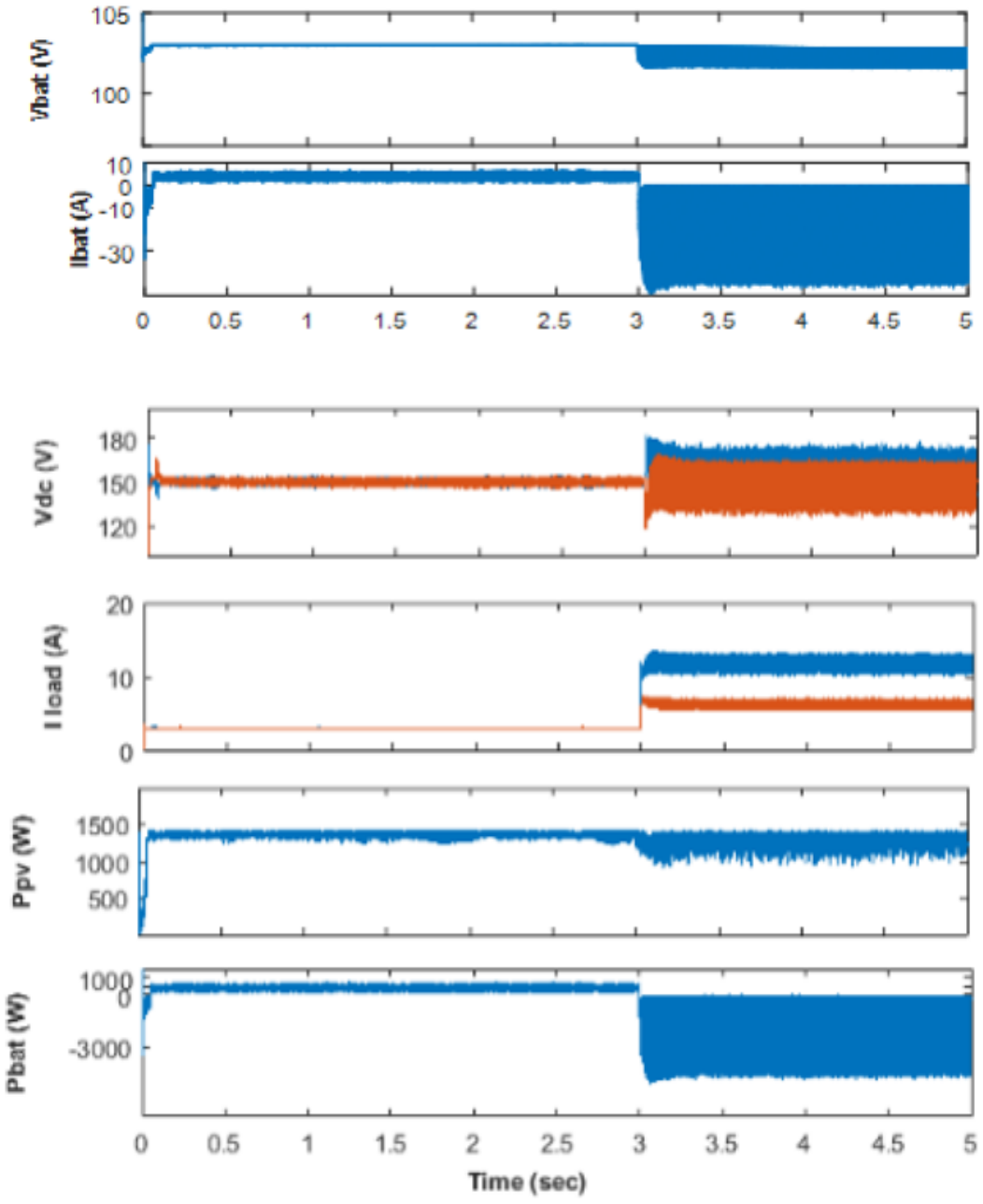

Figure 2.15: Simulation results for dc load change with PI

Simulated waveforms for changes in dc load connected. in buck and boost oper-

ation is evaluated in fig 2.15. DC load of 450W each connected to bipolar grid. For PV system, irradiation level kept at $600W/m^2$ each. Initially, battery is charging. At t= 3sec, dc loads connected is changed to 900W and 1800W respectively. Converter goes from buck to boost operation and battery discharge. From the simulation result waveforms, it is clear that although bipolar dc grid voltage is regulated and capacitor voltages V_{C1}, V_{C2} are balanced using PI controller, but with higher ripple/oscillations in the resultant waveforms under dynamic conditions.

2.11 Summary

In this chapter, operational modes, design and and state space modelling of three level bidirectional is put forward. Regulation of grid voltage, pole voltage unbalance mitigation and minimization of fluctuations during varying load and PV generation conditions are the main control objectives here. Investigation of operation with PI controller under during varying PV irradiation, sudden drop and rise of loads is also done. Power sharing between poles of grid is made feasible through BESS with bidirectional power flow capability.

Chapter 3

Model Predictive Control and Hardware in Loop Implementation

3.1 Introduction

This chapter, guides to the formulation of discrete model and predictive control of converters. Implementation of hardware in loop testing and validation in typhoon control center is discussed in this chapter. Comparative result analysis of MATLAB simulation and HIL validation is also done.

3.2 Control Methods in Power Electronics

The first control systems for power converters were based on linear cascaded control loops, assisted by coordinate transformations and modulation stages to linearize the power converter as much as possible. This enabled the use of the well-known proportional-integral (PI) controllers for almost every converter and application . The modulation stage generates the commutation signals for the converter based on a time-average operating principle to achieve the desired output. These are commonly based on a firing angle delay control for thyristor-based topologies working at fundamental switching frequency, and on pulsewidth modulation (PWM) for transistor-based topologies operating at higher switching frequencies. The practical implementation for both the control and modulation method was performed using analog circuitry, which became the early standard control platform for power electronics. Microproces-

sors were introduced in the early 1970s; nevertheless, they experienced an explosive development in computational power during the 1990s. During this decade, digital microprocessors. were introduced to control power electronics, which has continued since then. Currently, DSP and field-programmable gate array (FPGA) platforms are the dominant technology in power electronics applications.

The revolutionary development of microprocessing technology and the ever-increasing computational power has triggered the exploration of new and more sophisticated approaches to the control of power electronics, particularly in the last decade. Among them, fuzzy logic control, sliding mode control, and model predictive control (MPC) have attracted increasing attention for power electronics because of the nonlinear nature of the converters and motor drivess. All these control methods have unique advantages and disadvantages. Hence, it is fair to say that there is no control technology that outperforms all others in every aspect. Comparison of these most commonly used control techniques in power electronics is given in below figure 3.1 and table 3.1.

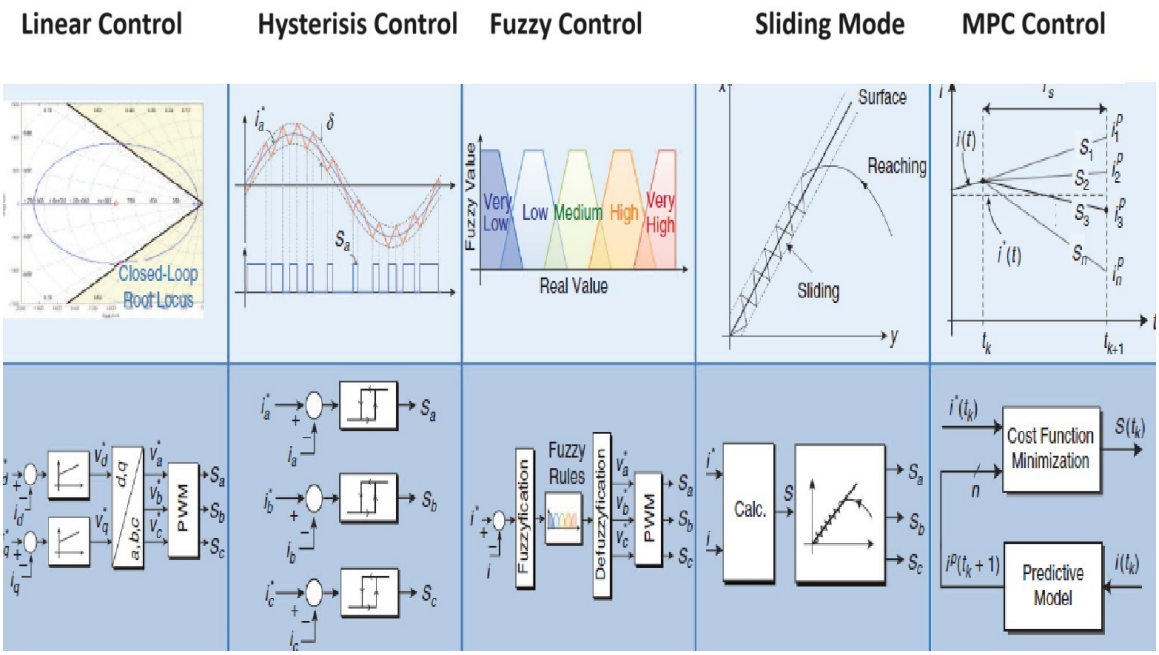

Figure 3.1: Control Methods in Power Electronics

Linear control is the most commonly used control strategy, employed in almost every industrial application because of its well-known design and simple implementation. However, there are several conditions present in many applications, such as

nonlinear plants, where linear control presents several restrictions in terms of dynamic response, handling of constraints, and even stability when parameters change.

Control theory has shown great advances during the last years, proposing new control techniques with higher capabilities, such as robust control, H-infinite, fuzzy logic, generalized control, passivity based control, etc. These advanced control strategies outnumbered linear control in applications with complex, nonlinear, and heavily constrained dynamical systems. Non-linear controllers are best suited for the control of real-time dynamic systems. It tends to have more accurate and faster responses. They obtain best results when complex control objectives are involved. Meanwhile, the classical linear controllers like PI/PID becomes relatively complex, when used for controlling multiple tasks. Advancement in computer technology made the implementation of non-linear control methodologies such as adaptive control, predictive control, sliding mode control, cur- rent programmed control, intelligent control such as Fuzzy and Neuro-Fuzzy control, Machine learning, Reinforced learning etc., relatively simple task. Model predictive control is emerging as one among the promising non-linear control techniques.

3.3 MPC in Power Electronics

Early digital processors appearing at the beginning of the 1970s had very restricted features regarding processing power and calculation speed. Features such as number of bits representation, floating point arithmetic, fast memory operations, and the number of processing cores have been continuously enhanced over time. On the other hand, the price of the digital processor has been continuously reduced. Although early generations of microprocessors did not have enough capabilities for control purposes, dedicated hardware such as DSPs and FPGAs appear from the early 1980s. The increasing of processing capabilities allows intense calculation tasks, such as audio, image, and video processing.

MPC has found successful application in the chemical and process industry for several decades, mainly because of its complex models and slow speed dynamics. Power electronics converters also have complex models and faster dynamics than chemical processes.The increase in processing capabilities and discrete modelling enabled the use of MPC in such converters. Most attractive features of predictive control is its intuitive and logical procedure to set out the control problem, which makes it easy to

Table 3.1: Control Methods in Power Electronics

Linear Control	**Hysterisis**	**Fuzzy Control**	**Sliding Mode**	**MPC Control**
Advantages:				
Known Bandwidth	Nonlinear Controller	Nonlinear Controller	Applicable to Switched Converters	Nonlinear Controller
Use of Modulator Makes Simple to Extend to Different Topologies	Very Robust	Simple Analogy to Human Response	Robust Against Model Uncertainties and Disturbances	No Modulation
Fixed Switching Frequency	No Modulator Required			Coordinate Transformation
Well Established (Mature, Used in Commercial Drives)	Very Fast Dynamic Performance	Linguistic Variables	Can Include Nonlinearities	Requirements and Constraints
Robustness for Nonlinear Systems	Simple Design and Mature control			Simple Design Based on Prediction Model and Cost Function
Disadvantages:				
Robustness for Nonlinear Systems	Requires High Sample Rate	Heuristic Design	Very High Control Activity, i.e., "Chattering"	High Computational
Not Easy to Adapt for Special Requirements (Constraints, Nonlinearities, etc.)	Variable Switching Frequency	Problems with Defuzzyfication	High Computational Requirements	Variable Switching Frequency
Requires Modulator (Slower Dynamics)	Resonance Issues			Heuristic Design of Weighting Factors
Requires Coordinate Transformation	Not Easy to Extend to Different Converter Topologies			Parameter Uncertainty

understand as a concept and simple to implement.

One of the key elements required in MPC is a precise model of the system to have an accurate prediction. These models depend directly on the application and the power converter used. For example, in drives, they are basically electrical machines whose physical models have been widely studied such as induction, synchronous, permanent magnets, switched reluctance, etc. For other applications, the loads, sources, and filters can be modeled as combinations of resistive, inductive, and capacitive components. These elements have well-known mathematical models established in the theory of electrical networks and machines. Power converters are composed by semiconductors operating in only two states: cutoff and saturation. Therefore, there always exist a finite number of possible combinations of the switching states in any power converter. This feature greatly simplifies the application of predictive control because, instead of a time consuming continuous optimization algorithm, direct evaluation of the switching states can be performed.

The control objectives in power electronics are usually to follow references of currents, voltages, power, torque, flux, etc. These objectives are represented in MPC by a cost function, which evaluates the errors between these references and the actual variables. Additional control objectives, such as commutation losses, common mode voltages, switching frequency and others, can be also included. Furthermore, nonlinear operation, such as restrictions and constraints, can be easily added greatly increasing the flexibility and reach of this control strategy. Today, it is possible to find very powerful microprocessors in the market, which can perform a large amount of calculations at a reduced cost. These calculations can be fast enough to predict the behavior of variables like electrical currents or voltages in real time without negatively affecting the performance of the system under control, enabling the use of predictive control in power electronics applications.

Over the last decade, MPC has been applied to a wide variety of applications, power converters, and control objectives. A classification of these applications is summarized in table below 3.2 .The references shown in the table are classified by application in power quality, machine drive, grid-connected converters, and controllable power supplies.

Table 3.2: Applications of MPC in Power Converters

Application	Converter Topology	Control Objective
Power Quality	Cascaded H-Bridge	Current Control,Active- Reactive Power,Voltage Balance
Power Quality	Flying Capacitor	Current Control, Voltage Control, Voltage Balance, Switching Frequency
Power Quality	NPC Inverter	Voltage Control, Current Control, Voltage Balance, Switching Frequency
Machine Drive	Direct Matrix Converter	Torque and Flux, Input Reactive Power, Common Mode Voltages, Switching Losses
Machine Drive	NPC Inverter	Current control, Torque and Flux, Switching Losses,Voltage Balance
Machine Drive	Voltage Source Inverter	Current Control, Switching Frequency Speed, Current Magnitude Minimization, Torque Ripple Torque and Flux,Current Limitation
Machine Drive	Voltage Source Inverter Hybrid	Torque, Current Magnitude Minimization
Grid Connection	Indirect Matrix Converter	Current Control, Input Reactive Power, Grid Synchronization
Grid Connection	Modular Multilevel Converter	Current Control, Voltage Balance
Grid Connection	NPC Rectifier	Active and Reactive Power, Capacitor Balance Current Control, Voltage Control, Resonance Damping, Switching Frequency
Grid Connection	Voltage Source Rectifier	Active and Reactive Power, Switching Frequency, Current Control, Current Ripple, dc Voltage

3.4 Challenges in MPC

The working principle of MPC is based on the prediction of the system behavior using a mathematical model of it and the optimization of the cost function defined using the predicted values to fulfill the control objectives. The MPC approach is widely used to control the high-power converters in various applications including motor drives, wind-energy conversion, power quality, and power conversion systems. Despite its popularity, the MPC has various challenges and issues when it comes to the MMCs. Some of the challenges that include,

1) Need for Accurate System model: The control performance obtained by MPC greatly depends on the discrete time model. .

2) Computational Complexity: In MPC approach, the control objectives are in-

cluded in a cost function and evaluated for all possible switching states. Finally, the switching state which minimizes the cost function is selected and applied to the converter. In MMC, the number of available switching states drastically increases with the number of submodules/switches. Hence, the computational burden on the digital controller is quite high, and it requires higher sampling time (Ts) to execute the optimization algorithm. The high sampling time deteriorates the steady-state and transient performance of the power converter. Further, the computational complexity varies with the optimization algorithm used to solve the cost function.

3) Variable-Switching Frequency: Modular Multilevel Converters are suited for high-power applications, where the average switching frequency is limited to kHz depending on the application. However,controlled with MPC, the average submodule switching frequency varies with the operating conditions. This leads to a variable harmonic profile and high switching power losses. Also, it is difficult to design the output filters in the grid-connected systems. In MPC, the switching frequency is controlled by penalizing the cost function with the weighting factors to some extent . However, this approach affects the performance of other control objectives of an MMC, which are included in the cost function.

4) Selection of Weighting Factors: In MPC approach, the multiple control objectives simultaneously can be included in a cost function. The relative importance of one control objective over other objective can be set by penalizing the cost function through the weighting factors . Due to the difference in the nature of control objectives, the variance in one control objective affects the performance of other control objectives as well. Further, the weighting factor has a direct influence on the system performance. Hence, the selection of weighting factors is one of important tasks in the MPC. Currently, the per-unit approach employed in the calculation of weighting factors in the MPC. This approach is only feasible if each control objective has a finite reference value. On the other hand, the heuristic method is still used in the calculation of weighting factors for control objectives with a zero reference value.

3.5 Discrete State Space Modelling

Model predictive control is based on discrete time model of a system . A discrete time model is used to predict the future values of currents and voltages in the next sampling interval (k+1),from the measured currents and voltages at the kth sampling

instant. Major goal of the predictive controller here is to balance the bipolar grid voltage during load variations and power generations and also to regulate the grid side voltage at reference value. Hence, state space model of the proposed converter is developed with bipolar grid capacitance voltages ;V_{C1}, V_{C2} ,inductor current I_{dc} as state variables and EV battery voltage V_{dc}, pole currents I_{01}, I_{02} as input variables. It can be referred in chapter 2. This model in continuous time domain has to be converted into discrete time domain. Methods often used for conversion of continuous time model to discrete time model are:

- Discretization by transformation of matrix
- Using Backward Euler's method
- Using Forward Euler's method

In discretization by matrix transformation ,state space equation in continuous time model is transformed to discrete state model by given transformations. Continuos time model is given by eqn.3.1

$$\frac{dX}{dt} = A.X(t) + B.U(t) \tag{3.1}$$

,where [A] is state matrix, [B] is input matrix, X(t) are state variables, U(t) is input. State space equation in discrete time model is given by eqn.3.2

$$x(k+1) = G.X(k) + H.U(k) \tag{3.2}$$

To convert A, B matrix to G, H , following transformation in eqn.3.3 is applied;

$$G = \mathrm{e}^{-\mathrm{A.Ts}} \mathrm{and} \mathrm{H} = \int_0^{\mathrm{Ts}} (\mathrm{I} + \mathrm{A}.\iota) * \mathrm{B}.\iota \tag{3.3}$$

Using the system model derivative $\dot{X}$ from Euler approximation, the discrete time model of predictive currents and voltages for the next (k+1) sampling instant of the power converter can be derived. Solving we get, equations of the (k+1)th states. The discrete model is in the form of $x(k+1) = [G].x(k) + [H].u(k)$.

Using Forward Euler's Method, discrete model can be derived in the form as in eqn.3.4 :

$$x(k+1) = [I + A.Ts].x(k) + [B].Ts.u(k) \tag{3.4}$$

Using Backward Euler's Method, discrete model can be derived in the form as in eqn. 3.5:

$$\frac{dx}{dt} = \frac{x(k) - x(k-1)}{Ts} \tag{3.5}$$

x(t) can be written as x(kTs) and u(t) as u(kTs) eqn.3.6;

$$x(k) = [I - A.Ts]^{-1}.x(k-1) + [I - A.Ts]^{-1}.[B].Ts.u(k) \tag{3.6}$$

Future values of currents and voltages for the (k)th sampling interval can be predicted from the measured currents and voltages at the (k-1)th sampling instant, given that discrete model is available. For a sampling time Ts, discrete time equations of proposed converter is derived by using Forward Euler's Method.

3.6 Model Predictive Control

Non-linear controllers are best suited for the control of real-time dynamic systems. It tends to have more accurate and faster responses. They obtain best results when complex control objectives are involved. Meanwhile, the classical linear controllers like PI/PID becomes relatively complex, when used for controlling multiple tasks. Advancement in computer technology made the implementation of non-linear control methodologies such as adaptive control, predictive control, sliding mode control, current programmed control, intelligent control such as Fuzzy and Neuro-Fuzzy control, Machine learning, Reinforced learning etc., relatively simple task. Model predictive control is emerging as one among the promising non-linear control techniques.
Model predictive control (MPC) is a very apt control technique for power electronic converters and electric drive applications. It is a very powerful control technique due to its intuitive features, easy implementation, adaptability in accommodating multiple constraints, easy inclusion of non-linearities and is easier to understand irrespective of the complexity of the converter (Rodriguez and Cortes, 2012). It also provides direct inclusion of control parameters into the cost function. Unlike the conventional linear control approach, model predictive control (MPC) technique is so desirable because it does not need the tuning of PID parameters for changes in the reference voltages and currents. It avoids the complexities of PWM modulation and other coordinate transformations. It gives less oscillations and peaks during transients and gives faster control. Non-linear controllers are the most suitable and faster techniques when com-

plex control objectives are involved.
Model predictive control utilizes the discrete behavior of the power converter (Akter et al., 2015). Given that discrete model is developed, future values of currents and voltages for the (k+1)th sampling interval can be predicted from the measured currents and voltages at the kth sampling instant. . Predictive control algorithm follows a cost function defined for the optimization of the control objectives. It is easier to formulate and accommodate multiple control objectives, and conflicting constraints into the cost function, once a proper discrete model of the system is developed. Cost function has an element called weighing factor, λ. Selection of weighting factor in the cost function is particularly important in model predictive control. If appropriate value selected, it works well for a wide range of changes in state and input variables. Hence fast acting model predictive scheme is better for the converter control in bipolar dc grid which is subject to fluctuating pv irradiation conditions and loads . Since model predictive control is based on discrete time model of a system, discrete state space equations of the interfacing converters are developed, which can be referred in below sections.

3.6.1 MPC Control of Two Level PV Converter

Non linear controllers like model predictive controllers gives faster response during dynamic conditions. PV generation systems are subjected to fluctuating irradiation conditions. So model predictive control is apt for the control of PV converters. Block diagram for the MPPT using predictive control is illustrated in fig.3.2. Either simple boost or three level boost converter can be used for interlinking PV panels to grid. Two-level boost converters are operated to extract maximum power corresponding to each irradiation level with MPPT technique. Perturb & Observe MPPT method was used, when PV boost converters were controlled with PI controllers as discussed in last chapter. Incremental Conductance method is used for maximum power tracking, for model predictive based control in PV boost converter. Incremental Conductance conductance method gives reference current to predictive model, in which inductor current tracks the reference current to extract maximum power from PV panel. Predictive model for PV boost converters developed are defined by eqn.3.7 -3.8:

$$i_{pv1}(k+1) = i_{pv1}(k) + \frac{T_S}{L} * .V_{pv1} - (1 - S_{PV1}) * .V_{C1} \tag{3.7}$$

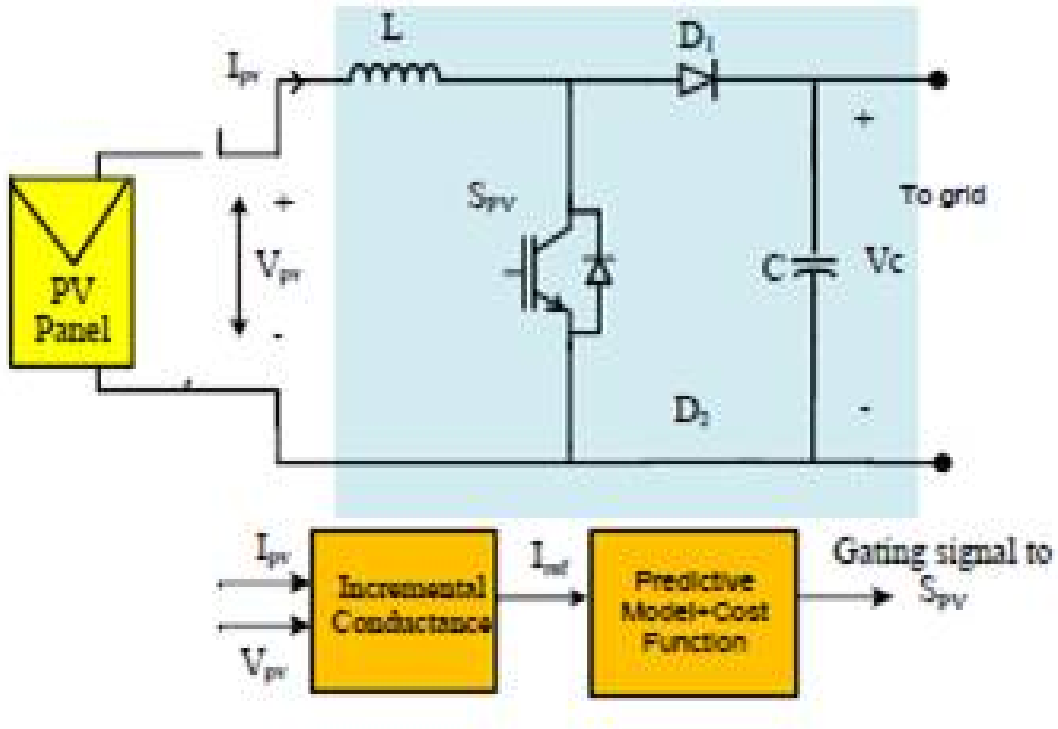

Figure 3.2: MPPT Control in PV Boost Converter with MPC

$$i_{pv2}(k+1) = i_{pv2}(k) + \frac{T_S}{L} * .V_{pv2} - (1 - S_{PV2}) * .V_{C2}] \tag{3.8}$$

3.6.2 MPC Control of Three Level Boost PV Converter

Conventional approach for maximum power point tracking (MPPT) is the implementation of any hill climbing method (Perturb & Observe or Incremental Conductance) using PID controller with PWM (Das et al., 2019) or hybrid modulation schemes (Sharaf and Şahin, 2017). Designing these controllers is a rather complicated task for the non-linear search of MPP (Mangu et al., 2016). Hence MPC is advisable for maximum power point tracking application. Since, MPC is based on discrete model, a predictive model of a three-level boost converter is developed for maximum power point tracking. The circuit diagram and modes of operation of three level boost converter is detailed in section 2.5. Control technique involves the incremental conductance MPPT and advanced MPC method for the system's efficient and faster performance. The predictive current control takes care of maximum power point tracking of the photovoltaic systems connected with the bipolar dc grid. The refer-

ence current is acquired from the current-based incremental conductance technique. PV current tracks the reference current to extract maximum power from PV panel.

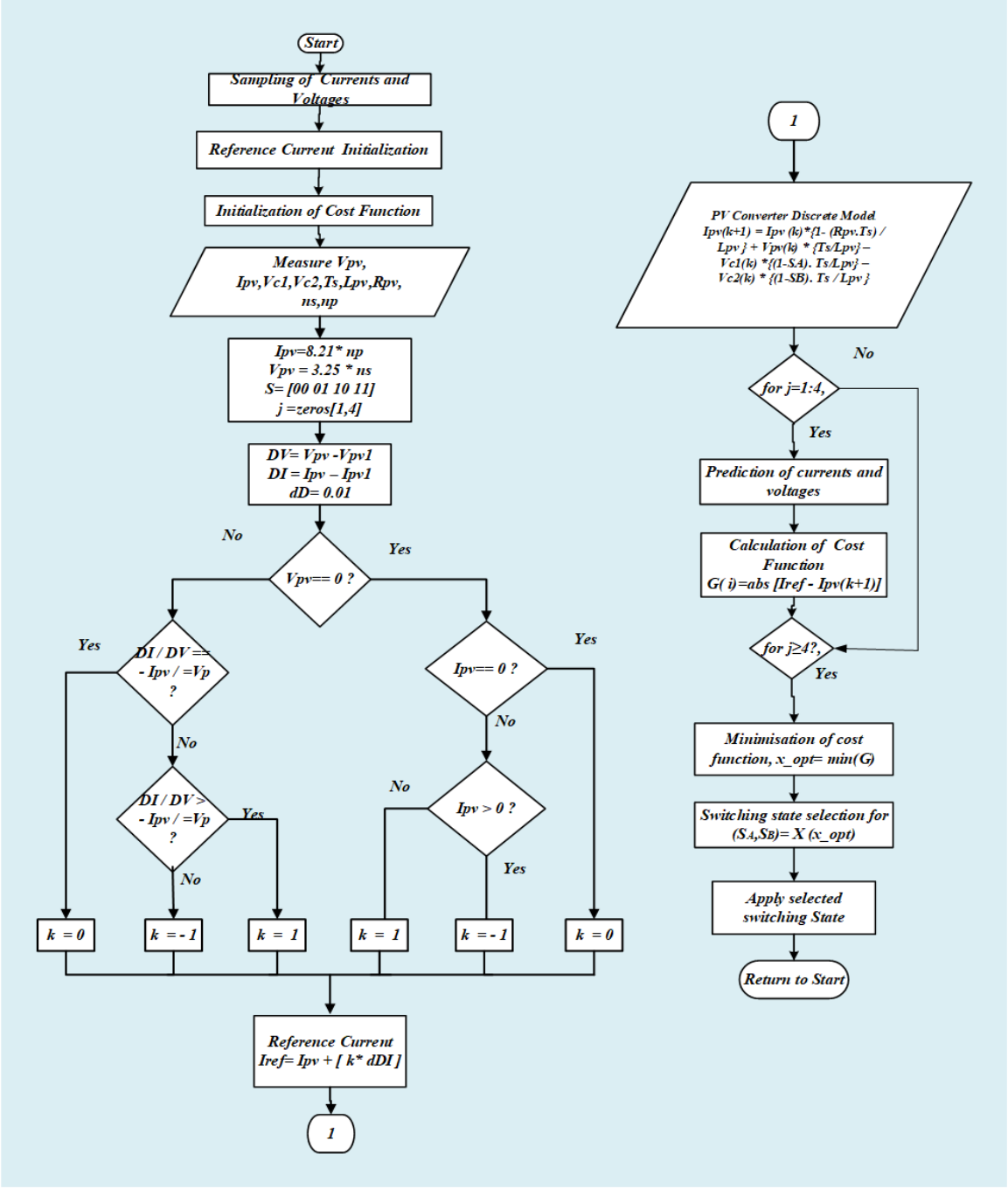

Figure 3.3: MPC Control Algorithm for TL boost PV converter

Discrete-time model equation for the PV converter is given below in eqn. 3.9;

$$\begin{bmatrix} i_{pv}(k+1) \\ V_{C1}(k+1) \\ V_{C2}(k+1) \end{bmatrix} = \begin{bmatrix} 1-\frac{R_{pv}.Ts}{L_{pv}} & \frac{-\bar{S_A}.Ts}{L_{pv}} & \frac{-\bar{S_B}.Ts}{L_{pv}} \\ \frac{-\bar{S_A}.Ts}{C_1} & 1-\frac{Ts}{R_{01}.C_1} & 0 \\ \frac{-\bar{S_B}.Ts}{C_2} & 0 & 1-\frac{Ts}{R_{02}.C_2} \end{bmatrix} . \begin{bmatrix} i_{pv}(k) \\ V_{c1}(k) \\ V_{C2}(k) \end{bmatrix} + \begin{bmatrix} \frac{Ts}{L_{pv}} & 0 & 0 \end{bmatrix} . \begin{bmatrix} V_{pv}(k) \\ 0 \\ 0 \end{bmatrix} \tag{3.9}$$

Cost function is given by absolute value of $g(i)_{s=1-4} = ||(iref - ipv(k+1))||$ and i_{ref} is given by the incremental conductance MPPT algorithm. Switching states of the three-level boost converter are selected such that the control objective stated in the cost functions is optimized, to transfer maximum power from PV generation to the grid side for varying irradiation irrespective of changing load conditions. The flowchart for the control algorithm is given in fig.3.3.

3.6.3 MPC Control for Three Level Bidirectional Converter

Fig 3.4 shows the schematics of the model predictive control of three level bidirectional buck/boost converter. This bidirectional converter used for connecting battery energy storage or electric vehicle charging stations has been assigned with multiple control objectives here with predictive control. The main control objective is grid voltage restoration and balancing of the pole capacitance voltage under transient conditions of load and power generations. It also has to ensure bidirectional power flow between battery and dc grid. Battery SOCs are constantly monitored. Mode of operation is selected by Power gap ΔP (difference between generated power P_{gen} and load demand P_{load} and SOC limits. If $\Delta P > 0$, the MPC controller selects buck mode and if $\Delta P < 0$, boost mode is selected. $Vref$ for grid regulation is 300V. Grid voltage error is processed using a PI controller to obtain I_{ref} .The inductor DC link current, I_{dc} is taken as the control variable for regulating grid voltage, with I_{ref} as reference current.

3.6.3.1 Predictive Model Formulation

Discrete model is developed using Forward Euler's Method, from the continuous state space model detailed in previous chapter. State variables for the next (k+1) th sampling instant are predicted from the measured variables at kth instant. Predictive model of proposed converter for buck operation for a sampling time Ts given below

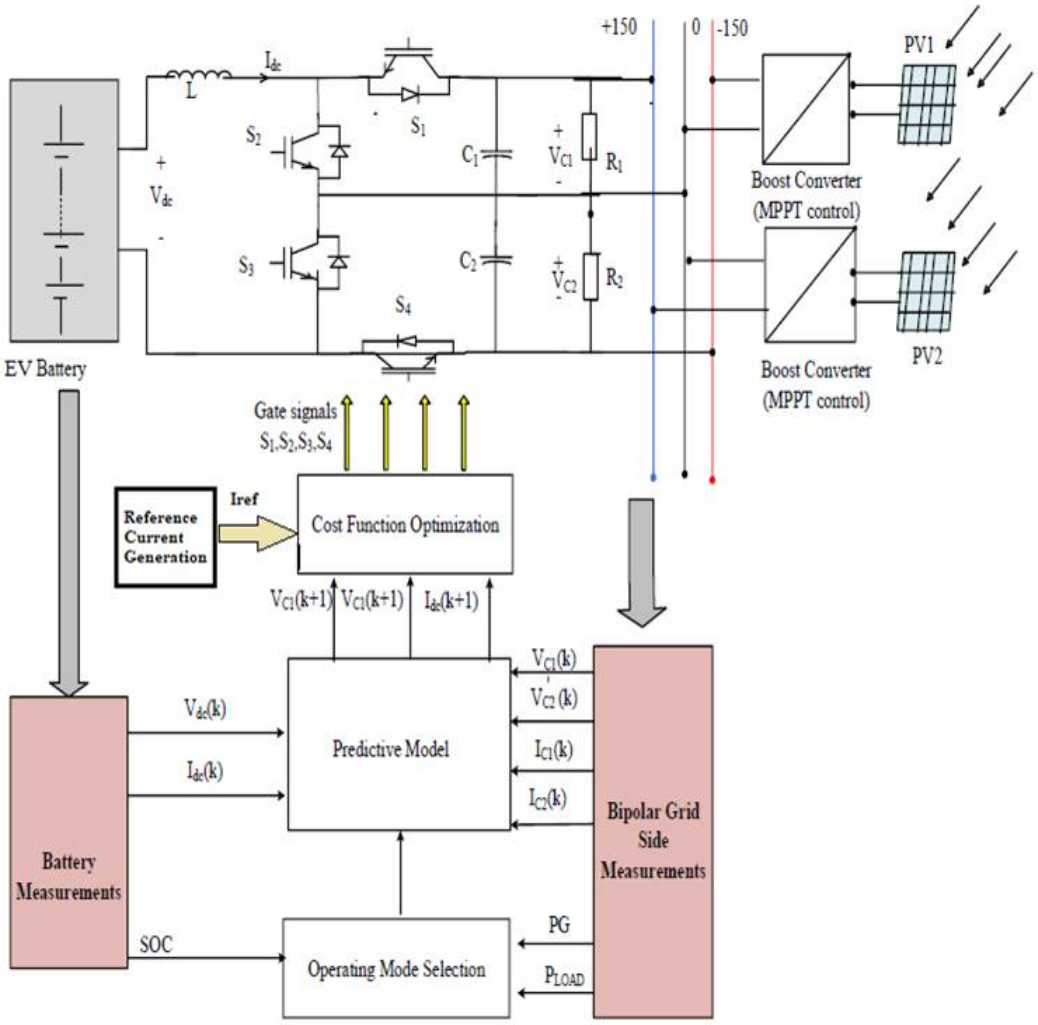

Figure 3.4: Model Predictive Control Diagram

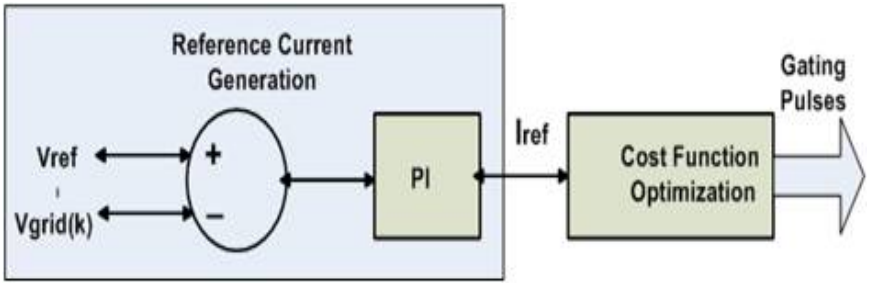

Figure 3.5: Reference Current Generation

in eqn.3.10-3.12 ;

$$i_{dc}(k+1) = \frac{1 - R_{dc}.Ts}{L_{dc}} * i_{dc}(k) + \frac{S_1.T_s}{L_{dc}} .* V_{C1}(k) + \frac{S_4.T_s}{L_{dc}} .* V_{C2}(k) - V_{dc}(k) * \frac{T_s}{L_{dc}} \quad (3.10)$$

$$V_{C1}(k+1) = \frac{-S_1.Ts}{C_1} * .i_{dc}(k) + \frac{1+T_s}{R_{01}.C_1} * .V_{C1} \tag{3.11}$$

$$V_{C2}(k+1) = \frac{-S_4.T_s}{C_2} * .i_{dc}(k) + \frac{1+T_s}{R_{02}.C_2} * .V_{C2}(k) \tag{3.12}$$

Predictive model for boost operation for a sampling time Ts is given below in eqn.3.13-3.15 ;:

$$i_{dc}(k+1) = \frac{1-R_{dc}.T_s}{L_{dc}} * .i_{dc}(k) - \frac{1-S_2.Ts}{L_{dc}} * .V_{C1}(k) - \frac{1-S_3.Ts}{L_{dc}} * .V_{C2}(k) + (V_{dc}(k).\frac{Ts}{L_{dc}} \tag{3.13}$$

$$V_{C1}(k+1) = \frac{(1-S_2).Ts}{C_1} * .i_{dc}(k) + \frac{1-Ts}{R_{01}.C_1} * .V_{C1}(k) \tag{3.14}$$

$$V_{C2}(k+1) = \frac{(1-S_3).Ts}{C_2} * .i_{dc}(k) + \frac{1-Ts}{R_{02}C_2} * .V_{C2}(k) \tag{3.15}$$

Objectives of the predictive controller in TL-bidirectional converter are pole capacitance voltage balancing and grid voltage regulation. This is stated by cost functions formulated with the predicted and reference values of control variables. Cost functions is given by :

$$G1 = \lambda_1 * ||V_{C1}(k) - V_{C2}(k)||$$

and

$$G2 = \lambda_2 * ||(I_{dc}(k) - I_{ref}||$$

where λ_1, λ_2 are weighing factors of each control objectives. The weighing factor, $\lambda 1$ and $\lambda 2$ decides the preference of optimization between the two cost functions. The higher the value of the weighing factor, the more focus will be given to that particular control objective during optimization. These are given a value such that $\lambda 1 + \lambda 2 = 1$. In this work, balancing the grid capacitance voltage is given more importance, hence we took $\lambda_1 = 0.65$ and $\lambda_2 = 0.35$. The switching states associated with the minimum cost function are finally selected for firing. Cost function for optimization is given in eqn. 3.16;

$$G = ||G1|| + ||G2|| = ||\lambda 1.(V_{C1(}k) - V_{C2}(k) + \lambda 2.(I_{dc}(k) - I_{ref})|| \tag{3.16}$$

3.6.3.2 Control Algorithm for TL Bidirectional Converter

Algorithm of predictive control implemented for bipolar converter is depicted in fig.3.6. The control algorithm starts with measuring and sampling the positive DC bus voltage Vdc1(k), Vdc2(k), current Io1(k), negative DC bus voltage Vdc2(k), current Io2(k); battery side voltage Vbat(k), current Ibat(k) for the kth sampling period. The reference currents Iref for regulating grid voltage to 300V are calculated and fixed. Cost functions are formulated and initiated. State of charge of the battery is monitored to check whether it is within the safe operating limit. SOC_{max} of 90% is taken as the upper safe operating range and SOC_{min} of 35% as the lower safe operating range. If SOC crosses this safe range, the floating mode is activated and BESS is isolated from the grid. Modes of operation are initiated by monitoring the following conditions;

- Buck Mode: $SOC_{max} > SOC \quad , \quad P_G > P_L$
- Boost Mode: $SOC > SOC_{min} \quad P_G < P_L$
- Float Mode: $SOC > SOC_{max}$, or $SOC < SOC_{min}$

If ΔP is +ve, control opts for buck mode of operation and battery is charged absorbing the excess power. If ΔP is -ve, MPC controller goes for boost mode of operation and battery discharges to provide the deficiency in power demanded by connected loads on the bipolar dc grid. Predicted current $i_{dc}(k+1)$, predicted voltages $V_{c1}(k+1), V_{c2}(k+1)$ the next (k+1) th sampling instant, are estimated for each of the four possible switching states of buck operation of the converter (j = 4,where j denotes the possible switching states) by utilizing the discrete model of the system as given in eqns.3.10,3.11, 3.12. Similarly, predicted currents $i_{dc}(k+1)$, predicted voltages $V_{c1}(k+1), V_{c2}(k+1)$ are determined for each one of the four possible switching states for boost mode of operation (j = 4, where j denotes the possible switching states), of the converter by utilizing the discrete model of the system given by eqns.3.13, 3.14, 3.15. Finally, the switching state associated with the minimum cost function is finally selected for firing the converter in the next sampling instant.

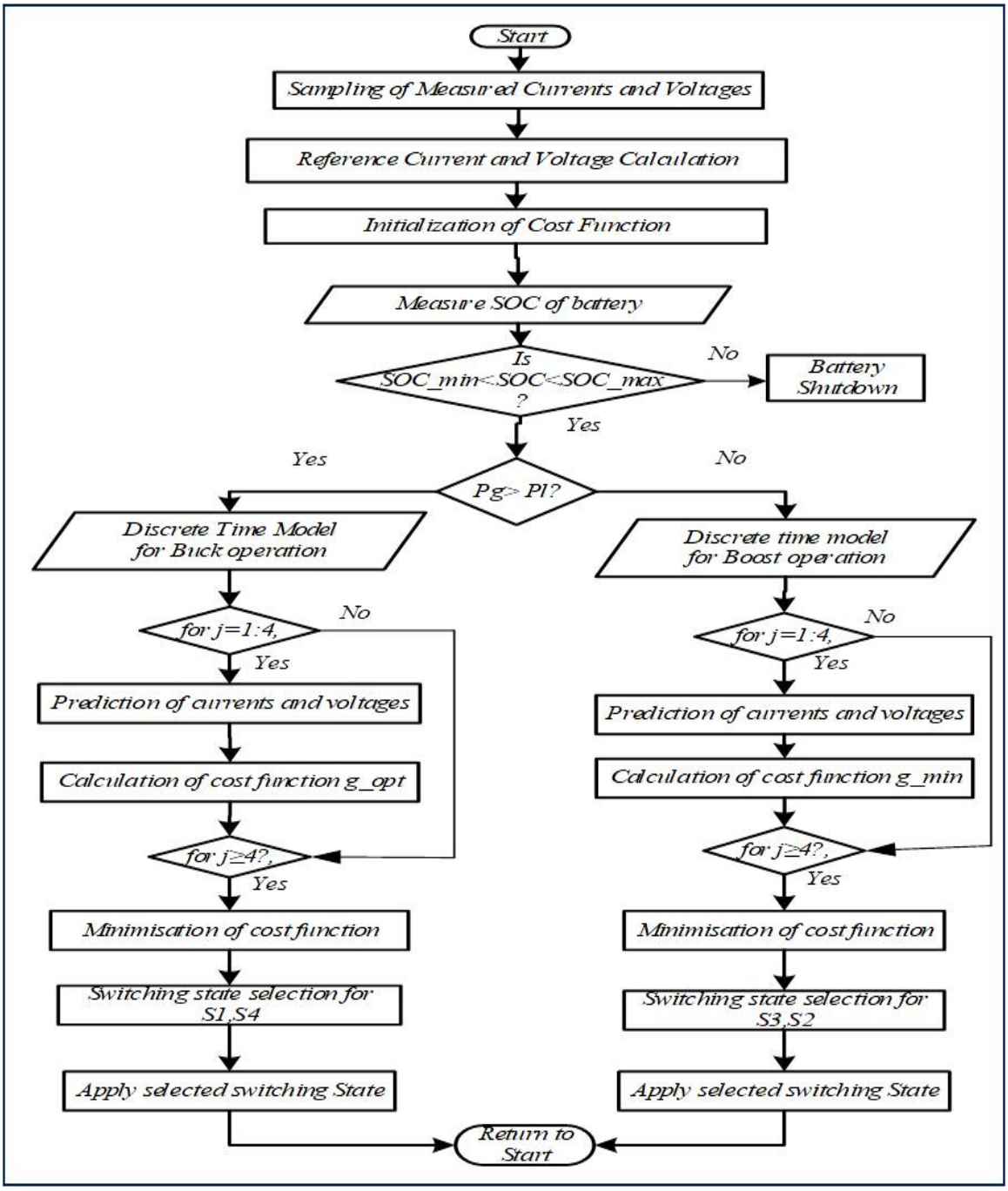

Figure 3.6: Flowchart of predictive algorithm

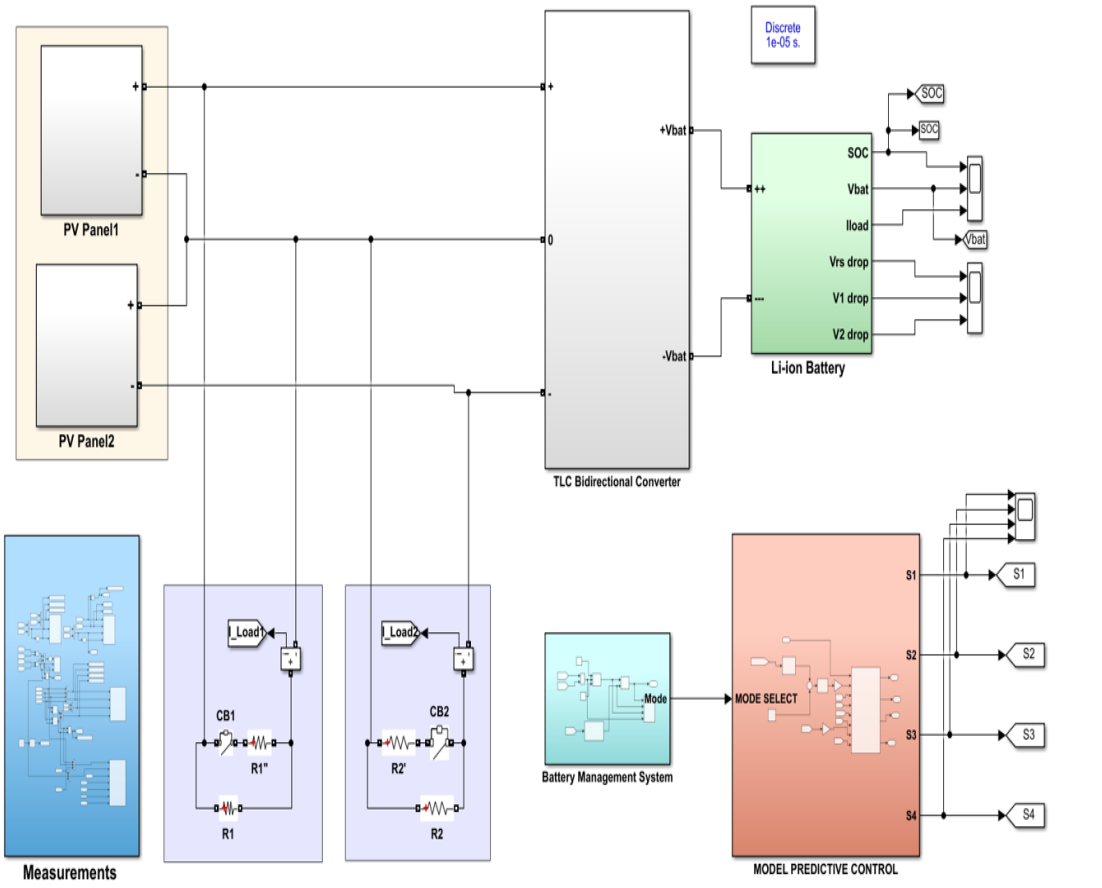

Figure 3.7: MATLAB simulation of proposed system

3.7 Simulation of Bipolar DC Grid System with Model Predictive Control

The proposed system of bipolar DC microgrid integrated charging stations for EV is simulated in MATLAB Simulink and analysed under dynamic conditions of power input and load changes. The battery energy storage or (can be replaced with EV charging stations) is connected to bipolar DC bus by three level bi-directional buck/boost DC-DC converter. The results are analysed for cases separately for unequal load changes and unequal pv irradiation. Fig.3.7 shows the MATLAB Simulink diagram of the bipolar dc grid with model predictive control. Parameters used in the simulation is described in table 3.3. Bipolar dc microgrid connected to solar photovoltaic systems PV_1,PV_2 are subjected to dynamic conditions like fluctuation in irradiation

level and changes in DC load connected. Converter has to maintain voltage balance across grid capacitance V_{C1} and V_{C2} and operate in buck and boost mode in accordance with these changes in generated PV power and load demand. Switches $S_1,\ S_2, V\ S_3,\ S_4$ are driven to obtain buck and boost operation of BESS in accordance with state of charge conditions of the battery, PV power generated (P_G) and power demanded by load (P_L).

3.7.1 Result Analysis

The proposed system with model predictive control is simulated in MATLAB/Simulink. Bipolar dc microgrid connected to solar photovoltaic systems PV1, PV2 are subjected to dynamic conditions like fluctuation in irradiation level and changes in DC load connected. Converter has to maintain voltage balance across grid capacitance VC1 and VC2 and operate in buck and boost mode in accordance with these changes in generated PV power and load demand. Switches S1, S2, S3, S4 are driven to obtain buck and boost operation of BESS in accordance with state of charge conditions of the battery, PV power generated (PG) and power demanded by load (PL).

Case. I: Change in dc load connected

Fig 3.8 illustrates simulation results for voltage balancing due to load imbalance. A load of 225W and 450W is applied on two poles of bipolar dc grid during 0-2sec. During this condition, two PV panels are operating at an irradiance of 500 W/m^2 and $400W/m^2$ at 25^{o}C. Total generated power is 1050W $\geq$ 675W, the excess amount of power 340W is taken by the battery. At t=2s, dc load connected is stepped to 1125W and 900W respectively. The additional load is supplied by the battery(-975W).

Case II.: Changes in irradiation level

Fig 3.9 shows simulation results for voltage balancing due to fluctuation in irradiation level. A constant dc load of 750W is connected on each pole throughout the operation. The two PV panels are operating at an irradiance of $500W/m^2$ and $300W/m^2$ at 25 ^{o}C temperature. Both the PV panels together are injecting a power of 920 watts. Since the load on the DC- bus is 1500W, the remaining amount of power 580W of power is provided by the battery [PG¡PL (920W$\leq$1500W)]. So, the battery discharges providing the deficient power (Ibat=-12A, Pbat=-620W). At t=2s, irradiation is stepped upto to $100W/m^2$ and $700W/m^2$. Here $P_G \geq P_L$ and the converter goes to buck mode charging battery with I_{bat} =9A and P_{bat} = 460W. When the

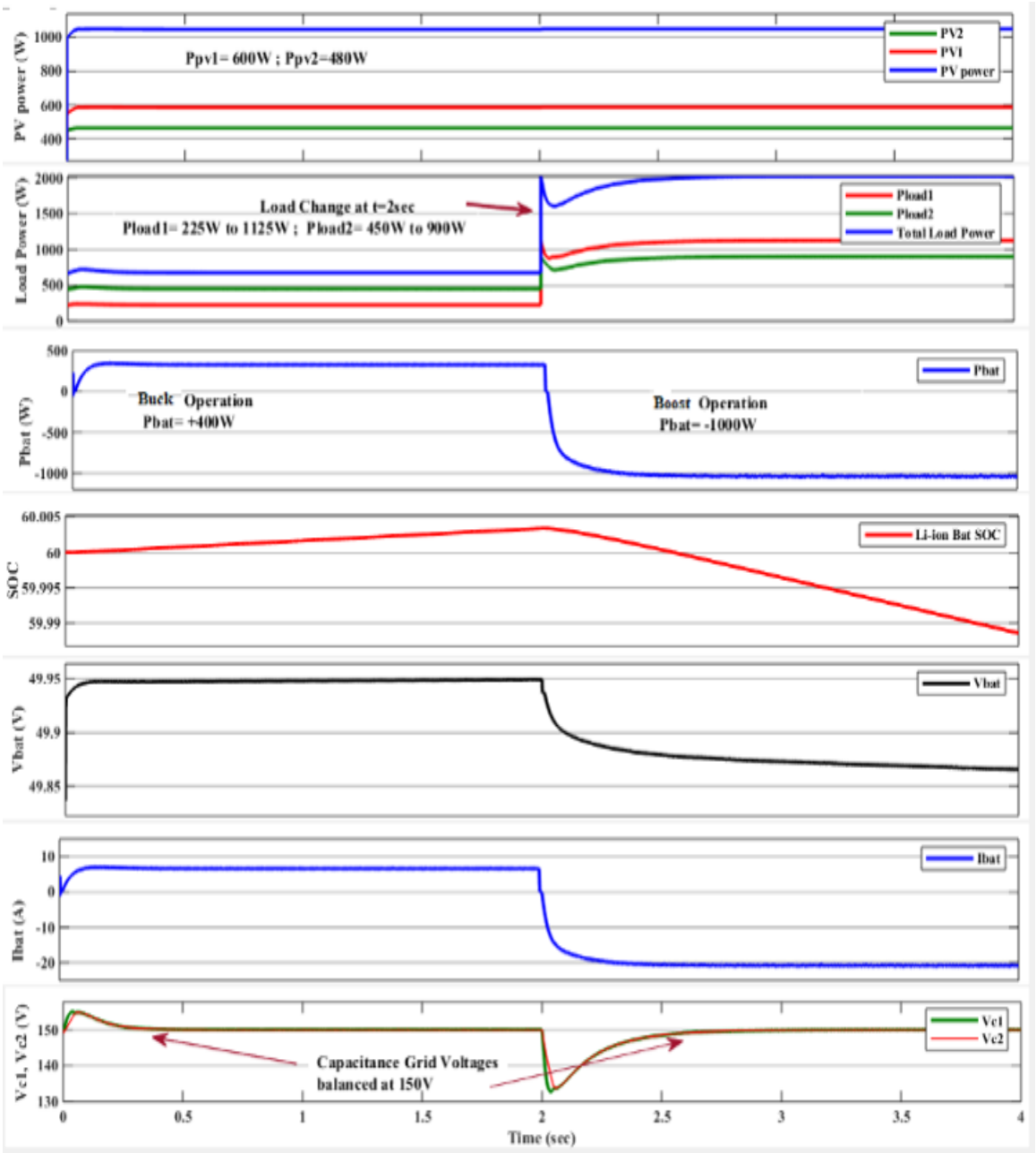

Figure 3.8: Simulation results of TLBiDC for changes in dc load a)P_G b)P_L c)P_{bat} d) SOC e) V_{bat} f)I_{bat} g)V_{c1}, V_{c2}

load is less in a bus, there is a sudden rise of capacitor voltage of corresponding bus. Similarly, when load is greater than generated power, there is tendency of voltage sag in a bus. Battery pans these power gap and TL-BDC makes the bidirectional power flow feasible. Along with that we are able to balance capacitor voltages V_{C1}, V_{C2} at

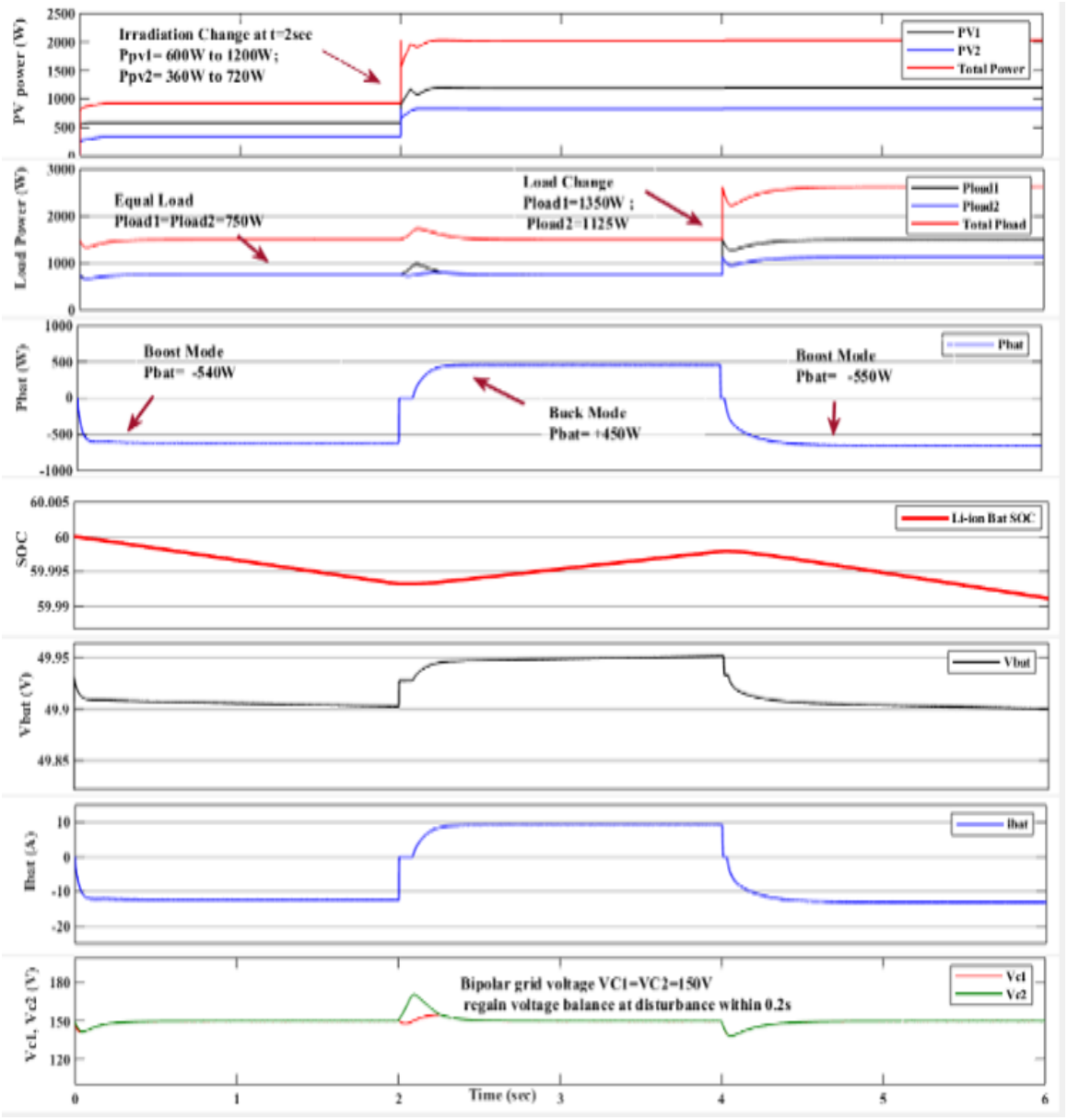

Figure 3.9: Simulation results for change in irradiation a)P_G b)P_L c) P_{bat} d)SOC e) V_{bat} f) I_{bat} g) V_{c1}, V_{c2}

$\pm$150V and bipolar dc grid voltage is regulated at 300V. From the simulated waveform results using model predictive control in fig.3.8 and fig.3.9, it is clear that MPC is able to balance capacitor voltages and regulate dc grid voltage with reduced ripples in $I_{bat}, P_{bat}, V_{C1}, V_{C2}, V_{grid}$. It also giver faster response during dynamic conditions compared with PI controller.

3.8 Hardware in Loop Testing and Validation

Hardware in loop testing is a method to test the controller and the control code of a plant model or a test system. Controller can be tested in real time, for various test cases, which is cost effective and advantageous to identify the fault and failure, before building the product or hardware in real. It is effective in avoiding destructive shoot through in the controllers, and also can account for power and thermal losses. HIL testing and validation is adopted wide spread for research and various stages of product development in the areas of microgrid,power systems,embedded system, software development, power electronics, drives, e-mobility, renewables etc. Power electronics is one of the major area, in which HIL testing is very essential, for validating new control techniques and control algorithms formulated in real time. Typhoon HIL is a major technological tool provider in controller and hardware in loop testing. Typhoon provides different types of testing platforms like Virtual HIL, Real Time HIL, Control in Loop, and Power HIL which can be referred in fig.3.10.

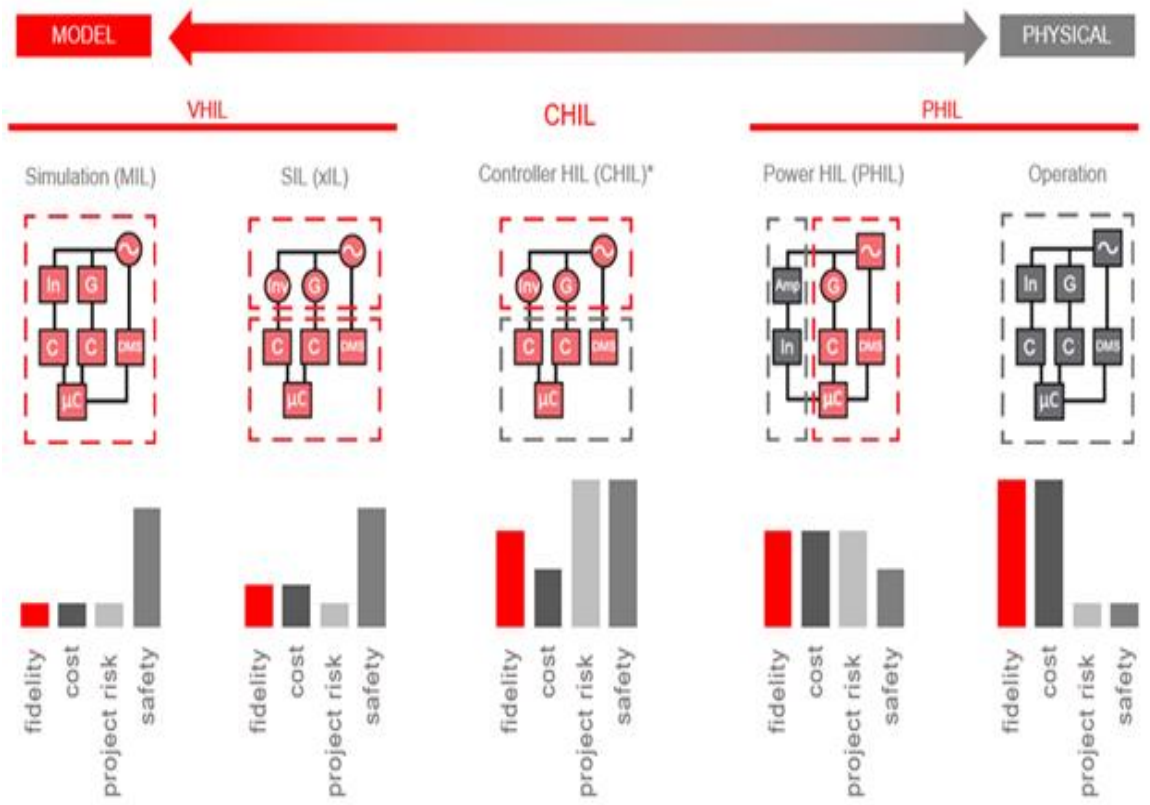

Figure 3.10: HIL methods in Typhoon HIL

In Virtual HIL , the plant/ model is developed inside the computer/simulation software and code generated for the controller is dumped into a real time processor and it is tested. Virtual HIL is also known as HIL Simulation in other testing platforms. In Real Time HIL, you dont need real plant for testing the controller. Plant /Model developed in the computer system and code is generated for the virtual plant with all its complexities of a real hardware and dumped in a real time processor (FPGA). Real controller placed outside, and tested in real time. Real Time Hardware in loop is also known as Control HIL. In Control in Loop testing, controller is developed inside and dumped to a real time processor and actual hardware is placed outside and tested. CIL is also known as rapid control prototyping (RCP) in other HIL test platforms like OPAL-RT.

3.8.1 Typhoon HIL Test Set Up

Figure 3.11: . Hardware in loop set up using Typhoon HIL 402

Hardware in loop testing and validation is done with Typhoon HIL 402. HIL 402 is a compact and powerful simulation hardware with 20ns PWM sampling time and

simulation steps in the range of $0.5\mu s/1\mu s/2\mu s$ (i.e. it has a sampling rate as high as of 1MHz). It has 16 I/O analog channels and 32 digital I/O channels. It has a built in 32 channel oscilloscope and support 12V/5V analog external power supply and 3.3V digital inputs. Digital input signal can be sampled at 20ns, that PWM converters with $f_s \geq$200kHz can be accurately modelled. Hardware in loop experimental set up is shown in fig. 3.11. Typhoon HIL Control Center is the software for plant and controller modelling hardware by Typhoon. This consists of Schematic Editor, HIL SCADA, Typhoon HIL Test Suite etc (Typhoon, 2018).

Schematic Editor allows you to create high-fidelity models of the power stage for your real-time simulations. Bipolar dc microgrid plant modelled in Typhoon HIL Schematic Editor is shown in fig.3.12.

Typhoon HIL SCADA is a simple, easy to use graphical environment that allows you to create your own specific interface with the real-time (RT) model. SCADA panel or .cus file developed for the testing in given in fig.3.13. Through this SCADA panel, real time inputs and variations is given and also observe the changes occuring in parameters using meters, plots etc. In this monitoring panel, we can see PV irradiation and temperature can be varied, Battery System can be turned on/off manually using a toggle switch. Battery SOC,load parameters, etc can be given as real time inputs. The HIL SCADA application downloads simulation models to the HIL platform from Schematic Editor and controls the emulation process, parameters and outputs. Also, we can control and observe not only HIL simulation but also our own external device. Control Panel and Customized User Interface is created for the proposed system using HIL SCADA widgets, with the Python scripts. It is tested in both virtual and real time (RT) HIL platform of Typhoon HIL 402.

Control interface board used HIL DSP 180 Interface. This enables connection between HIL device and Texas Instruments C2000s microcontrollers, for testing power electronics applications. It has a Texas Instruments HSEC control card with 180 pin, RJ45 CAN bus connector of 3.3.V, 24 hil digital inputs, including 16 PWM signals.

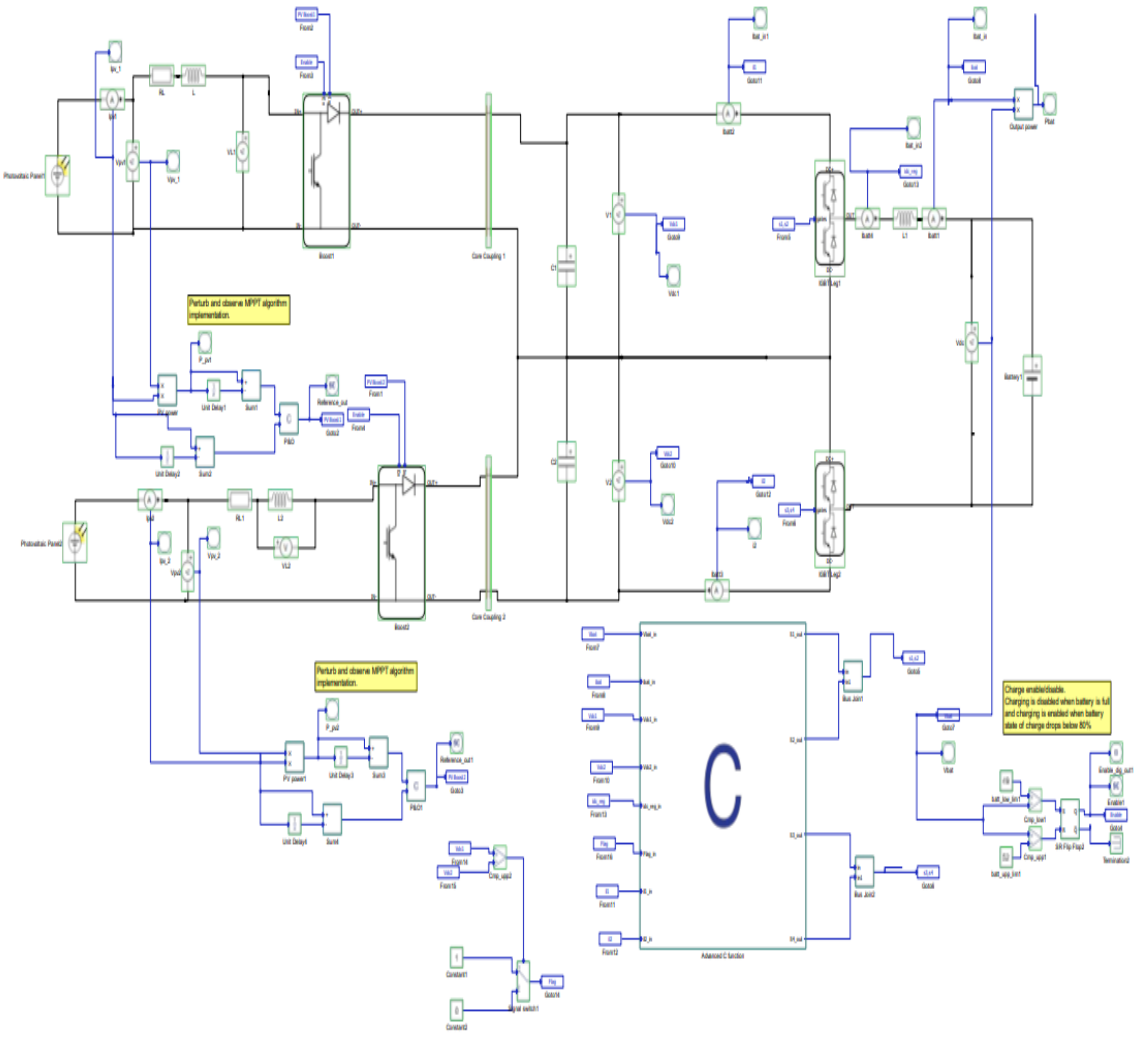

Figure 3.12: Developed plant in Typhoon Schematic Editor

3.8.2 HIL Result Analysis

Table 3.3 gives the parameters used for the hardware in loop testing. The plant model developed and model predictive controller was tested both in Virtual HIL (VHIL) and Real Time HIL (RT-HIL) test set up. System responses obtained in HIL testing validated the effective and faster control of the test system with model predictive controller. HIL test results matches with the simulation results. Grid conditions taken for hardware in loop testing of the predictive controller is sudden changes in PV irradiation with BESS charging,sudden changes in PV irradiation with BESS in discharging, sudden changes in dc load with BESS charging and sudden changes in

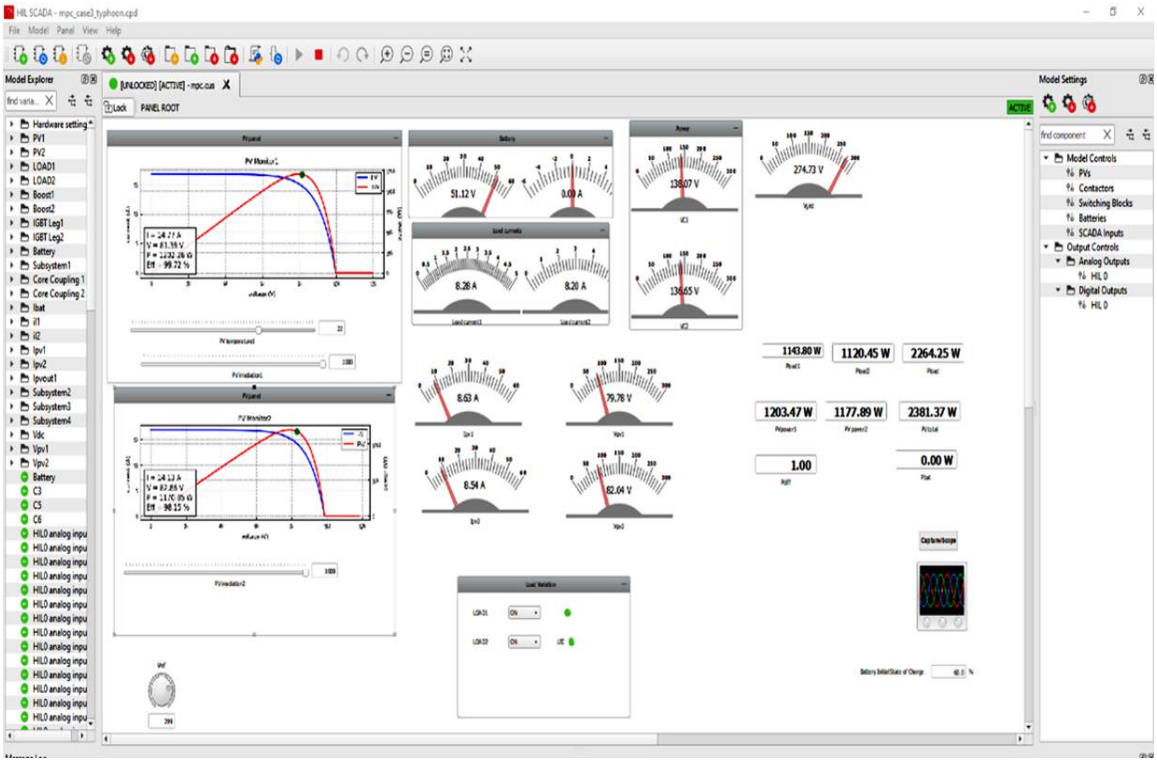

Figure 3.13: HIL SCADA control panel of the developed HIL plant

dc load with BESS discharging.

Table 3.3: Test Parameters (HIL and SIMULINK)

Symbol	Parameter	Value
Ts	Sampling Time	10 μs
C1/C2	DC link capacitance	2500 μF
Ldc	Inductance at battery side	15 mH
Rdc	Inductor series resistance	0.05
Vgrid	Grid voltage (H.V Side)	300 V
VC1,VC2	Bipolar voltage level	+ 150 V, 150 V
PV1, PV2	Photovoltaic systems	1.2 KW, 80 V, 15 A
Li-ion Cell	Battery Cell model	3.7V ,4.2Ah

Case I: Changes in dc load connected (unequal loading)

Initial conditions of irradiation levels and dc loads is same as in simulation test case I. The converter is in buck mode and battery is charging with P_{bat}=340W. At t = 3.8s, load demand at +ve bus is increased to 1125W. Since $P_G \leq P_L$ (1080W $\leq$ 1575W), converter goes to boost mode and battery discharges(P_{bat} = - 500W, I_{bat}

= -10A). At t=4.8s, load power at with I_{bat} = -23A, supplying deficient power (P_{bat} = - 945W). Output waveforms obtained for change in connected dc load is shown in fig.3.14.

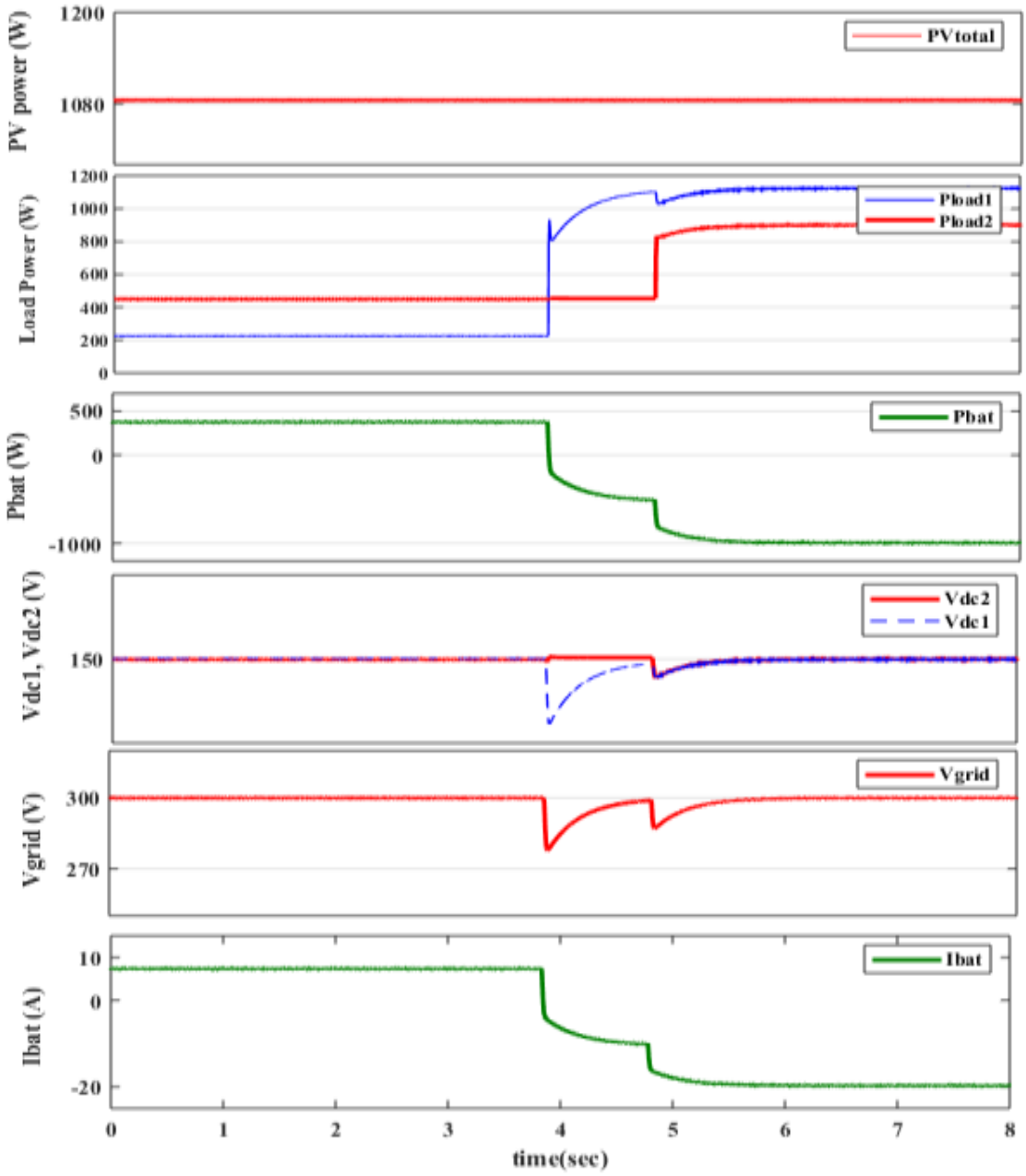

Figure 3.14: Case I. Changes in load connected (RT- HIL)

Case II: Unequal PV irradiations with excess power (buck)

In this case, bipolar dc buses ae equally loaded with 1500W ($P_{L1} = P_{L2} = 750$W

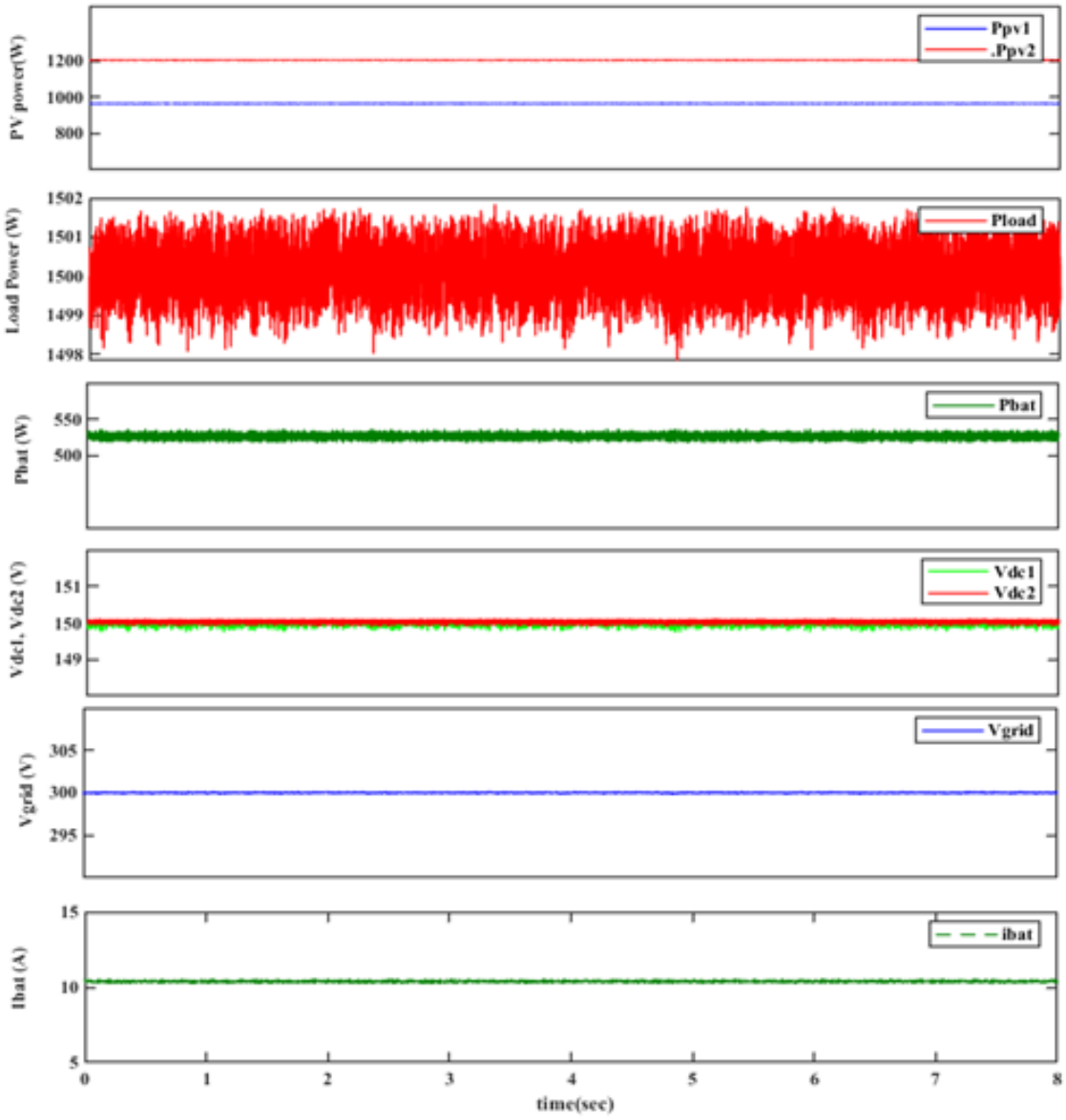

Figure 3.15: Case II. Unequal PV irradiations with excess power (buck)

). PV1 generate 840W and PV2 generate 1200W. Excess power is fed to the battery through buck operation (I_{bat}= +11A , P_{bat} = 540W). Real time HIL responses is shown in fig.3.15.

Case III: Unequal PV irradiation with deficient power(boost)

In this case, bipolar buses are equally loaded with 750W each. PV_1 is kept at 720W and PV_2 at 360W. Total PV power generated is 1080W. Deficient power 1080-

1500 = -420W is supplied by the battery through boost operation. Results obtained in HIL platform is shown in fig.3.15- 3.16. It can be observed that, grid capacitance voltage get unbalanced when power mismatch occurs between generated power and load power. It takes less than 0.5s for predictive controlled three level bidirectional buck/boost converter to mitigate this unbalance

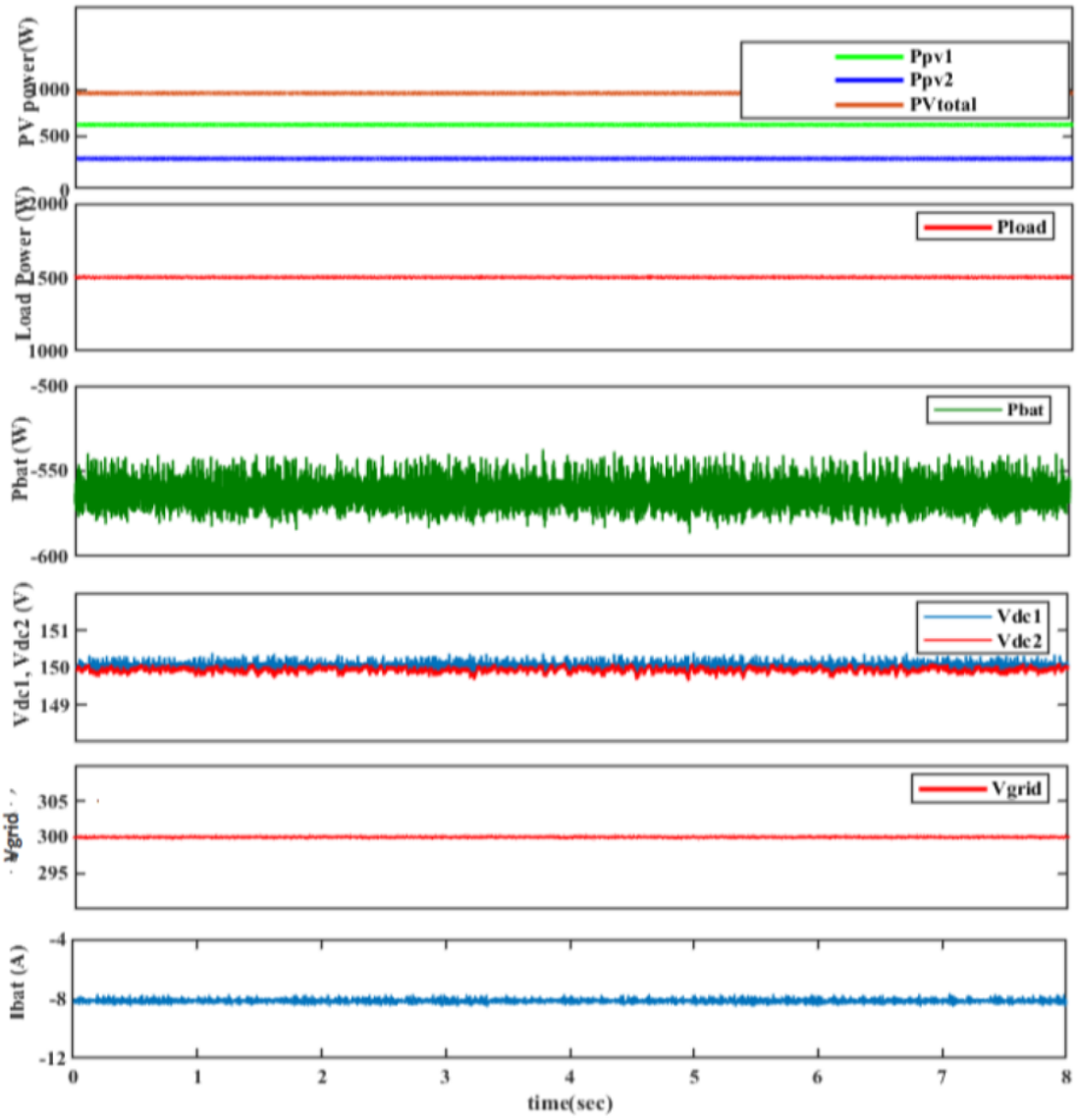

Figure 3.16: Case III: Unequal PV irradiation with deficient power(boost)

3.9 Summary

The proposed model predictive controlled (MPC) three level (bipolar) bidirectional buck/boost DC–DC converter is modelled and simulated in MATLAB/Simulink and Typhoon HIL Schematic Editor. It is tested for real time performance using Typhoon HIL 402, in Virtual HIL and Real Time HIL platforms. Both virtual and real time HIL results go hand-in-hand with MATLAB Simulink results. Dynamic conditions of sudden change in dc loads, solar irradiation variations are analyzed for both buck and boost mode of operations. DC grid voltage is regulated at 300V, unbalance in the dc bus voltages ($V_{C1,}V_{C2}$) are mitigated and balanced at ±150V. Maximum power is being extracted from both PV sources in correspondence with the irradiation level. Proposed converter with model predictive control technique gives faster response (less than 0.5sec) and lesser ripple in mitigating the voltage unbalance and grid voltage regulation issues arising in bipolar dc microgrid during transient conditions within the power ratio limit $0.9 \geq$ —Pload/Pg— $\leq$ 1.1. Hence, MPC proves to be an efficient, powerful, and faster control technique for optimal power conversion. As future work, instead of EV battery, electric vehicle fast charging stations can be modelled and integrated using proposed bipolar bidirectional buck/boost converter. V2G & G2V operations between bipolar dc microgrids and EV charging stations as well as management of other power quality issues arising in bipolar dc microgrids can be further investigated .

- Developed model predictive control of TLC to meet control objectives; voltage regulation, voltage balancing, mppt tracking and bidirectional power flow.
- Performance study through simulation and hardware in loop validation of proposed MPC controller and energy management strategy.
- Effective decentralized control of all the components of multi-node bipolar dc microgrid (BESS, PV, dc loads and EV charging loads).
- Efficient and faster voltage balancing, grid voltage regulation and power sharing achieved within 0.2sec in multi-node bipolar dc microgrid under dynamic conditions

Chapter 4

Modelling of EV load Profile and V2G/G2V Energy Management

4.1 Introduction

In this chapter, the architecture of bipolar dc microgrid with electric load profile is described followed by its decentralized model predictive control. Extensions of multi-port three level converter suitable for connecting charging stations to bipolar grid is also proposed. An ev charging load profile, for different categories of vehicles is also is modelled and integrated to the bipolar dc grid with V2G/G2V control. The simulation results for operation and control of the multi-node bipolar dc grid with ev loads is detailed with transient and steady state analysis.

4.2 Bipolar DC Microgrid Integrated with EVCS

The overview of the proposed bipolar DC microgrid integrated with EV charging profiles taken into consideration is depicted in fig.4.1. Bipolar dc bus voltages are taken as +200V, 0, -200V. Lower rating loading can be connected between +200 V and 0 or -200V and 0, heavy loads can also be connected directly to 400 V. Power generated in the microgrid is provided by two solar photovoltaic units. An energy storage system is required to regulate the surplus/ deficient energy demand in the grid, which can be a battery energy storage or hybrid energy storage system with

bidirectional converters (Sharaf and Şahin, 2017).

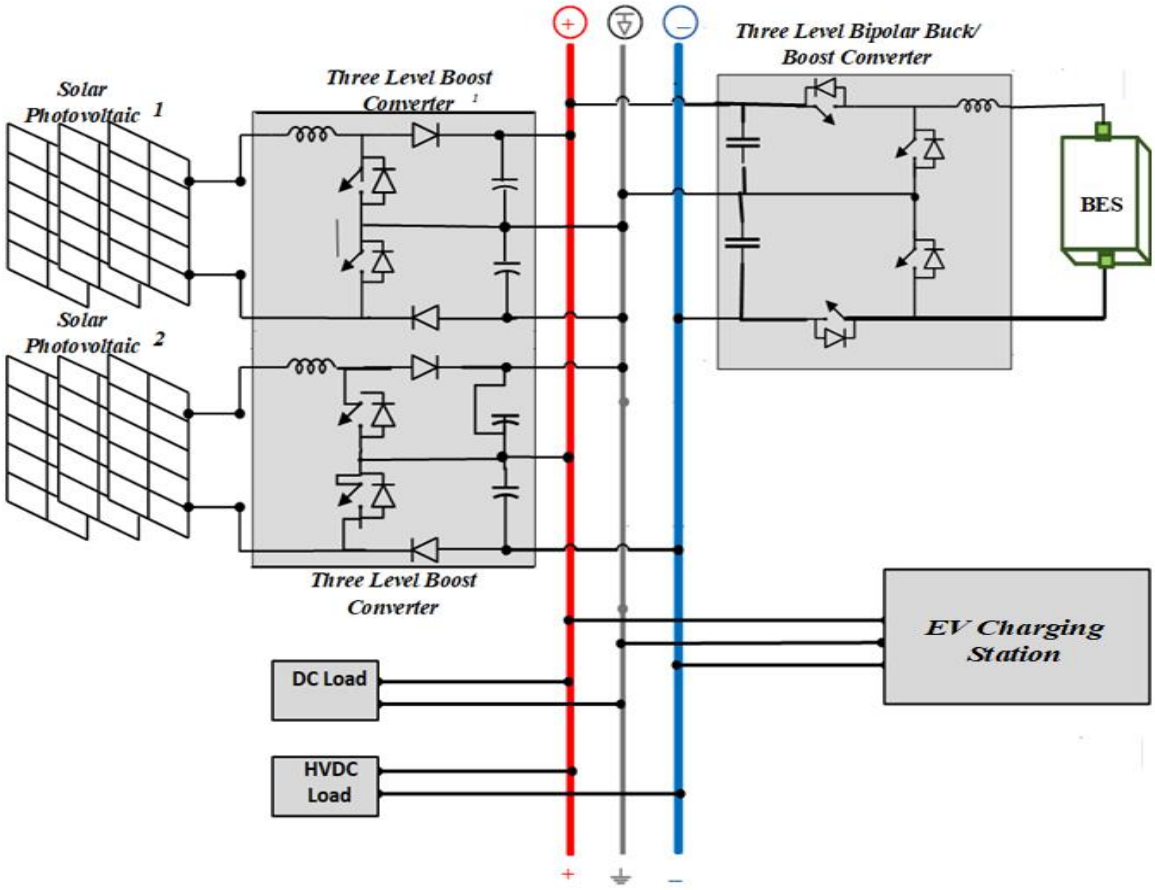

Figure 4.1: Architecture of the proposed system.

Two PV generation units PV_1, and PV_2 rated at 16kW, 190V, 80A is taken as the power feeding units to the bipolar DC microgrid. PV converters are needed to extract the maximum power from the PV units. Three-level boost converters (TLBC) are used to interface PV systems to bipolar DC microgrids. Instead of a normal boost converter, a three-level boost converter is used so the power from each generation unit can be fed equally to both poles of the bipolar DC grid. This converter has two switches in series which reduce the voltage stress across the switch by half. Another advantage of using a three-level or bipolar converter is capacitance-voltage balancing; i.e. if properly switched, the voltage imbalance between two poles due to unbalanced generation or loading can be eliminated. The circuit diagram of TL-Boost converter is given in fig.2.6. The modes of operation of TL boost converter is depicted in fig.2.7.

A battery energy storage (BES) system of 15kWh, with terminal voltage 150V

is developed as auxilliary storage. It is used to bridge the power gap that occurs between load (ev charging load and dc load here) and generated power(pv power and ev discharge power). It is connected to grid with three level buck/boost bidirectional converter which enables bidirectional power flow. To balance the capacitance-voltage at the bipolar terminals and regulate the grid voltage, this converter is used. The circuit diagram of TL bidirectional converter is given in fig. 2.8. The modes of operation of TL bidirectional converter is depicted in fig. 2.9.

Varying DC loads is connected to bipolar grid and range between 8kW-32KW. Resistive loads of 5-20 ohm are connected as dc loads and sudden variation of this dc loads are given by circuit breaker opening and closing in the simulation. An EV charging station with charging load profiles of maximum 45kW is modelled and integrated to grid with multi-port three level converters. The charging station can be connected directly connected to the grid or through a BESS in between to buffer the load. A three-level bidirectional DC-DC buck-boost combined with multi-interleaved buck converter is used to connect EVCS with bipolar DC microgrid which enables the power flow from the grid to vehicle and vehicle to grid. Using multiple interleaved buck converters, multiple charging terminals are created to connect the EVs. This is detailed more in the below section.

4.3 Multi-port Three level Converter for connecting BESS and EVCS

The charging station can be connected directly connected to the grid or through a BESS in between to buffer the load. A three-level multi-port converter is used to connect EVCS with bipolar DC microgrid which enables the power flow from the grid to vehicle and vehicle to grid. The circuit topology for this multi-port three-level bidirectional DC-DC converter (TL-BiDC) illustrated in fig. 4.2. This configuration is derived by extending TL bidirectional converter with provisions of interleaved inductor. This three-level configuration gives it a bipolar structure with a positive output terminal, a negative output terminal, and neutral in between. This structure has numerous advantages; reduction of voltage stress across the switches by half, inherent capacitance-voltage balancing, multiple output voltage levels, and reduced reverse recovery losses of the anti-parallel diodes. Operational modes, switching pattern, and

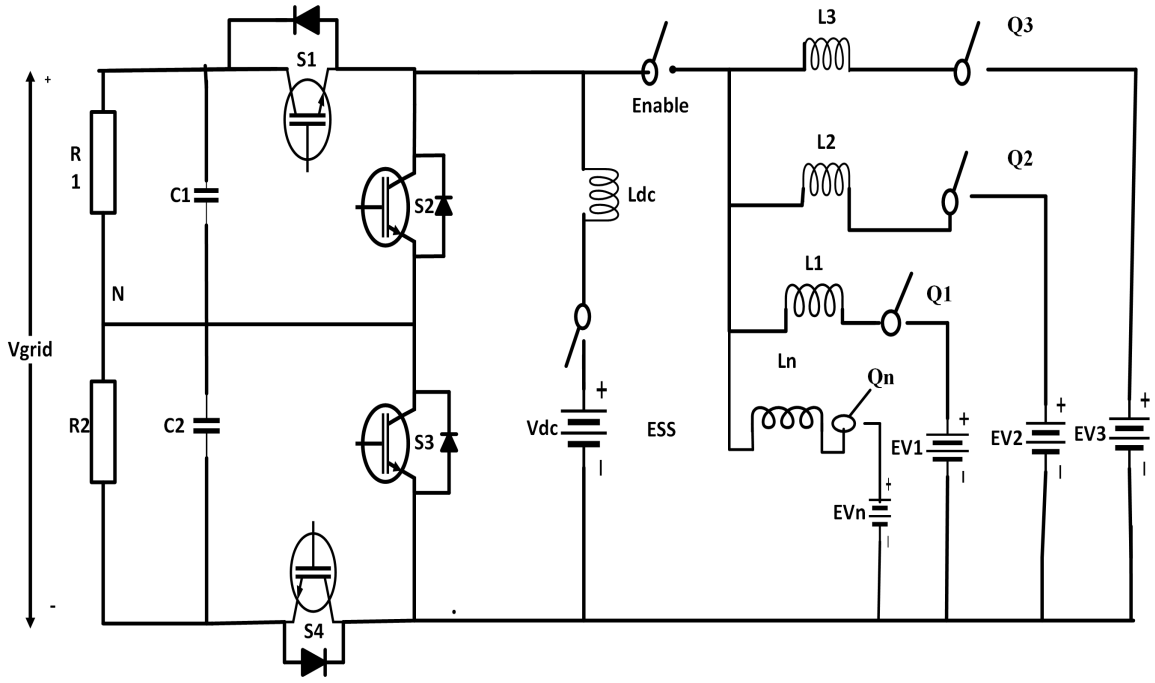

Figure 4.2: Three level bidirectional multi-interleaved buck converter for connecting EVCS/ multiple EVs.

small signal modeling of this converter is similar to that of TL bidirectional converter. Battery energy storage system (BESS) can be connected in between EVCS and grid as buffer storage. Multi-port converters are an advantage when EV charging is considered, whether it is off-board charging, onboard charging, or for powering auxiliary components inside EV (Aden et al., 2021). The configuration of the three-level bidirectional converter (TLBiC) used for connecting the battery energy storage system in parallel is depicted in fig. 4.3 and the multi-interleaved three-level bidirectional converter used for connecting BESS in series is depicted in fig. 4.4. This configuration has multi-output structure due to the interleaving and three-level (bipolar) structure at the input side. This facilitates easier integration to the bipolar dc grid and has voltage balancing capability, which is an inherent feature of a three-level converter. Multi-output structure can be used for connecting multiple EVs in an EVCS with a bipolar grid or for the parallel connection of EVCS and BESS with a bipolar dc grid. Moreover, interleaved inductor incorporated in converter reduce adverse ripple current and circulating current effects.

Design equations of multi- interleaved buck converter (Garcia et al., 2006), (Chen

et al., 2013) is given by eqns. 4.1 - 4.2.

$$L_{int} = \frac{(Vs - Vo). * D}{\Delta I_L * 2f} \tag{4.1}$$

and interleaved inductor value given by L1 = L2 .....=Ln = L_{int}/n.
The capacitor value is given by;

$$C_{int} = \frac{1 - 2D}{32 * L_{int} * (dV/Vo) * f^2.} \tag{4.2}$$

This three-level bidirectional converter can be further extended or modified for parallel and series connection of charging station and BESS. Fig. 4.3 shows the non-isolated multi-port bipolar bidirectional converter configurations with parallel connection with EV charging stations and auxillary battery energy storage. Figure 4.4 shows the non-isolated multi-port bipolar bidirectional converter configurations with series connection with EV charging stations and auxilliary battery energy storage. Advantages of the improved multi-port three level converters are :

- provision of multiple outputs
- Reduced inductor ripple current
- reduced switching voltage stresses
- voltage balancing capability
- controlled V2G/G2V bidirectional power flow

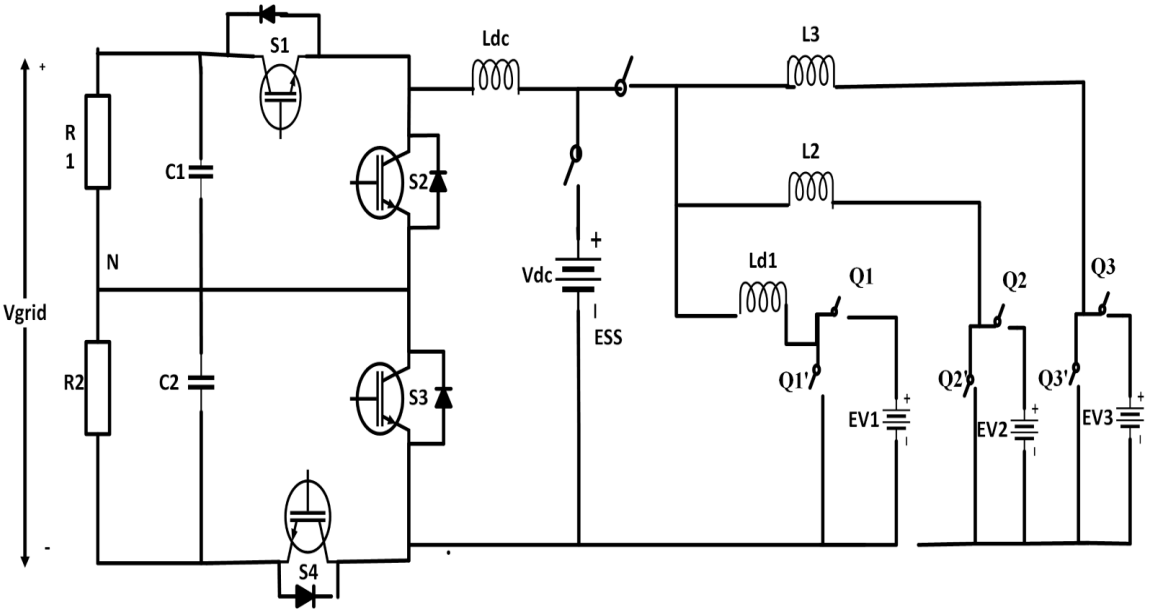

Figure 4.3: Modified Multi-port TLC Configuration for parallel connection of EVCS and BESS

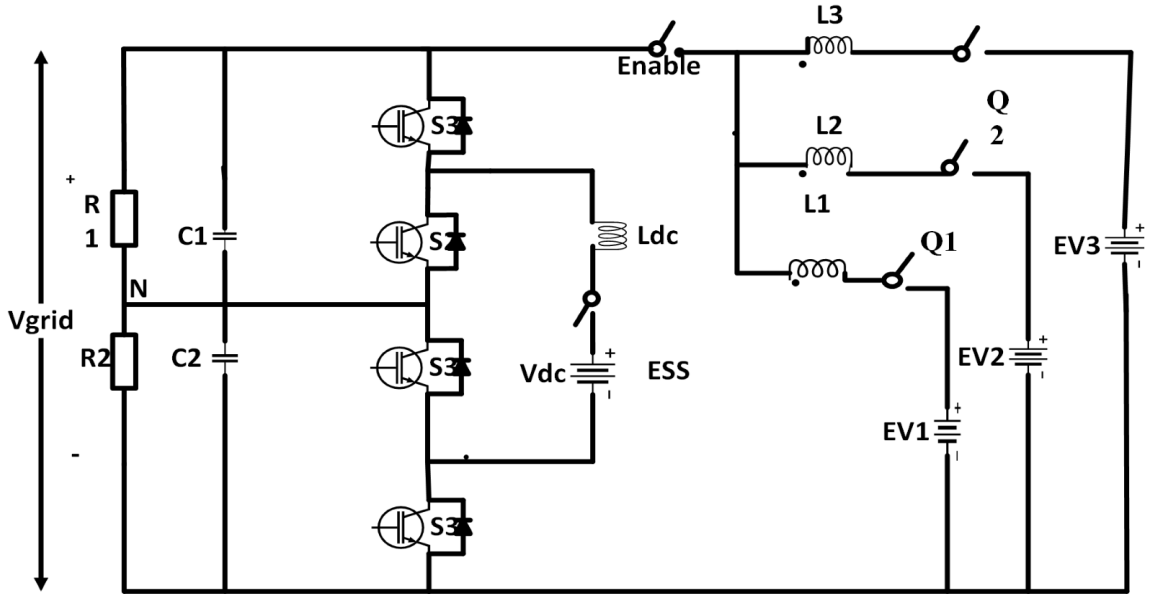

Figure 4.4: Modified Multi-port TLC Configuration for series connection of EVCS and BESS

4.4 Decentralized Model Predictive Control and Energy Management

Non-linear controllers are best suited for the control of real-time dynamic systems. It tends to have more accurate and faster responses. Advancement in computer technology made the implementation of non-linear control methodologies such as adaptive control, sliding mode control, current programmed control, intelligent control such as Fuzzy and Neuro-Fuzzy control, Machine learning etc., relatively simple task. Unlike the linear controllers, non-linear controllers are quite reliable and fast acting for the control of complex, multi-variant systems. Among the non-linear control techniques, model predictive control has wide applications when it comes to applications of power electronics converter. Model predictive control is based on discrete time model of a system. Methods often used for conversion of continuous time model to discrete time model are discretization by matrix transformation, backward Euler's method or forward Euler's method. In this section, the developed discrete models and predictive control of the proposed system is detailed.

Model predictive control (MPC) is emerging as a promising control technique for power electronic converters and electric drive applications due to its intuitive features, easy implementation, easy inclusion of system constraints and nonlinearities, direct inclusion of control parameters into the cost-function etc. Figure 4.5 shows the overall decentralized control techniques used in the proposed system of bipolar DC microgrid. Schematics of model predictive control of three level boost converter for PV and three-level bidirectional buck/boost converter for battery (BESS) is given in fig. 3.3 and fig.3.4 respectively.
The proposed decentralized model predictive control takes care of the following in the proposed system :
i. control of PV systems with maximum power point tracking,
ii. control of BESS with power sharing to and from the grid according to the load demands,
iii. eliminates the voltage unbalance issue with three level bidirectional converter and regulates the grid voltage and enables power sharing,
iv. enables the V2G and G2V controlled power flow between EV charging station and microgrid.

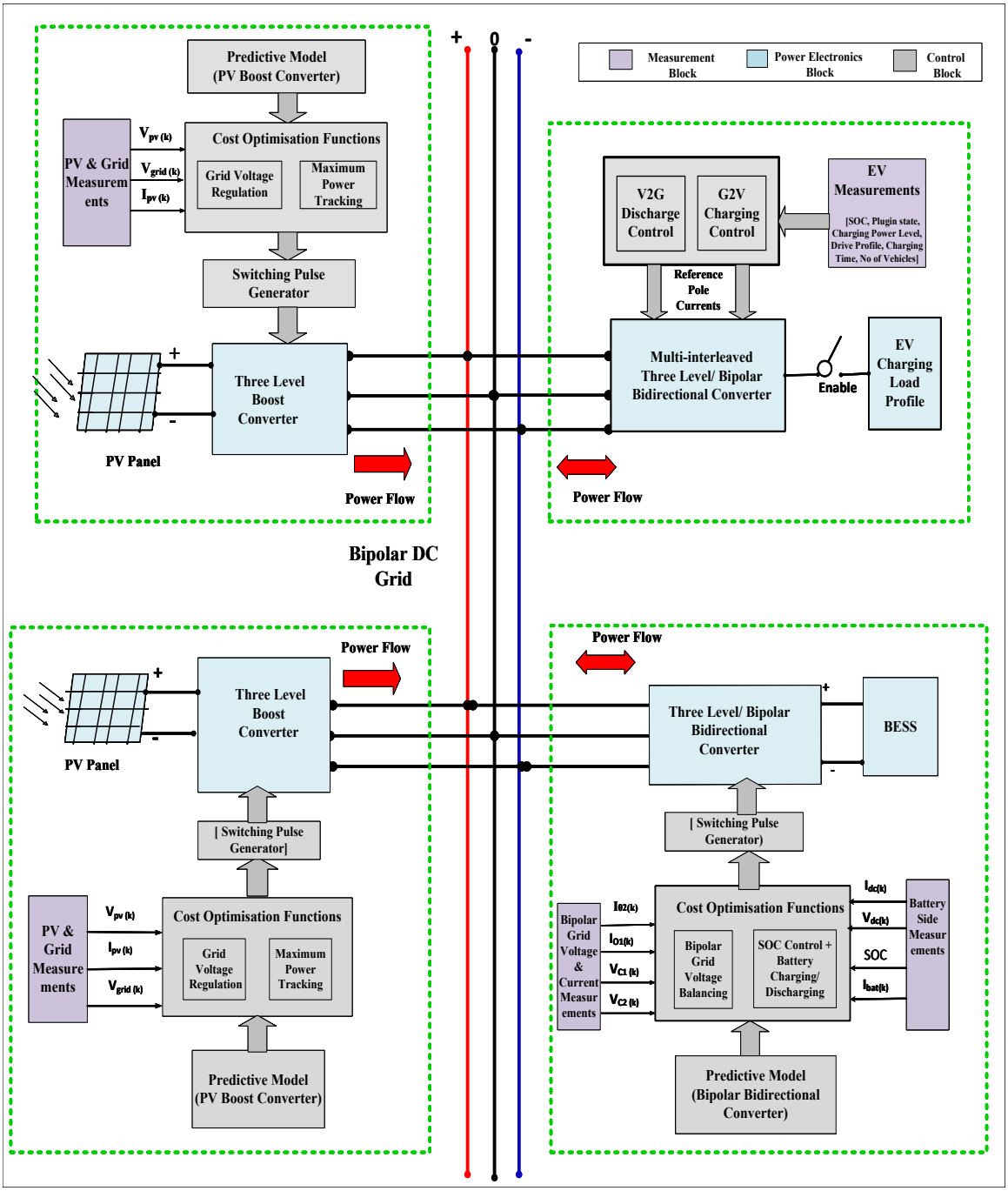

Figure 4.5: Block diagram of complete control of the proposed system: decentralized model predictive control

4.5 Modeling of Charging Load Profile of Multiple Electric Vehicles

4.5.1 Review of ELectric Vehicle Load Models

Charging of electric vehicles is going to be a major electrical load in the near future, as more and more population shift to electric auto-motives from conventional internal combusted engine-powered vehicles. Usually, EV loads are represented by a battery at the load side. The number of EVs that get connected to the grid at any time is highly random and the nature of these loads varies with various factors. Representing EV load as a constant power load (CPL) or by a lumped battery for investigating the real-time impact of EV charging on the power grid is not accurate and will not reflect the actual nature of the EV loads that might get interfaced with microgrid (Haidar et al., 2014). For reliability and safety of grid, (Amara-Ouali et al., 2021), and for effective adaption of EV technology, (Xiang et al., 2019), the challenges in EV charging control and EV charging load modeling need to be addressed. In certain literature, EV loads are modeled for power system numerical simulation considering EV quantities, initial state-of-charge distributions, load change processes during charging, and the effect of grid side parameters(Fan et al., 2015). In (Haidar et al., 2014), a multistage time-variant EV load modeling based on polynomial/mathematical function is used and implemented constant impedance-constant current-constant power (ZIP) model on the IEEE test bus system. An accurate EV load model is developed by determining the relationship between power consumption by EV, grid voltage and state of charges of fast charging EV load Battery charging behavior thus obtained is fitted on standard exponential load model and compared with ZIP load and CPL load model. The exponential load model is a better representation of fast-charging EV load than the existing CPL model (Shukla et al., 2018). Data obtained by measuring current and active power under different operating conditions of EVCS connected to IEEE-13 bus is also taken as EV load model (Gil-Aguirre et al., 2019). The load model of different charging stations based on the probability distribution of characteristic variables in a trip chain is established (Gong et al., 2017) and solved by the Monte Carlo Simulation method in some recent works. EV load models so far discussed in literature are power system based models and cannot be connected as loads to analyze the effectiveness of the controller and power converters in EV charging control. So

we need to develop an EV load model which can be connected to power electronic converters.

4.5.2 Modelling of EV Load Profile

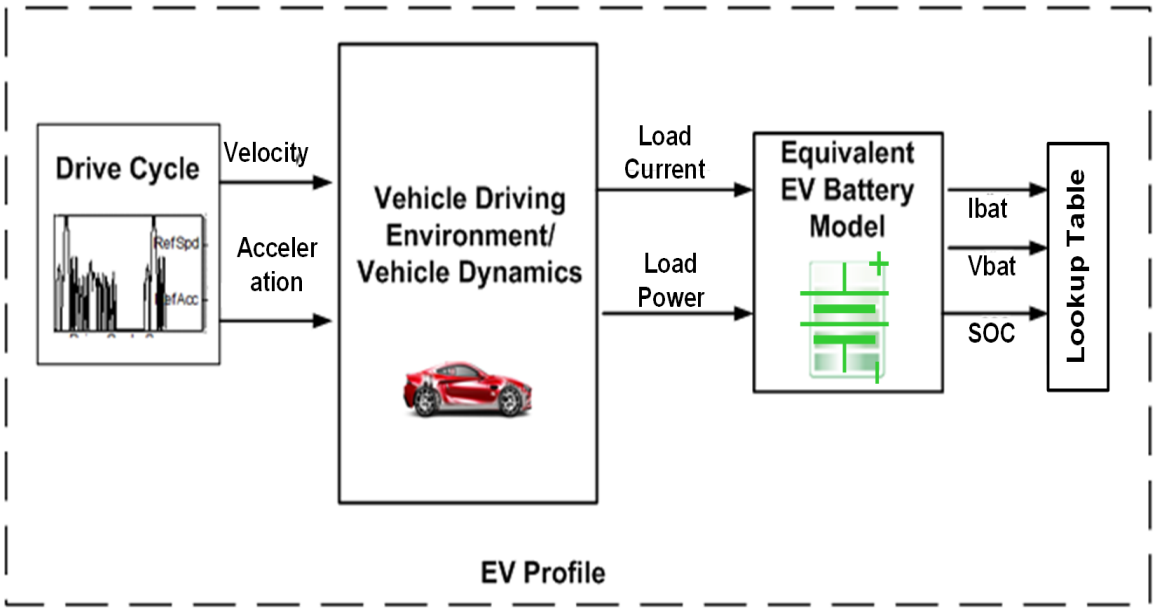

Figure 4.6: Modelling of EV load profile

Fuel economy, driving range, and equivalent emissions of diesel and petrol vehicles can be assessed by testing under different driving cycles and ambient conditions (Jehlik et al., 2015). Similar way, EV energy consumption can be estimated by analyzing real-world driving cycles (Zhao et al., 2020). Combining these ideas, an EV load profile is developed here which reflects the variations of the driving cycles and EV battery conditions. A charging profile of multiple EVs connected to the grid at random intervals of time is developed, which reflects the variations of the driving cycles and (FTP-75,IDC,WLTP,HWFET) along with specific vehicle dynamics (drag coefficient Cd, frontal area Af, mass M) and resultant EV battery conditions (eg: state of charge, battery capacity, charging power). Schematics of developed EV load profile is given in fig. 4.6. The state of the EV battery is highly dependent on driving behavior and vehicle dynamics. So we categorized vehicles into different types as EV1-passenger vehicles, EV2-goods carrier vehicles, EV3-three wheelers, EV4-trucks.

Respective vehicle dynamics like drag coefficient Cd, frontal area Af, mass M etc is given to each category of vehicle. Drive cycle followed for testing each category of vehicle is assigned to the respective vehicle model. Then analyzed the effect of the different driving cycles on the battery equivalent circuit model of the respective vehicles to produce actual equivalent charging load profiles of EVs that might be encountered by microgrids in the future. EV load is constrained to be within 60kW. Tbl.4.1 gives the number and type of EVs taken for the study.

Table 4.1: EV Profile.

Cluster	Drive Cycle	Vehicle Dynamics	No.of Vehicles
EV1	FTP-75	Cd=0.38, W=1200kg, Af= 1.8m^2	3
EV2	WLTC	Cd=0.19, W=1500kg, Af= 1.8m^2	2
EV3	IDC	Cd=0.44, W=700kg, Af= 2.09m^2	4
EV	HWFET	Cd=0.74, W=2500kg, Af= 3.2m^2	1

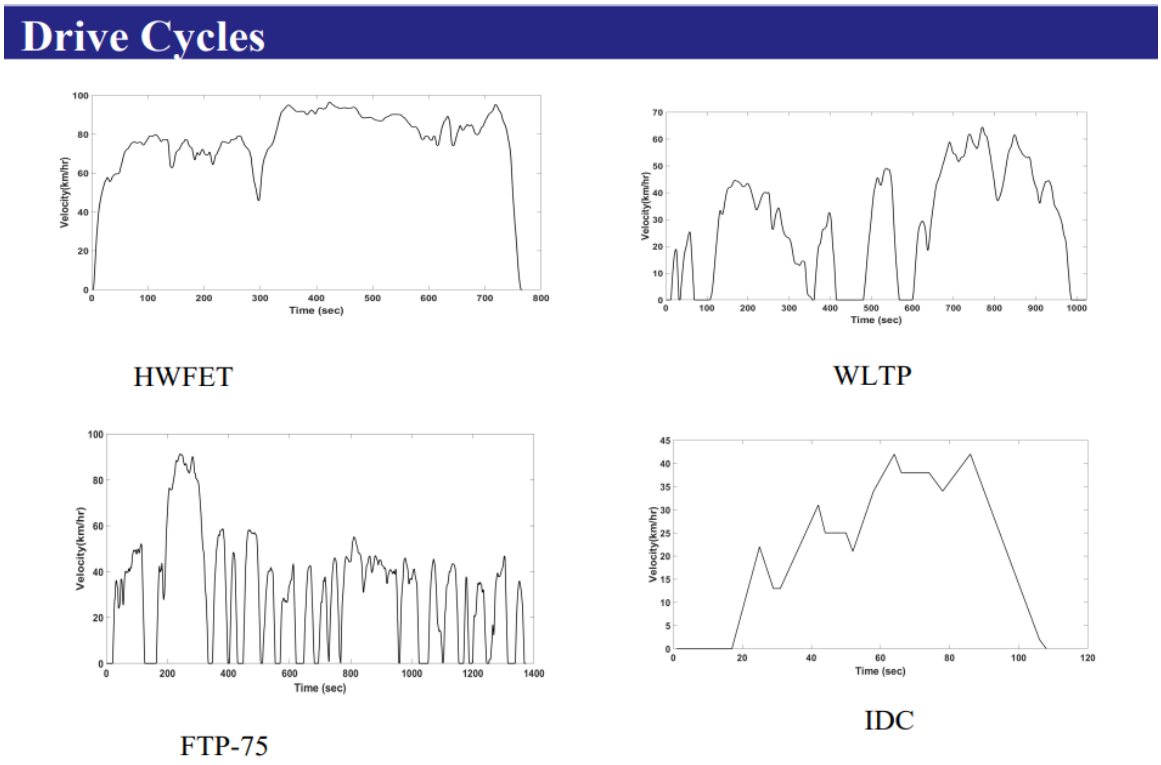

Figure 4.7: Drive cycles

The standard drive cycles recognized internationally for testing fuel efficiency like Federal Test Procedure (FTP-75), Worldwide Harmonised Light Vehicle Test Pro-

cedure (WLTP), Highway Fuel Economy Test (HWFET) and Indian Driving Cycle (IDC) (refer 4.7 is given as input to the vehicle dynamics model for each cluster of EVs.

Vehicle dynamics model developed in MATLAB can be referred in 4.9. From the vehicle model, required load current and power needed at each instant is retrieved and fed to the equivalent EV battery model (reference for model vehicle in each sector given in A.2 and A.1 in appendix). The EV battery parameters ($V_{bat}, I_{bat}, \& SOC$) thus obtained is taken as EV charge demand profile for each cluster of vehicles. This can be stored in a lookup table as EV load profiles and used for further simulation studies. Battery capacity and voltage of different segments of vehicles is given tbl. 4.2.

Table 4.2: Vehicle Segments and Battery Capacity

Vehicle Segment	Battery Capacity	Battery Voltage
E-2W	1.2kWh-3.3kWh	48-72V
E-3W	3.6kWh -8kWh	48-60V
E-Cars (1st Gen)	21kWh	72V
E-Cars (2nd Gen)	30-80kWh	
Trucks	80-200kWh	350-500V

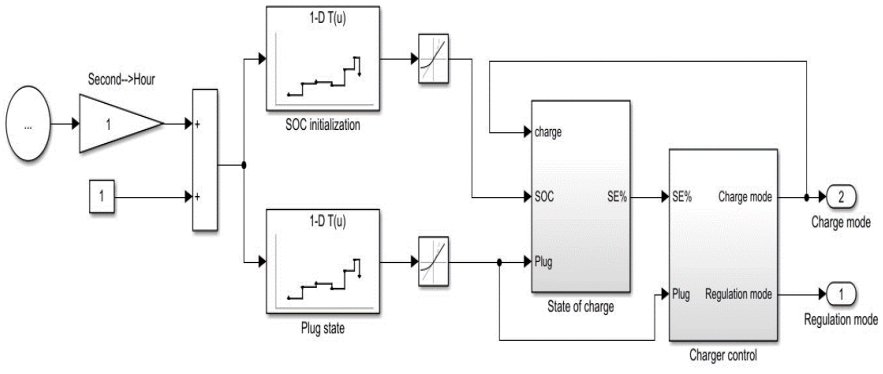

Figure 4.8: EV Battery Model in Simulink

Figure 4.9: Vehicle dynamics model in simulink

4.6 EVCS Charging and Grid Regulation Control

The schematics of the control strategy used for the connection and operation of EV charging profiles with the bipolar grid is illustrated in Fig. 4.10. EVs connected to grid can be used in G2V mode, i.e taking power from grid for charging EVs or in G2V mode, i.e feeding back power from EV to grid. Hence, there is separate control algorithm for G2V/Charging control and V2G/Grid regulation control. The connection between a particular car profile and the bipolar grid is enabled by a plug-in enable signal and V2G/G2V mode selection based on the SOC of the EV battery and plug-in state, which is illustrated in Fig.4.11.a. The number of vehicles available for charging and the number of vehicles available for feeding power back to the grid at each instant is obtained from the V2G/G2V mode selection module. If $SOC_{ev} < 85\%$, then G2V mode or charging of EV battery and $SOC_{ev} > 90\%$, then V2G mode or discharging EV power fed to the grid. Vehicles assigned with V2G mode are subjected to the V2G discharge/grid regulation control. Vehicles assigned with G2V mode are subjected to the G2V charging control. Vehicles assigned with V2G mode are subjected to the V2G regulation control.

The flowchart and control diagram for mode selection and charging/regulation

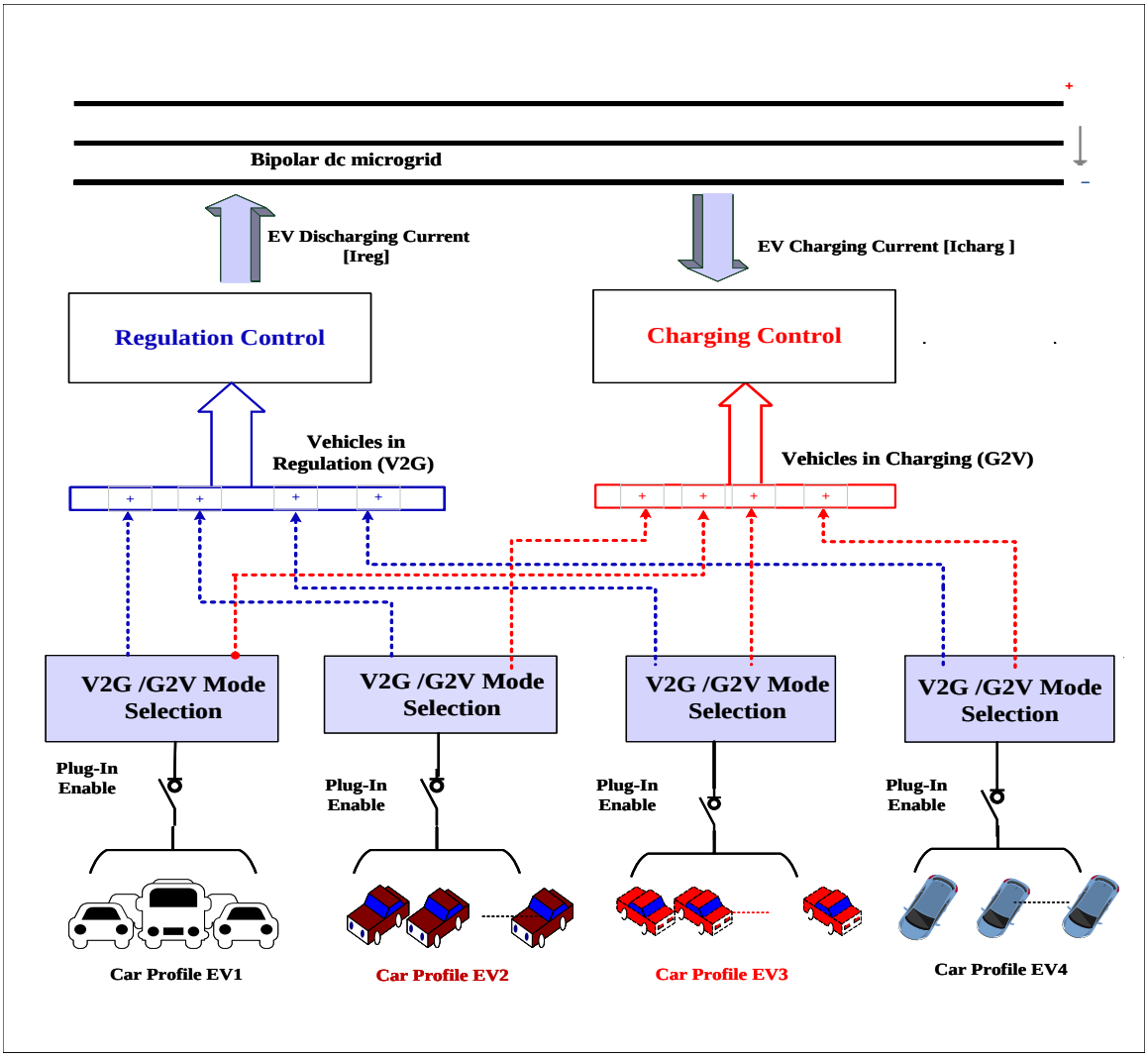

Figure 4.10: Schematics of complete control of EV charging load profile

control is detailed in Fig.4.11.b. In regulation control, the power available for discharge to the grid from each EV load profile is calculated and reference regulation current is found out. The regulation current I_{reg} is split on the ratio load demands on the respective pole and total load power as I_{reg1}=$\frac{P_{load1}}{P_{load}}$ and I_{reg2}=$\frac{P_{load2}}{P_{load}}$. Vehicles assigned with G2V mode are subjected to the G2V charge control. In this, the power required by each EV profile for charging to the grid is calculated and the charging current is found. The charging current, I_{charg} is split on the ratio of generated power fed on the respective pole and total generated power fed by PV system as I_{charg1}=$\frac{P_{gen1}}{P_{gen}}$ and I_{charg2}=$\frac{P_{gen2}}{P_{gen}}$. Splitting the charging and regulating currents this way, ensures

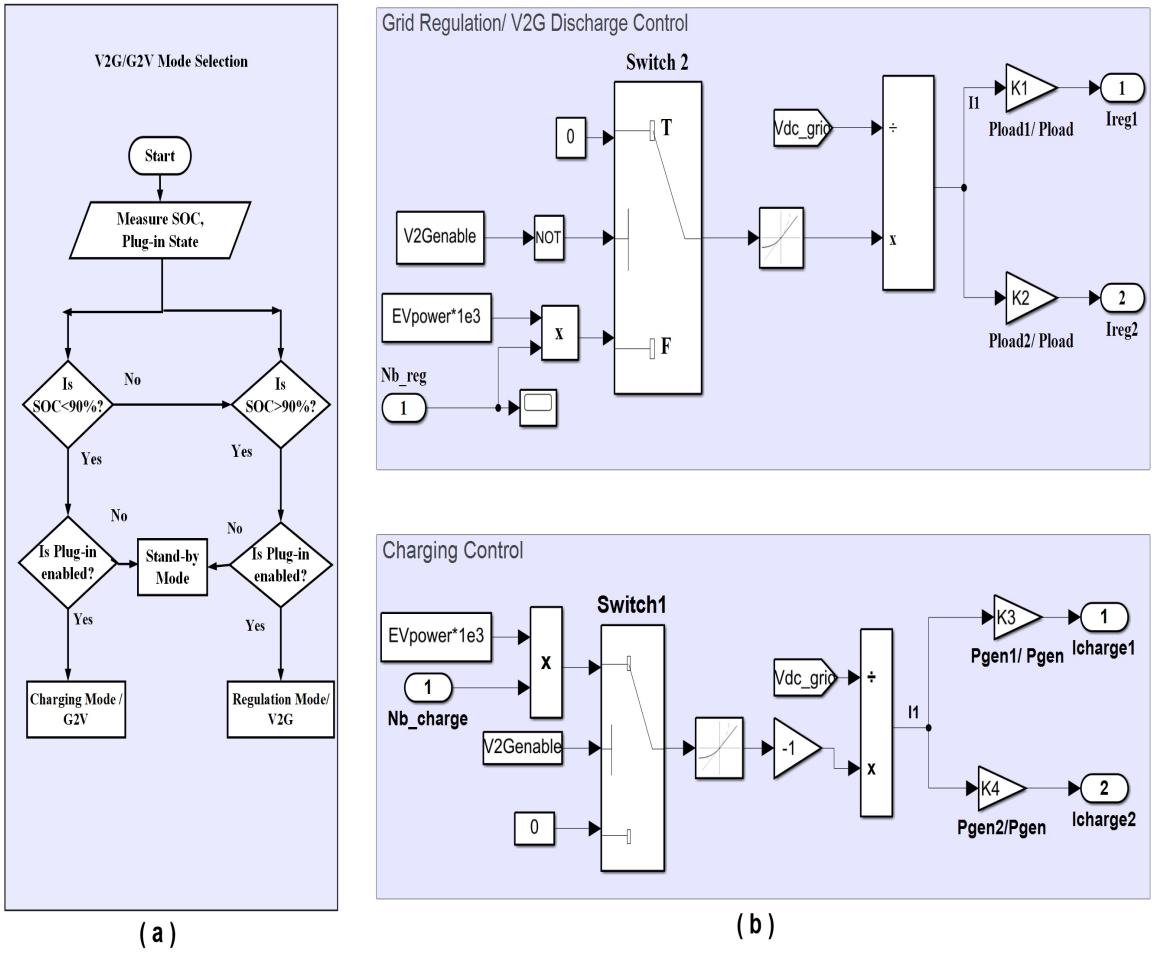

Figure 4.11: a) V2G /G2V charging control b) Grid regulation control

EV current fed to both poles of the bipolar dc microgrid will be distributed equally and proportionately.

4.7 Simulation Result Analysis

The model of the proposed multi-node bipolar DC microgrid including the complete decentralized predictive control is established and validated in Matlab/Simulink environment. EV charging load profile is modeled and simulated based on different driving cycles, vehicle parameters, and battery parameters so that it would emulate effectively EV load variations that might be added to the grid in the future. A total of 10 EVs of four different car profiles are connected in EVCS here for the simulation

study. Based on the SOC conditions detailed in Section 3.3, G2V mode (charging of EV from the grid) or V2G mode (discharging EV battery to feed power to the grid) is enabled.

Table 4.3: Simulation Parameters

Parameter	Specification
Photovoltaic Systems PV-1, PV-2	16kW, 195V, 82A
Battery Cell model	3.7V ,4.2Ah, Li-ion Cell
Terminal Battery Voltage,V_{bat}	150V
Battery Capacity	15kWh
Grid voltage V_{grid}	400V
Bipolar Voltage Level, V_{C1}, V_{C2}	200V
Inductance at battery side, L_{dc}	15mH
Inductance at PV side, L_{pv}	12mH
DC link capacitance ,C_1, C_2	$2500\mu F$
Sampling Time, Ts	$10\mu s$

A simulated waveform from the EV load profile is shown in Fig. 4.12, from which I_{EV} represents EV load current distributed between terminals of the DC grid, V2G-power represents the net EV power available from the connected EVs for grid regulation, G2V-power indicates the net EV power demanded by the connected EVs, and n_{EV} represents the number of vehicles connected for charging and discharging. Parameters and specifications used for the simulation study are given in Table 4.3.

4.7.1 Steady State Analysis

The bipolar DC microgrid system with proposed decentralized predictive control is modeled and developed in MATLAB/Simulink. For the simulation study of the proposed bipolar DC grid, solar photovoltaic systems PV-1, and PV-2 are exposed to the same solar irradiance level and equal DC loads under steady-state operating conditions. Under these steady-state conditions, the voltage balance across grid capacitance V_{C1} and V_{C2} is to be maintained in accordance with changes in generated PV power and load demand. BESS is driven to charging/discharging mode by three level-bidirectional converters considering the state of charge conditions of the battery, PV power generated P_{gen}, and power demanded by load P_{load}. Steady-state operation results are given in the fig. 4.13 and 4.14.

For analyzing the operation of the system under boost mode, solar irradiation is

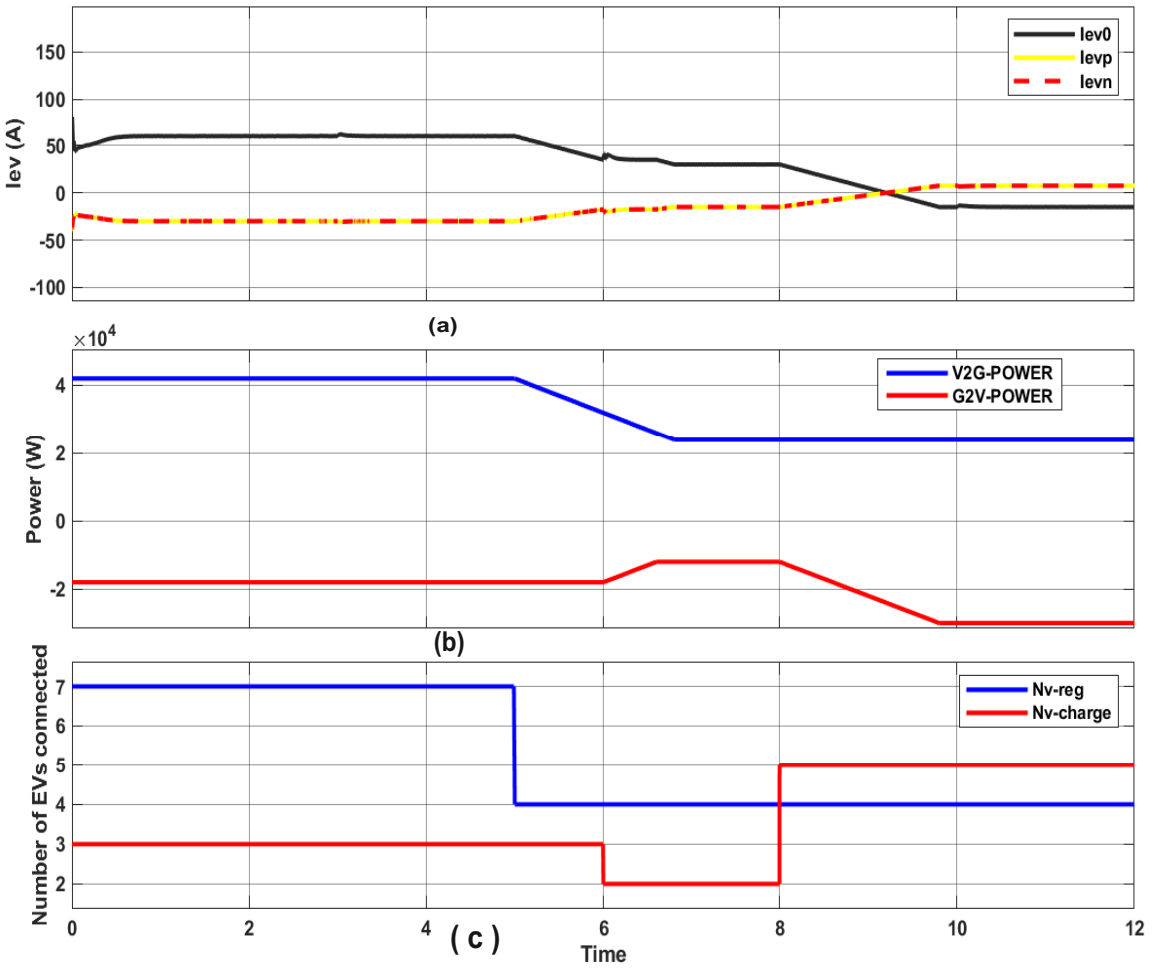

Figure 4.12: EV load profile: resultant waveform. a) I_{EV} b) P_{EV} c) n_{EV}

kept at 300 W/m^2 (4.5kW) and a DC load of 8kW is connected on each bus. Hence, the total load demand is (16kW) greater than PV-generated power (9kW). Hence, battery and EV loads in V2G mode provide the deficient power of 7kW by boost operation of the three-level bi-directional converter as shown in fig. 4.13.

For analyzing the operation of the system in buck mode, initially PV irradiation is kept at 1000 W/m^2 (15kW) and a DC load of 8kW is set at each pole. The total load power needed is 16kW. The rest of the power (14kW) is taken up by the battery and the EV loads in G2V mode as shown in fig.4.14. Simulations carried out in the bipolar DC microgrid system under steady state also observe the following: i) TL Boost converter obtaining maximum power from PV-1, and PV-2, ii) TL Bidirectional Buck/Boost Converter with BESS balancing pole voltages and sharing power.

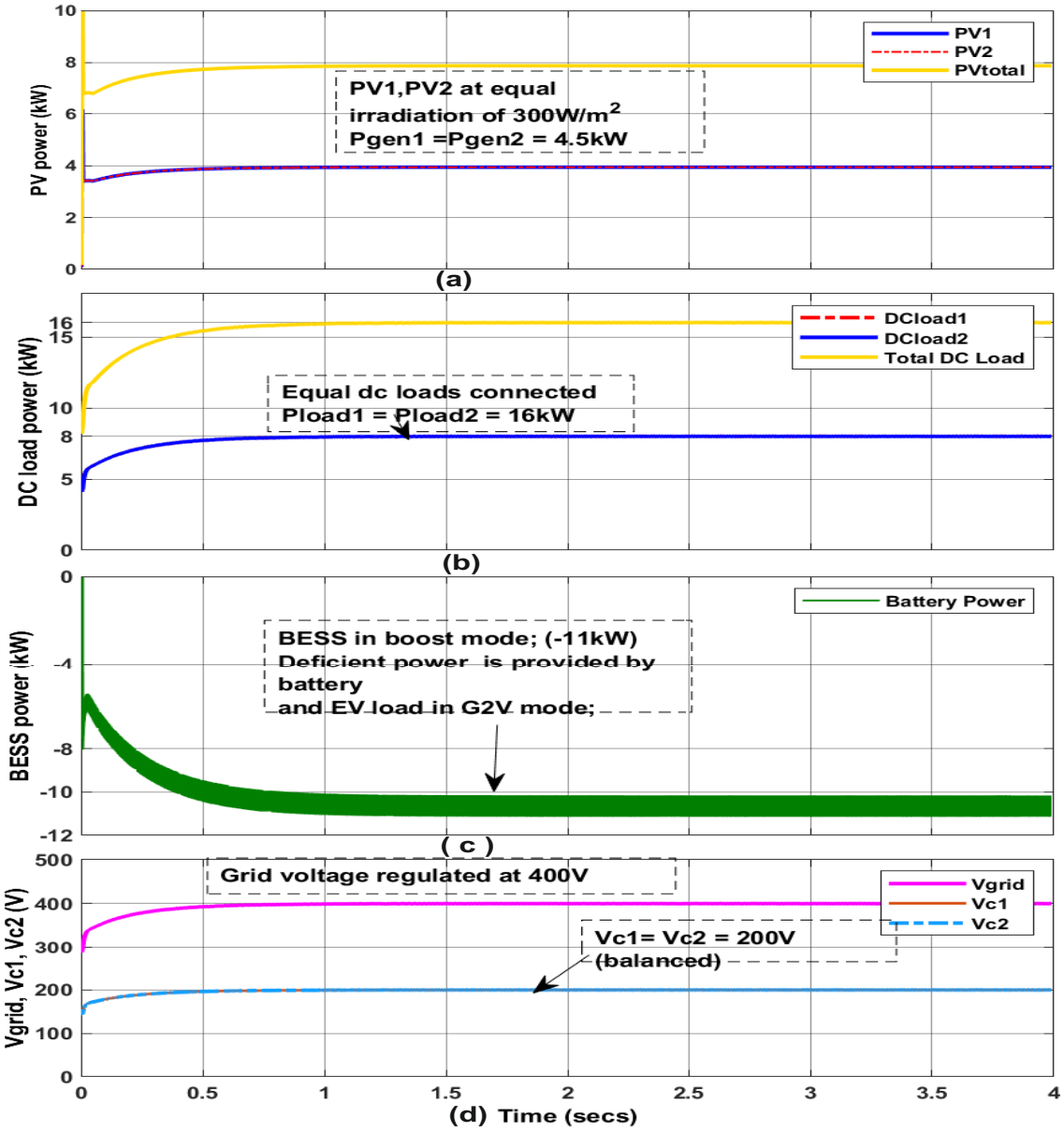

Figure 4.13: Steady state operation in boost mode: resultant waveforms a) P_{gen} b) P_{load} c) P_{bat} d) V_{grid}, V_{C1}, V_{C2}

4.7.2 Dynamic State Analysis

Bipolar DC microgrids connected to solar photovoltaic systems PV-1, and PV-2 are subjected to dynamic conditions like fluctuation in solar irradiance, sudden changes in connected DC load, and changes in the EV load profile connected. EV profile waveforms are given in fig. 4.12 and the complete output waveform is given in fig.

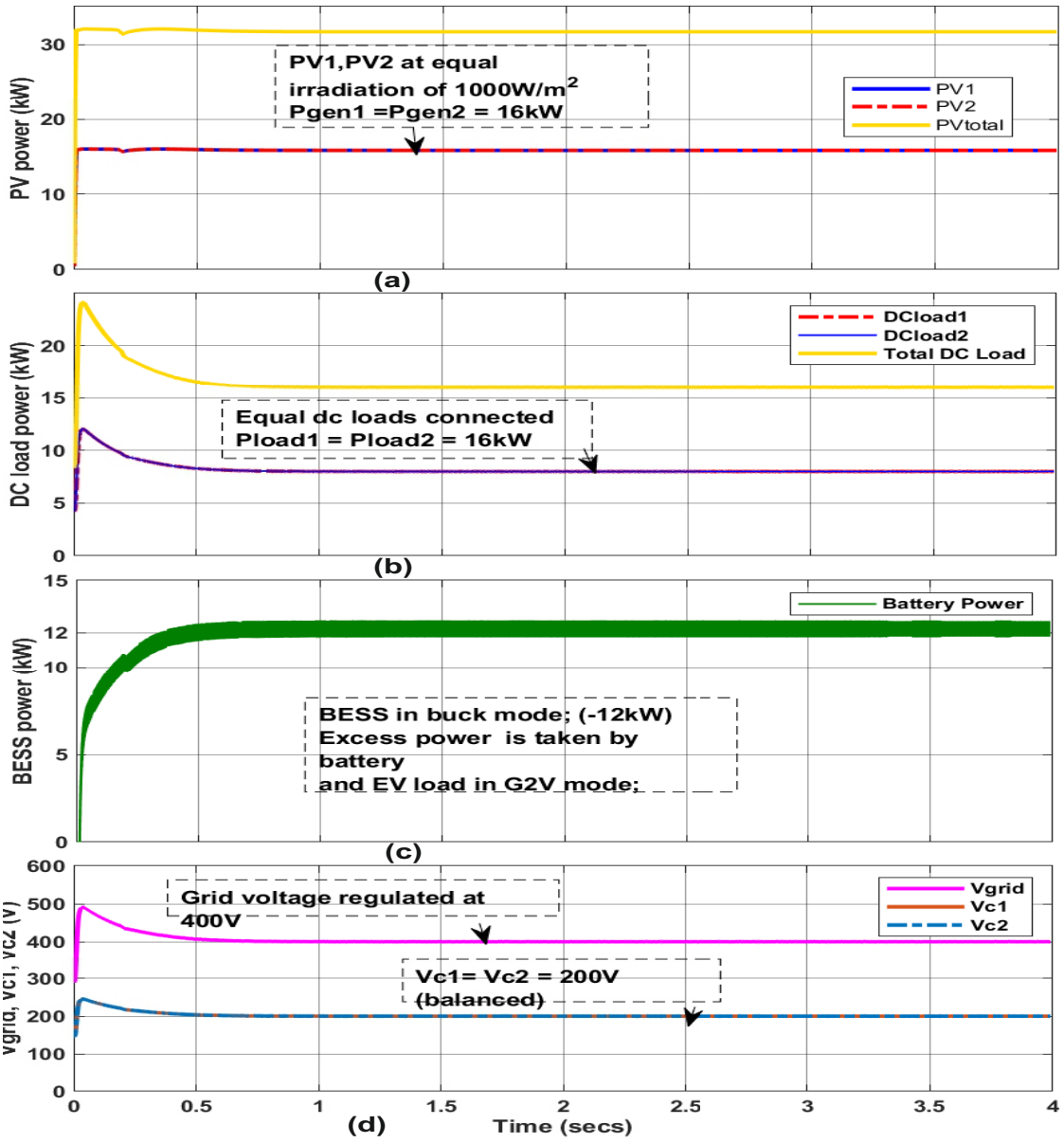

Figure 4.14: Steady state operation in buck mode: resultant waveforms a) P_{gen} b) P_{load} c) P_{bat} d) V_{grid}, V_{C1}, V_{C2}

4.15, with transients conditions of sudden load change (50% load increase) triggered at t= 3sec, solar irradiance change (50% decrease of PV generation) initiated at t= 6s, varying EV loads given at t=8sec and solar irradiance change (50% increase of PV generation) at t=10sec. It can be inferred from the simulation results that, power and voltage quality issues occurring during transients are mitigated within a

short period of time (within 0.2s). Grid voltage sag, swell, and capacitance-voltage imbalance is eliminated with efficient power sharing between subsystems of the bipolar DC microgrid with decentralized MPC control.

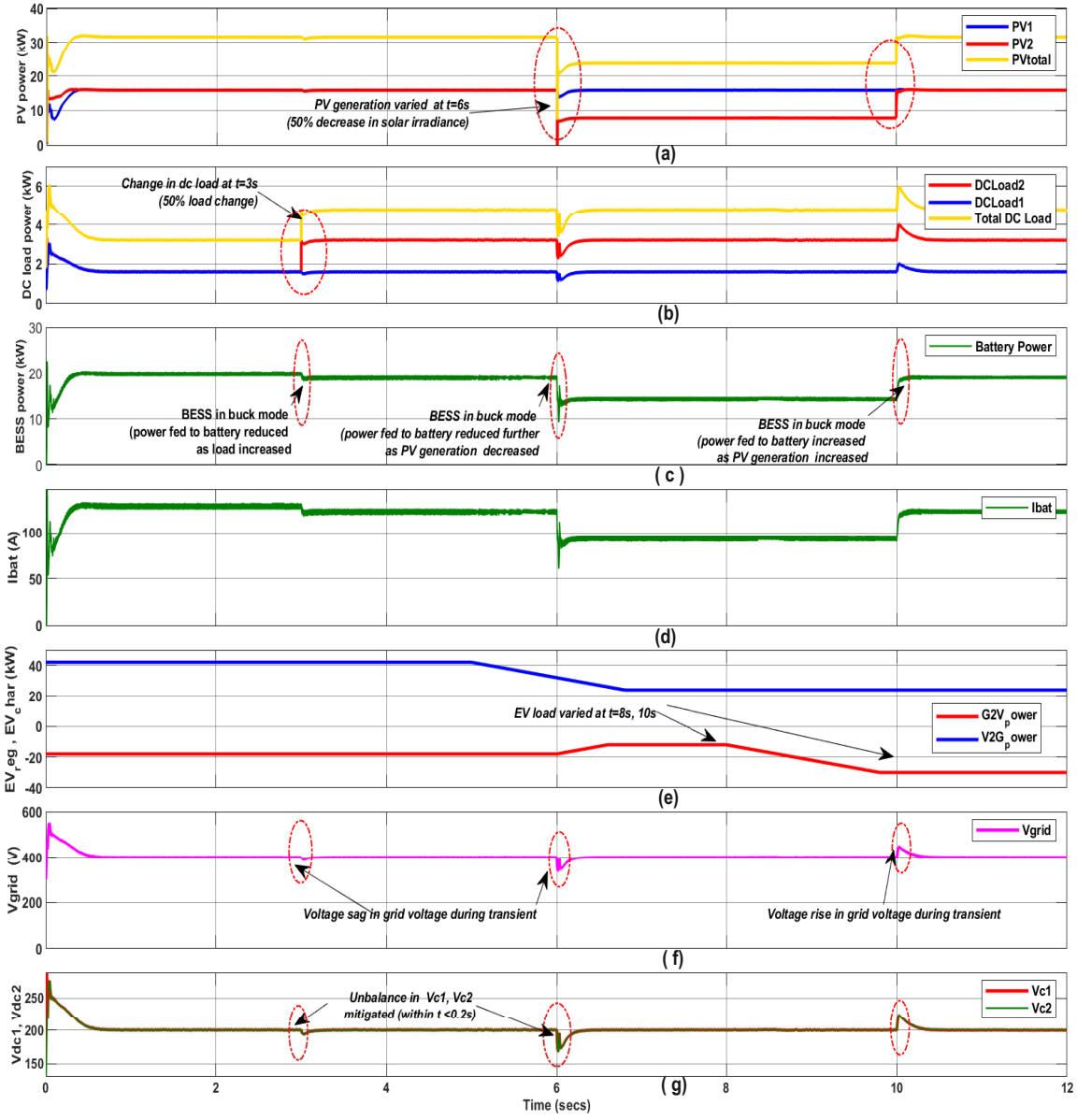

Figure 4.15: Simulation resultant waveform for transient conditions in bipolar grid a) P_{gen} b) P_{load} c) P_{bat} d) I_{bat} e) EV_{power} f) V_{grid} g) V_{C1}, V_{C2}

Case I: Sudden change in connected DC loads

The simulation results obtained for the operation of the proposed bipolar DC microgrid under transient conditions created by sudden variation in DC loads are given in fig. 4.16. DC load-1 is changed from 1.6kW to 3.2kW at t=3s and DC load-2 is kept at 1.6kW. The irradiation level is 1000W/m^2 with a corresponding maximum power of 16kW extracted from each PV system. Total PV power fed to the grid is 32kW and power demanded by DC loads is 4.8kW. Power demand from EV charging stations is 24kW and EV power available for regulation from EVCS is 42kW. i.e. net EV power is 18kW. This is consumed taken by BESS. TL-Bidirectional converter operates in voltage balancing buck mode and BESS charges with I_{bat}=120A. Whenever the load demand power in a DC bus goes down, there occurs a sudden surge in the grid capacitance voltage of that respective DC bus. Similarly, when the load demand power increases, there will be a dip/sag in the grid capacitance voltage of the corresponding bus. The use of battery energy storage acts as a buffer to bridge the power difference and the bidirectional power flow between the battery and the grid is made feasible by the TL-bidirectional converter. From fig. 4.16, it is observed that a change in load demand (50% increase in DC load-2) at t=3sec, causes grid voltage, V_{grid} to dip around 385V, pole capacitance-voltage V_{C1}, V_{C2} dip around 192V and high ripple in battery current. It is also obvious from the above result that pole capacitance-voltage V_{C1}, V_{C2} become balanced at ±200V, and bipolar DC grid voltage, V_{grid} is maintained constant at 400V within a time span of t= 3.15s, i.e. model predictive control is able to achieve faster voltage balancing, grid regulation and stable operation of the bipolar grid.

Case II.: Changes in solar irradiance level

The simulation results obtained for the operation of the proposed bipolar DC microgrid under transient conditions created by sudden variation in PV irradiance level are given in figure 4.17. DC load of 3.2kW and 1.6kW is connected to the bipolar grid. Solar irradiance of 1000W/m^2 is made available on both PV panels initially, giving out a power of 15kW each. At t=6s, solar irradiation at PV-2 is decreased to 500W/m^2 (8kW). Total PV generation is 24kW. The net power demand from the EV charging station is 12kW(36-24kW). This power is taken up by BESS, which

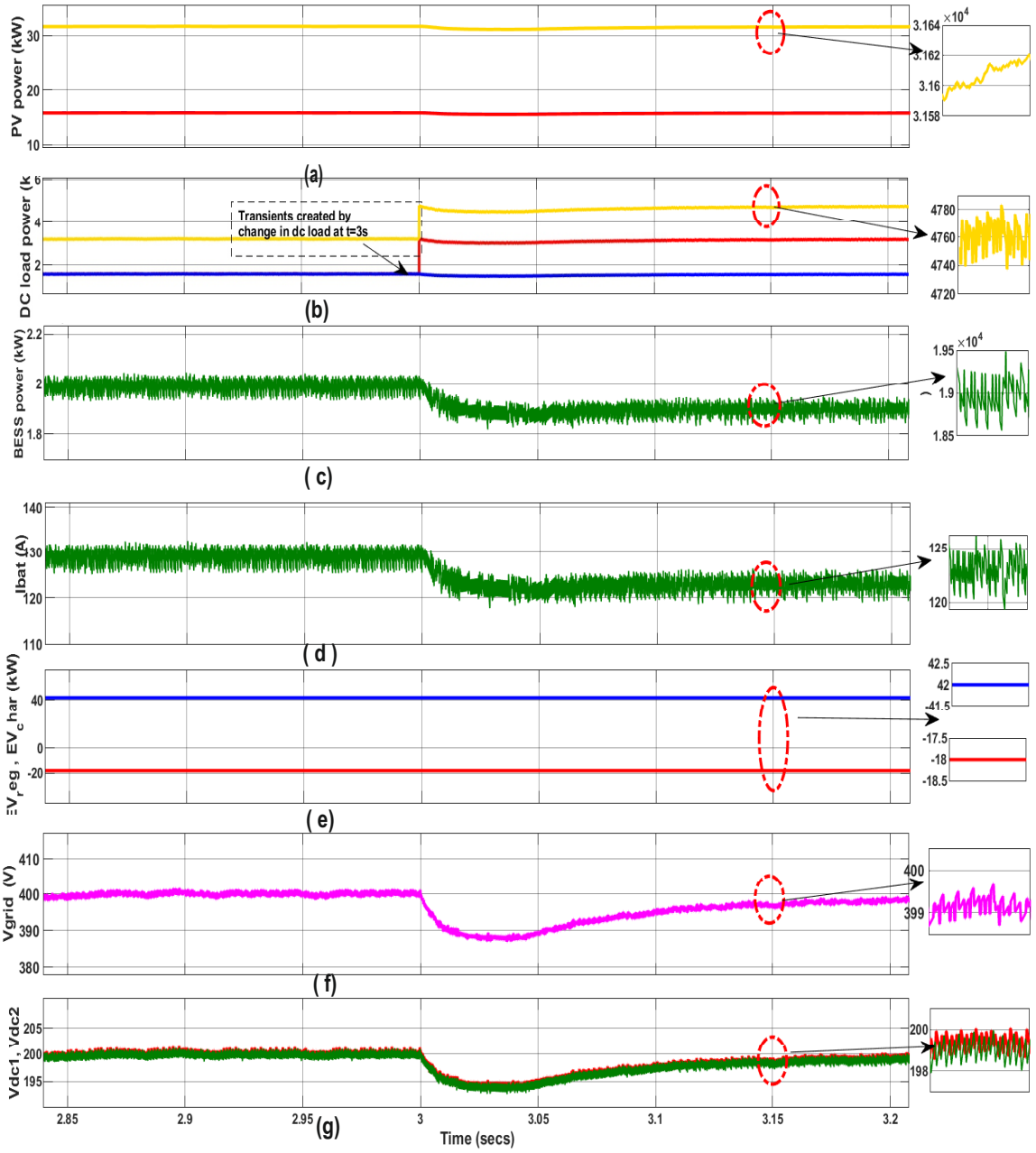

Figure 4.16: Simulation results for transient conditions (changes in dc load) a) P_{gen} b) P_{load} c) P_{bat} d) I_{bat} e) EV_{power} f) V_{grid} g) V_{C1}, V_{C2}

goes into buck mode of operation. Whenever the power generation in a DC bus goes up, there occurs a sudden surge in the grid capacitance voltage of that respective DC bus. Similarly, when there is a decrease in generated power fed, there will be a dip/sag in the grid capacitance voltage of the corresponding bus. The use of battery

energy storage acts as a buffer to bridge the power difference and the bidirectional power flow between the battery and the grid is made feasible by the TL-bidirectional converter.

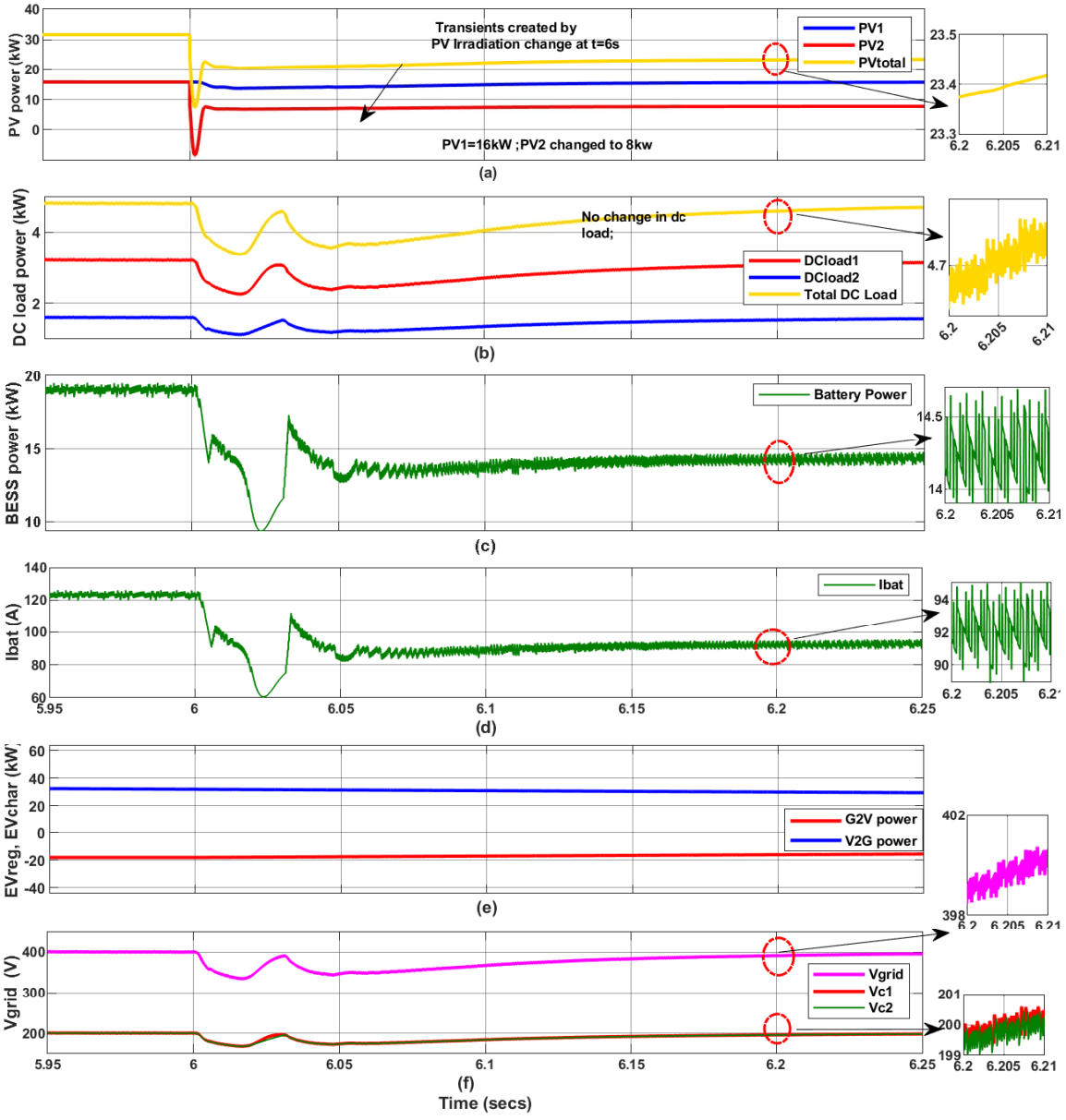

Figure 4.17: Simulation results for transients (change in irradiation) a) P_{gen} b) P_{load} c) P_{bat} d) I_{bat} e) EV_{power} f) V_{grid}, V_{C1}, V_{C2}

From the fig. 4.17, it is observed that change in PV generation (50% decrease in PV-2) at t=6sec, causes grid voltage, V_{grid} to dip around 340V, pole capacitance-voltage V_{C1}, V_{C2} become unbalanced and dip around 120-150V and high ripple in

battery current. It is also obvious from the above result that pole capacitance-voltage V_{C1}, V_{C2} become balanced at ±200V, and bipolar DC grid voltage, V_{grid} is maintained constant at 400V within a time span of t= 6.15s, i.e. model predictive control is able to achieve faster voltage balancing, grid regulation and stable operation of the bipolar grid. In case of sudden increase of PV irradiation (around 50% increase in PV-2) as depicted in figure 4.15 at t=10s, grid voltage, V_{grid} surges around 460V and pole capacitance-voltage V_{C1}, V_{C2} also surges around 230V along with unbalance. But with effective control with model predictive control, the pole capacitance-voltage V_{C1}, V_{C2} become balanced at ±200V, and bipolar DC grid voltage, V_{grid} is maintained constant at 400V within t=10.2s. Simulations carried out in the bipolar DC microgrid system under transient state observe the following: a) TL Boost converter obtaining maximum power from solar PV generation systems PV-1, PV-2 corresponding to solar irradiation, b) TL Bi-directional Buck/Boost Converter with battery energy storage (BESS) balancing pole voltages and sharing power, C) V2G and G2V controlled power flow between multiple EV charging load profiles and grid.

4.7.3 Stability Analysis

From case studies I and II, it is clear that for 50% unbalance in the load connected to poles and 50% unbalance in PV power fed to poles, the decentralized model predictive controller is able to stabilize the grid conditions, perform battery management and mitigate the voltage unbalance. i.e. the proposed system and control are effective for handling 50% power unbalance/ disturbance in the system. On further testing, the MPC controller is able to mitigate power unbalance in the ratio of $\frac{P_{gen}}{P_{load}} > 1.2$ & $\frac{P_{gen}}{P_{load}} < 0.8$ To test the limits of stability of system and find DC bus voltages upto which controller can take care of unbalance, we incultivated a voltage imbalance of 60% between poles. When DC bus voltage drops below 100V, MPC controller not able to balance the bus voltage. (eg : when DC load2=10ohm, Vdc2 drops to 65V, in this case controller not able to balance the grid voltages back to 200V. But when DC-load2 =15ohm, Vdc2 drops to 82V, and MPC controller is able to balance the bus volatge back to 200V in this case). MPC controller can mitigate in ratio of unbalance in bus voltages up to $\frac{V_{C1}}{V_{C2}} < 50\%$.

4.8 Summary

In this chapter, a varying EV load profile with V2G discharge and G2V charge mode is modelled taking into consideration the standard drive cycles and vehicle dynamics. It is integrated with bipolar DC microgrid to study the performance of bipolar DC microgrid under transient and steady state conditions. Configurations of novel multi-interleaved three level bidirectional converter suitable for integrating EV charging stations is also put forward. Simulations carried out in MATLAB /Simulink to validate the effectiveness of the model predictive control for the proposed system of bipolar DC grid and EV fast charging stations. Various case studies are presented and analyzed, confirming the effectiveness and stability of the control strategies proposed for the islanded grid system. Performance under steady state and dynamic state conditions with sudden change in solar irradiation, variation in the DC loads connected and fluctuations in EV load profiles are investigated. Model predictive control takes care of the following in the proposed system; i) TL Boost converter obtaining maximum power from solar PV generation systems, ii) TL Bidirectional Buck/Boost Converter with battery energy storage system balancing pole capacitance voltages,V_{C1} and V_{C2}, iii) V2G and G2V controlled operations between multiple EV charging load profiles and grid and iv) regulation of grid voltage,V_{grid} and power sharing. Thus, effective decentralized control of all the components of multi-node bipolar DC microgrid is implemented with model predictive control.

Chapter 5

Conclusion and Future Scope

5.1 Conclusions

In the proposed research work, modelling and design of three level converters for efficient operation and control of bipolar dc microgrid by model predictive control is the major research contribution. Three level/bipolar converter are designed to operate such that voltage unbalance issues in bipolar dc grid is mitigated and by enabling power sharing between BESS and grid. Discrete state space modelling of three level converters are done for formulating predictive model. EV load profile is modelled and simulated. A novel multi-interleaved three level converter is proposed to integrate EV charging stations to bipolar dc grid. Performance investigation of the above proposed system for fast and efficient operation under dynamic conditions with model predictive control is tested and validated with Hardware in Loop set up. Significance of bipolar dc microgrid in future transportation electrification is highlighted through this research.

In Chapter 1, a brief introduction to the bipolar dc microgrid and basics of electric vehicle charging is covered. An extensive literature survey of the power electronic interface and control techniques to overcome voltage unbalance issues in bipolar dc grid, EV charging converter configurations are reviewed. Identified research gaps leading to the major contributions of this research works.

In Chapter 2, modelling and design of the proposed bipolar dc microgrid and three level converter is discussed. It details mathematical modelling of PV cells, Li-ion battery, circuit description and state space modelling of three level buck/boost converters.Operation of the TLC converter and PV boost converter with PI control

and its simulation result analysis is also covered.

In Chapter 3, Implementation of the model predictive controller and an energy management strategy which mitigates voltage unbalance issues and ensures stable operation of proposed bipolar dc microgrid are discussed. Further, hardware in loop testing using Typhoon Control Center is done to validate the effectiveness of the predictive controller.

In Chapter 4, modelling of EV load profiles which reflects the variations in driving cycles, vehicle dynamics and battery conditions EV load profile is discussed. V2G/G2V energy management system suitable for bipolar dc microgrid and its effective operation in the proposed bipolar dc microgrid is also explained. Moreover, an improved bipolar bidirectional converter suitable for integrating Electric Vehicle Charging Stations to bipolar dc microgrid is also put forward. Possibilities of bipolar dc microgrid in the transportation electrification is emphasized through this work. The major contributions of this research work are:

- Emphasized the concept of bipolar DC microgrid as the best solution to power EV charging stations

- Effective decentralized control of multi-node bipolar dc microgrid (BESS, PV generation system, DC loads, and EV charging loads) implemented with model predictive control.

- Model predictive control takes care of the following in the proposed system;

  * TL boost converter obtaining maximum power from solar photovoltaic generation systems

  * TL bidirectional buck/boost converter with battery energy storage to meet three control objectives; balancing pole capacitance voltages,V_{C1} and V_{C2}, voltage regulation, and bidirectional power flow.

  * Model predictive technique gives faster response(less than 0.2sec) and less ripple during transient conditions within power ratio limit $0.9 \geq \|P_{load} \ / \ P_g\| \geq 1.1$.

- Hardware in loop testing is done to validate the effectiveness of the predictive controller

- EV charging load profile is developed which reflects the variations of the driving cycles, vehicle dynamics, SOC conditions, and power demand of multiple vehicles to study the effect of unpredictable varying EV loads in the bipolar DC microgrid
- Incorporation of the vehicle to grid (V2G)/grid to vehicle (G2V) power flow between EV charging load and bipolar DC microgrid
- Configurations of novel multi-interleaved three level bidirectional converter suitable for integrating EV charging stations is put forward.

5.2 Suggestions for Future Work

Based on the research carried out in this thesis, the recommendations for future research are presented:

- HIL testing and validation of EV Load Profiles with Typhoon Control Center.
- Performance Investigation of Proposed Bipolar DC microgrid with Grid Tied Neutral Point Clamped/Multi-level Inverters
- Typhoon HIL implementation and testing of improved bipolar converter configurations.
- Incorporating effects of driving patterns, optimal charging scheduling in the EV load profile with additional features like smart charging, timed slot charging etc.
- More studies on the optimal positioning or placement of bipolar dc grid along the highways and roads for powering charging stations.
- Developing a prototype EV charging station connected to bipolar dc grid.

Publications

Patents

1. **Nisha K.S.**, Dattatraya N. Gaonkar, Jayalakshmi N.S., A Non-isolated Multi-Port Interleaved Bipolar Bidirectional Converter for EV Charging in Bipolar DC Grid, *Patent No: 509391, Application No:202341033747, Patent granted :10-02-2024.*

Journals

1. **Nisha K.S.**, Dattatraya N. Gaonkar, Jayalakshmi N.S., Operation and control of multiple electric vehicle load profiles in bipolar microgrid with photovoltaic and battery energy systems, ***Journal of Energy Storage, Elsevier***,Volume 57,2023,106261. https://doi.org/10.1016/j.est.2022.106261.

2. **Nisha K.S.**, Gaonkar, D.N., Model predictive controlled three-level bidirectional converter with voltage balancing capability for setting up EV fast charging stations in bipolar DC microgrid, ***Electrical Engineering, Springer***, 104, 2653–2665 (2022). https://doi.org/10.1007/s00202-022-01492

Conferences:

1. **K. Nisha**, and D. N. Gaonkar, "Predictive Control of Three Level Bidirectional Converter in Bipolar DC Microgrid for EV Charging Stations," ***2020 IEEE International Conference on Power Electronics, Smart Grid and Renewable Energy (PESGRE2020)***, Cochin, India, 2020, pp. 1-6.
doi: 10.1109/PESGRE45664.2020.9070356

2. **K. S. Nisha** and D. N.Gaonkar,"Model Predictive Control of Three Level Buck/Boost Converter for Bipolar DC Microgrid Applications," ***2019 IEEE 16th India Council International Conference (INDICON)***, Rajkot, India, 2019, pp. 1-4.
doi: 10.1109/INDICON47234.2019.9029051.

Bibliography

Aden, I. A., Kahveci, H., and Şahin, M. E. (2021). Design and implementation of single-input multiple-output dc–dc buck converter for electric vehicles. *Journal of Circuits, Systems and Computers*, 30(13):2150228.

Ahmadi, T. (2020). Voltage unbalances mitigation in bipolar dc microgrids using a novel three-port multidirectional buck–boost converter. *IET Power Electronics*, 14:192–200.

Ahmadi, T. (2021). Voltage unbalances mitigation in bipolar dc microgrids using a novel three-port multidirectional buck–boost converter. *IET Power Electronics*, 14(1):192–200.

Ahmadi, T., Hamzeh, M., and Rokrok, E. (2018a). Hierarchial control scheme for three-port multidirectional dc-dc converters in bipolar dc microgrids. *J. Power Electron.*, 18(5):1595– 1607.

Ahmadi, T., Rokrok, E., and Hamzeh, M. (2018b). Mitigation of voltage unbalances in bipolar dc microgrids using three-port multidirectional dc-dc converters. *J. Power Electron.*, 18(4):1223– 1234.

Akter, P., Mekhilef, S., N.Tan, L., and Akagi, H. (2015). Model predictive control of bidirectional ac–dc converter for energy storage system. *Journal of Electrical Engineering and Technology*, 10:165–175.

Amara-Ouali, Y., Goude, Y., Massart, P., Poggi, J.-M., and Yan, H. (2021). A review of electric vehicle load open data and models. *Energies*, 14:2233.

Bevrani, H., François, B., and Ise, T. (2017). Microgrid dynamics and control. *John Wiley & Sons:Hoboken, NJ USA .*

Bull, S. R. (2001). Renewable energy today and tomorrow. *Proceedings of the IEEE*, 89(8):1216–1226.

Chen, M. and Rincon-Mora, G. A. (2006). Accurate electrical battery model capable of predicting runtime and iv performance. *IEEE transactions on energy conversion*, 21(2):504–511.

Chen, Y., Q. Huang, A., and Yu, X. (2013). A high step-up three-port dc–dc converter for stand-alone pv/battery power systems. *IEEE Trans. Power Electron.*, 28:5049–5062.

D Broeck, V., J Berten, G., Dalla Vecchia, M., Ravyts, S., and Driesen, J. (2019). Operation of the full-bridge three-level dc–dc converter in unbalanced bipolar dc microgrids. *IET Power Electron.*, 12(9):2256– 2265.

Das, M., Pal, M., and Agarwal, V. (2019). Novel high gain, high efficiency dc–dc converter suitable for solar pv module integration with three-phase grid tied inverters. *IEEE J. Photovolt.*, 9:528–537.

Debnath, D. and Chatterjee, K. (2015). Two-stage solar photovoltaic-based stand-alone scheme having battery as energy storage element for rural deployment. *IEEE Trans. Ind. Electron.*, 62:4148–4157.

Du, Y., Zhou, X., Bai, S., Lukic, S., and Huang, A. (2010). Review of non-isolated bi-directional dc–dc converters for plug-in hybrid electric vehicle charge station application at municipal parking decks. *IEEE APEC, Palm Springs, CA*, page 1145–1151.

Fan, Y., Zhang, H., and Shi, F. (2015). Modeling of electric vehicle loads applicable to power system quasi-steady state analysis. In *2015 5th International Conference on Electric Utility Deregulation and Restructuring and Power Technologies (DRPT)*, pages 301–305.

Garcia, O., Zumel, P., de Castro, A., and Cobos, A. (2006). Automotive dc-dc bidirectional con-verter made with many interleaved buck stages. *IEEE Trans Power Electron*, 21(3):578–586.

Gharibeh, H. F., Yazdankhah, A. S., Azizian, M. R., and Farrokhifar, M. (2021). Online energy management strategy for fuel cell hybrid electric vehicles with installed pv on roof. *IEEE Transactions on Industry Applications*, 57(3):2859–2869.

Gil-Aguirre, J., Perez-Londoño, S., and Mora-Flórez, J. (2019). A measurement-based load modelling methodology for electric vehicle fast-charging stations. *Electric Power Systems Research*, 176:105934.

Golchoubian, P. and Azad, N. (2017). Real-time nonlinear model predictive control of a battery–supercapacitor hybrid energy storage system in electric vehicles. *IEEE Trans Veh Technol*, 66(11):9678–9688.

Goli, P. and Shireen, W. (2014). Pv powered smart charging station for phevs. *Renewable Energy*, 66:280–287.

Gong, L., Cao, W., and Zhao, J. (2017). Load modeling method for ev charging stations based on trip chain. In *2017 IEEE Conference on Energy Internet and Energy System Integration (EI2)*, pages 1–5.

Guo, C., Jianquan, L., and Zhang, Y. (2022). Adaptive droop control of unbalanced voltage in the multi-node bipolar dc microgrid based on fuzzy control. *International Journal of Electrical Power & Energy Systems*, 142,PartB:1142.

Haidar, A. M., Muttaqi, K. M., and Haque, M. H. (2014). Multistage time-variant electric vehicle load modelling for capturing accurate electric vehicle behaviour and electric vehicle impact on electricity distribution grids. *IET Generation, Transmission & Distribution*, 9(16):2705–2716.

Huang, H., Balasubramaniam, S., Todeschini, G., and Santoso, S. (2021). A photovoltaic-fed dc-bus islanded electric vehicles charging system based on a hybrid control scheme. *Electronics,MDPIPhys. Rep.-Rev. Sec. Phys. Lett.*, 10:1142.

Ingersoll, J. and Perkins, C. (1996). The 2.1 kw photovoltaic electric vehicle charging station in the city of santa monica. *IEEE Photovoltaic Specialists Conference*, pages 1509–1512.

Jamroen, C. and Dechanupapritta, S. (2019). Coordinated control of battery energy storage system and plug-in electric vehicles for frequency regulation in smart grid. In *2019 IEEE PES GTD Grand International Conference and Exposition Asia (GTD Asia)*, pages 286–291.

Jehlik, F., Rask, E., Magand, S., and Condemine, E. (2015). Fuel consumption effects of a diesel hybrid electric vehicle across a range of driving styles and ambient conditions. In *2015 IEEE Transportation Electrification Conference and Expo (ITEC)*, pages 1–6.

JPMorgan (2018). Driving into 2025:the future of electric vehicles.

Kakigano, H., Miura, Y., and Ise, T. (2010). Low-voltage bipolar-type dc microgrid for super high-quality distribution. *IEEE Trans. Power Electron.*, 25(12):3066–3075.

Kang, T., Suh, Y., Park, H., Kang, B., and Kim, S. (2013). A design and control of rapid electric vehicle charging system for lithium-ion battery. *The Transactions of the Korean Institute of Power Electronics*, 18:26–36.

Kim, H., Lee, Y., Lee, J., and Han, B. (2014). Operation analysis of bipolar dc distribution system with voltage balancer. *Australasian Universities Power Engineering Conference (AUPEC), Perth, WA*, page 1–6.

Kim, S., G.Kim, H., and Cha, H. (2018). A new voltage balancer with dc–dc converter function. *Asian conference on energy power and transportation electrification (ACEPT)*, 10:1–7.

Lucas, A., Bonavitacola, F., Kotsakis, E., and Fulli, G. (2015). Grid harmonic impact of multiple electric vehicle fast charging. *Electr. Power Syst. Res.*, 127:13–21.

Mangu, B., Akshatha, S., Suryanarayana, D., and G. Fernandes, B. (2016). Grid-connected pv-wind-battery-based multi-input transformer-coupled bidirectional dc-dc converter for household applications. *IEEE J. Emerg. Sel. Top. Power Electron.*, 4:1086–1095.

Pillai, R., Suri, R., Singh, H., Roy, S., and Dhuri, S. (2018). Electric vehicle charging stations business models for india. *India Smart Grid Forum White Paper,*, Version 1.0.

R. Chandra Mouli, G., Bauer, P., and Zeman, M. (2016). System design for a solar powered electric vehicle charging station for workplaces. *Applied Energy*, 168:434–443.

Rafi, M. A. H. and Bauman, J. (2021). A comprehensive review of dc fast-charging stations with energy storage: Architectures, power converters, and analysis. *IEEE Transactions on Transportation Electrification*, 7(2):345–368.

Rodriguez, J. and Cortes, P. (2012). Predictive control of power converters and electrical drives. *Wiley, Hoboken*, 40:1–6.

Sadiq, M., Aragon, C. A., Terriche, Y., Ali, S. W., Su, C.-L., Buzna, L., Elsisi, M., and Lee, C.-H. (2022). Continuous control set model predictive control for three level dc dc converter with unbalanced loads in bipolar electric vehicle charging stations. *Mathematics*, 10:19.

Sharaf, A. M. and Şahin, M. E. (2017). A flexible pv-powered battery-charging scheme for electric vehicles. *IETE Technical Review*, 34(2):133–143.

Shukla, A., Verma, K., and Kumar, R. (2018). Voltage-dependent modelling of fast charging electric vehicle load considering battery characteristics. *IET Electrical Systems in Transportation*, 8(4):221–230.

Singh, A. K., Mishra, A. K., Gupta, K. K., Bhatnagar, P., and Kim, T. (2020). An integrated converter with reduced components for electric vehicles utilizing solar and grid power sources. *IEEE Transactions on Transportation Electrification*, 6(2):439–452.

Tan, L., Wu, B., Yaramasu, V., Rivera, S., and Guo, X. (2016). Effective voltage balance control for bipolar-dc-bus-fed ev charging station with three-level dc–dc fast charger. *IEEE Trans. Ind. Electron..*, 63:4031–4041.

Tavakoli, A., Negnevitsky, M., and Muttaqi, K. M. (2017). A decentralized model predictive control for operation of multiple distributed generators in an islanded mode. *IEEE Transactions on Industry Applications*, 53:1466–1475.

Tavakoli, S.D., e. a. (2013). Decentralised voltage balancing in bipolar dc microgrids equipped with trans-z-source interlinking converter. iet renew. power gener. 10(5), 703–712 (2016). *IEEE Trans. Vis. Comput. Graph.*, 19:2486–2495.

Tremblay, O., A. Dessaint, L., and I. Dekkiche, A. (2007). A generic battery model for the dynamic simulation of hybrid electric vehicles. *IEEE Vehicle Power and Propulsion Conf.*, page 284–289.

Typhoon, H. (2018). Introduction to the typhoon hil toolchain. *HIL Academy*.

UNFCCC (2015). Paris agreement. *United Nations Framework Convention on Climate Change,*, 28.

Wang, F., Lei, Z., Xu, X., and Shu, X. (2017). Topology deduction and analysis of voltage balancers for dc microgrid. *IEEE J Emerg Sel Top Power Electron*, 5(2):672–680.

Xiang, Y., Hu, S., Youbo, L., Zhang, X., and Liu, J. (2019). Electric vehicles in smart grid: A survey on charging load modelling. *IET Smart Grid*, 2.

Xiong, X. and Yang, Y. (2020). A photovoltaic-based dc microgrid system: Analysis, design and experimental results. *Electronics*, 9:941.

Yaramasu, V. and Wu, B. (2014). Predictive control of a three-level boost converter and an npc inverter for high-power pmsg-based medium voltage wind energy conversion systems. *IEEE Trans Power Electron*, 29(10):5308–5322.

Yilmaz, M. and Krein, P. (2013). Review of the impact of vehicle-to-grid technologies on distribution systems and utility interfaces. *IEEE Transactions on Power Electronics*, 28:5673–5689.

Yong, J., Ramachandaramurthy, V., Tan, K., and Mithulananthan, N. (2015). A review on the state-of-the-art technologies of electric vehicle, its impacts and prospects. *Renew. Sustain. Energy Rev.*, 49:365–385.

Zhang, X., Gong, C., and Yao, Z. (2015). Three-level dc converter for balancing dc 800-v voltage. *IEEE Trans Power Electron*, 30(7):3499–3507.

Zhao, X., Ye, Y., Ma, J., Shi, P., and Chen, H. (2020). Construction of electric vehicle driving cycle for studying electric vehicle energy consumption and equivalent emissions. *Environmental Science and Pollution Research*, 27:37395–37409.

Zubieta, L. E. (2016). Are microgrids future of energy? dc microgrids from concept to demonstration to deployment. *IEEE Electrification Magazine*, June.

Appendix A

EV Segments: Current Market Study

Table A.1: Charging power level of EV segments

	Power Level	Compatible Vehicle
Normal Power Charging	P $\leq 7kW$	E-2W,E-3W
.	7kW $\leq P \leq 22kW$	E-cars (LCV upto 1ton)
High Power Charging	22kW $\leq P \leq 50kW$	E-cars, LCV (upto 1.6 tons)
.	50kW $\leq P \leq 200kW$	MCV
Extra High Power Charging	200 kW $\leq P \leq 500kW$	Trucks, Buses

Table A.2: EV currently available in the market

EV Model	Charge Power(kW)	Battery Capacity (kWh)	Range
Hyundai Ioniq-E	6.6	28	
Tesla Model 3LR	11.5	74	
VW e-golf	7.2	35.8	31km
BMW i3	7.4	33	245km
Mercedes B Class	10	28	
Nissan Leaf	6.6	40	270km
Volvo VNR Trcuk	250	200	
Bajaj-RE 3W	3kW	3.51kWh/48V	60km
Small medium cars	6kW	36kWh	

Appendix B

Vehicle Dynamic Equations

The following are the resistive forces that need to be overcome by the vehicle traction unit to achieve the required acceleration for the vehicle.

Frictional Force

Frictional forces, F_{roll} occur due to the friction between the tire and the road. Reference values of rolling coefficient f_r vary for different road types as shown in Table B.1. Therefore, the resistive force is expressed as:

$$F_{ad} = M_T.g.f_r.cos(\alpha) \tag{B.1}$$

where M_T is the gross weight of the vehicle, g is the acceleration due to gravity, f_r the rolling resistance coefficient, α the gradeability angle.

Aerodynamic Drag Force

The aerodynamic drag force, F_{ad} is the resistive force due to wind opposition during the motion. The force varies based on wind velocity, the frontal area A_f of the vehicle, and the drag coefficient, C_D which varies for different vehicles. The opposing force is expressed as:

$$F_{roll} = \frac{1}{2}.\rho.A_f.C_D.V^2 \tag{B.2}$$

where ρ the air density, A_f the frontal area of the vehicle, C_D the drag coefficient, V the velocity of the vehicle.

Table B.1: Reference values for the rolling resistance coefficient .

Conditions	**Rolling resistance coefficient (f_r)**
Tire on smooth tarmac road	0.01
Tire on concrete road	0.011
Tire on a rolled gravel road	0.02
Tar macadam road	0.025
Unpaved road	0.05
Bad earth tracks	0.16
Loose sand	0.15-0.3
Truck tire on concrete or asphalt road	0.006-0.01
Wheel on iron rail	0.001-0.002

Grading Force

The grading force, F_g is the resistive force that occurs during the uphill of the vehicle on a slope road. It opposes the tractive force during the uphill slope and aids during the downhill slope. The main parameter that defines grading force is the angle of the uphill which varies based on road conditions or terrains. The grading force is given :

$$F_g = M_T.g.sin(\alpha) \tag{B.3}$$

where M_T is the gross weight of the vehicle, g is the acceleration due to gravity, α the gradeability angle.

Acceleration Force

The acceleration force, F_a, is significant in moving the vehicle forward at the required speed the driver decides. It varied with the driver behavior and expressed as in equation B.4, (**?**):

$$F_a = \lambda.M_T.\frac{dV}{dt} \tag{B.4}$$

where λ the rotational inertia constant, M_T is the gross weight of the vehicle, V the velocity of the vehicle. The total resistive force which opposes the motion of the vehicle is the summation of all the forces as shown in Equation B.5. The motor must deliver the power in order to overcome these opposing forces:

$$F_{res} = F_{roll} + F_{ad} + F_g + F_a \tag{B.5}$$

Vehicle dynamics equation

$$P_{LOADT} = \frac{(M.g.f_r.cos(\alpha) + \frac{1}{2}.\rho.A_f.C_D.V^2 + M.g.sin(\alpha) + \lambda.M.\frac{dV}{dt}).V}{\eta_{HESS}.\eta_T.\eta_M} \tag{B.6}$$

$$P_{LOADB} = (M.g.f_r.cos(\alpha) + \frac{1}{2}.\rho.A_f.C_D.V^2 + M.g.sin(\alpha) + \lambda.M.\frac{dV}{dt}).V.\eta_R \tag{B.7}$$

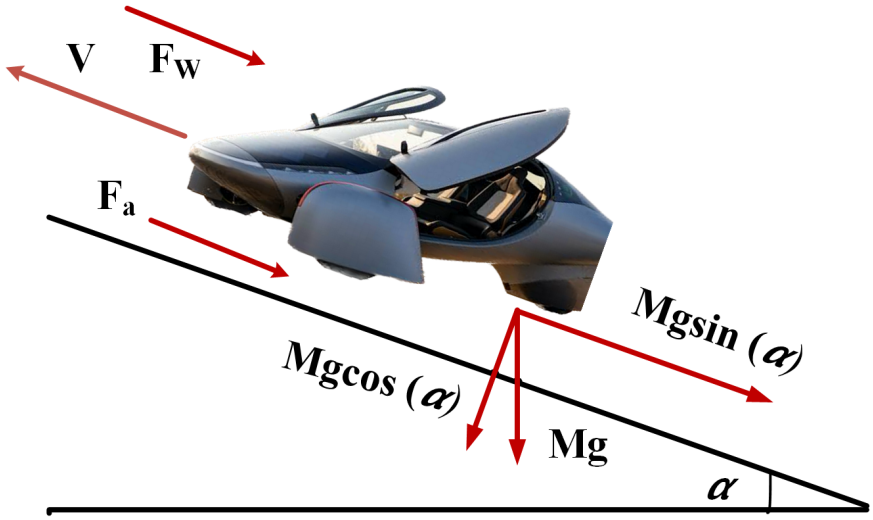

Figure B.1: Dynamics of Vehicle

PI Control Loop Parameters

Table B.2: PI Controller loops parameters

Parameters	**Values**
Bandwidth of inner current battery loop	rad/sec
Phase margin of inner current battery loop	60 °
Control parameters current loop	Kp = 0.045 ,Ki = 5
Bandwidth of outer voltage loop	rad/sec
Phase margin of outer voltage loop	55 °
Control parameters outer voltage loop	Kp = 0.4 ,Ki =10

Biodata

Bio-Data

Name : Nisha K S
Date of birth: 05-05-1989
Marital status: married
E-mail: nishaks.187ee012@nitk.edu.in
E-mail: nishaksathian@gmail.com
Mobile: +91 9946194884

Address
Research Scholar
Department of Electrical & Electronics Engineering
National Institute of Technology Karnataka
Surathkal, Mangaluru, India-575025, India.

Education

- **M.Tech.**, Power Electronics and Control, Government Engineering College Idukki, Mahatma Gandhi University, Kerala, CGPA - 8.24, 2015.
- **B.Tech**, Electrical & Electronics Engineering, NSS College of Engineering, Palakkad, Kerala, Percentage - 69.80, 2012.